

Heat Pump Simulation Model and Optimal Variable-Speed Control for a Wide Range of Cooling Conditions

By

Tea Zakula

Dipl. Ing.

Faculty of Mechanical Engineering and Naval Architecture

University of Zagreb, 2007

Submitted to the Department of Architecture
in Partial Fulfillment of the Requirements for the
Degree of Master of Science in Building Technology
at the

MASSACHUSETTS INSTITUTE OF TECHNOLOGY

June 2010

© Massachusetts Institute of Technology

All rights reserved.

Author:

Department of Architecture

May 20, 2010

Certified by:

Leslie K. Norford

Professor of Building Technology

Thesis Supervisor

Accepted by:

Julian Beinart

Professor of Architecture

Chair of the Department Committee on Graduate Students

Leslie K. Norford
Professor of Building Technology
Thesis Supervisor

Heat Pump Simulation Model and Optimal Variable-Speed Control for a Wide Range of Cooling Conditions

By
Tea Zakula

Submitted to the Department of Architecture
On May 20, 2010, in Partial Fulfillment of the Requirements for the
Degree of Master of Science in Building Technology

Abstract

The steady-state air-to-air heat pump model presented in this thesis was developed from the first principles. The main objective was to develop a heat pump model that can be used as a part of larger simulation models, and that will make a connection between simple models that do not describe equipment behavior accurately enough and complicated models that are computationally very expensive. The model consists of the evaporator, compressor and condenser sub-model, each modeling the steady-state behavior of a particular component. To confirm the model accuracy, simulation results are compared with the experimental data from the Mitsubishi “Mr. Slim”[®] heat pump. The reported COP prediction errors are up to 20% under-prediction when the evaporating temperature is more than 2 K under-predicted, and \pm 10% when the evaporating temperatures are more accurately predicted (less than 2K under-predicted). The model is strongly sensitive on the evaporator temperature prediction errors, since they influence the compressor inlet density. A grid search optimization algorithm is used to find the heat pump optimal performance map. The map defines the optimal evaporator fan speed, condenser fan speed and compressor speed needed to achieve the lowest total power consumption for the given cooling rate, ambient and zone temperature.

Thesis Supervisor: Leslie K. Norford

Title: Professor of Building Technology, Department of Architecture

Acknowledgement

I would like to acknowledge certain people and groups who were tremendously helpful in this process. First, thanks to MIT Energy Initiative and MIT/Masdar Institute of Science and Technology Collaborative Research Program for believing in me and in my research. Without your financial support none of this would be possible.

Professor Armstrong, your skills and aspiration for perfection are priceless. Without your helpful insight this work definitely would not be as meaningful or complete. Thank you so much for mentoring me from the other side of the world.

Last, but not least, Professor Norford, you are the best advisor that a person could wish for. You offered your friendship and support whenever I needed them and your challenging questions and constructive criticism helped me to advance not only in my knowledge but also in my thoughts and approach to problems.

At the end, I dedicate this work to my grandmother Zlata who recently passed away and to my grandmother Beba. You both mean so much to me. Among all my traits, I am most proud of my strength and integrity, and both of those things I inherited from you. Thank you for passing those virtues to my parents and for showing me their true meaning. Grandma Zlata, I am so sorry that I cannot call you on my graduation day. But I know you will be there with me.

Table of Contents

Chapter 1: Introduction.....	18
Chapter 2: Literature review.....	23
Chapter 3: Heat pump model	31
3.1. Evaporator sub-model.....	33
3.2. Compressor sub-model.....	40
3.3. Condenser sub-model	47
3.4. Whole system model	52
3.5. Heat transfer coefficient correlations	57
3.6. Pressure drop correlations	61
Chapter 4: Heat pump model validation	65
4.1. Evaporator sub-model validation.....	68
4.2. Compressor sub-model validation	82
4.3. Condenser sub-model validation	85
4.4. System validation	91
Chapter 5: Heat pump optimization	107
5.1. Condenser airflow optimization	108
5.2. Condenser airflow and subcooling optimization	111
5.3. Evaporator airflow and condenser airflow optimization	113
5.4. Heat pump optimal performance map	120
Chapter 6: Conclusion and future work.....	123
References.....	127
Appendix A: Constant UA value estimate.....	131
Appendix B: Optimization results.....	133
B.1. Condenser airflow optimization results	133
B.2. Condenser airflow and subcooling optimization results	137
B.3. Evaporator airflow and condenser airflow optimization results	139
Appendix C: Measurement data.....	141
Appendix D: Code.....	147

List of Figures

Figure 1-1: Use of electricity in commercial buildings	18
Figure 1-2: Results of mid-performance building annual energy simulations.....	20
Figure 3-1: Schematic of the heat pump cooling cycle.....	33
Figure 3-2: T-s diagram of the heat pump cooling cycle.....	33
Figure 3-3: Condenser fan speed vs. airflow dependence	36
Figure 3-4: Condenser fan power vs. airflow	37
Figure 3-5: Approximated evaporator fan power vs. airflow dependence	37
Figure 3-6: Evaporator sub-model flow chart.....	39
Figure 3-7: Compressor sub-model flow chart	46
Figure 3-8: Condenser sub-model flow chart	51
Figure 3-9: Whole system solver flow diagram.....	54
Figure 3-10: Whole system solver schematic	55
Figure 3-11: Effectiveness of cross-flow exchanger with both fluids unmixed	57
Figure 3-12: Rectangular tube array	58
Figure 3-13: Heat exchanger geometry.....	59
Figure 4-1: Schematic of the heat pump test stand	65
Figure 4-2: Components of the heat pump test stand	66
Figure 4-3: Evaporator inlet temperature absolute error.....	70
Figure 4-4: Cooling rate to airflow ratio for each measurement point	71
Figure 4-5: Temperature difference between the refrigerant evaporating temperature and zone temperature as a function of Q_e/V_z	72
Figure 4-6: Temperature difference if the evaporating region thermal effectiveness is set to constant value of 0.95	73
Figure 4-7: Temperature difference if the evaporator airflow is 20% larger than the measured values	74
Figure 4-8: Evaporator outlet temperature absolute error.....	74
Figure 4-9: Evaporator inlet pressure relative error.....	75
Figure 4-10: Compressor inlet pressure relative error	76
Figure 4-11: Refrigerant mass flow rate relative error	77
Figure 4-12: Evaporator inlet temperature absolute error for 20% larger evaporator airflow than the measured values	78
Figure 4-13: Evaporator outlet temperature absolute error for 20% larger evaporator airflow than the measured values	79
Figure 4-14: Evaporator inlet pressure relative error for 20% larger evaporator airflow than the measured values	79
Figure 4-15: Compressor inlet pressure relative error for 20% larger evaporator airflow than the measured values	80
Figure 4-16: Refrigerant mass flow rate relative error for 20% larger evaporator airflow than the measured values	81
Figure 4-17: Compressor shaft speed relative error.....	83
Figure 4-18: Compressor power relative error.....	84
Figure 4-19: Discharge temperature relative error.....	84
Figure 4-20: Condensing temperature relative error.....	87
Figure 4-21: Temperature difference between the refrigerant evaporating temperature and zone temperature as a function of Q_e/V_z	87
Figure 4-22: Condenser outlet temperature absolute error	88
Figure 4-23: Condenser outlet enthalpy relative error	89

Figure 4-24: Compressor outlet pressure relative error	90
Figure 4-25: Condenser heat relative error	90
Figure 4-26: Evaporator inlet temperature absolute error.....	92
Figure 4-27: Evaporator outlet temperature absolute error.....	93
Figure 4-28: Evaporator inlet pressure relative error.....	93
Figure 4-29: Compressor inlet pressure relative error	94
Figure 4-30: Refrigerant mass flow rate relative error	95
Figure 4-31: Condenser outlet enthalpy relative error	95
Figure 4-32: Compressor outlet pressure relative error	96
Figure 4-33: Pressure ratio relative error	96
Figure 4-34: Compressor shaft speed relative error.....	97
Figure 4-35: Compressor power relative error.....	98
Figure 4-36: Compressor outlet temperature relative error	99
Figure 4-37: Condenser heat relative error	99
Figure 4-38: Condensing temperature absolute error	100
Figure 4-39: Condenser outlet temperature absolute error	100
Figure 4-40: COP relative error	101
Figure 4-41: Evaporator outlet temperature absolute error for 20% larger evaporator airflow than the measured values	103
Figure 4-42: Compressor inlet pressure relative error for 20% larger evaporator airflow than the measured values	103
Figure 4-43: Pressure ratio relative error for 20% larger evaporator airflow than the measured values	104
Figure 4-44: Compressor power relative error for 20% larger evaporator airflow than the measured values	104
Figure 4-45: COP relative error for 20% larger evaporator airflow than the measured values	105
Figure 5-1: Total power consumption versus condenser airflow.....	109
Figure 5-2: Total power consumption versus condenser airflow.....	110
Figure 5-3: Cooling process T-s diagram for measured and optimal predicted condenser airflow and subcooling temperature difference for point 8	112
Figure 5-4: Total power consumption versus condenser airflow and subcooling temperature difference for point 8	112
Figure 5-5: Total power consumption versus evaporator	114
Figure 5-6: Cooling process T-s diagram for measured and optimal predicted evaporator and condenser airflow for point 40.....	115
Figure 5-7: Total power consumption versus evaporator	116
Figure 5-8: Cooling process T-s diagram for measured and optimal predicted evaporator and condenser airflow for point 8.....	117
Figure 5-9: Total power consumption versus the evaporator and.....	119
Figure 5-10: Heat pump performance map for the zone temperature 25 °C.....	120
Figure 5-11: Evaporator airflow to compressor speed ratio map.....	121
Figure 5-12: Condenser airflow to compressor speed ratio map	122
Figure B- 1: Optimal condenser airflow for M1 – M4	133
Figure B- 2: Measured and optimal condenser airflow for M4	134
Figure B- 3: COP_m^* and COP_{max} for model M1	135
Figure B- 4: COP_m^* and COP_{max} for model M2	135
Figure B- 5: COP_m^* and COP_{max} for model M3	136
Figure B- 6: COP_m^* and COP_{max} for model M4.....	136
Figure B- 7: Measured and optimal condenser airflow for M4	137

Figure B- 8: Measured and optimal condenser subcooling for M4	138
Figure B- 9: COP_m^* and COP_{max} for model M4	138
Figure B- 10: Measured and optimal evaporator airflow for M4	139
Figure B- 11: Measured and optimal condenser airflow for M4	140
Figure B- 12: COP_m^* and COP_{max} for model M4	140
 Figure D- 1: The code map	 148

List of Tables

Table 2-1: Summary of predicted capacity and COP discrepancies based on comparisons against actual test data	25
Table 3-1: Coefficients and RMS errors for four different models	43
Table 3-2: Coefficients and RMS error for power model.....	44
Table 4-1: Overview of the 4 compared models.....	67
Table 4-2: Evaporator RMS errors for output variables for 4 different model variations.....	77
Table 4-3: RMS errors for 20% larger evaporator airflow than the measured values	81
Table 4-4: Compressor RMS errors for the compressor sub-model output variables	85
Table 4-5: Condenser RMS errors for output variables for 4 different models.....	91
Table 4-6: System RMS errors for output variables for 4 different models	102
Table 4-7: System RMS errors for output variables for 20% larger evaporator airflow than the measured values	105
Table 5-1: Parameters for condensing region of the condenser for measured and optimal condenser airflow for measurement point 8.....	109
Table 5-2: Parameters for measured and optimal condenser airflow for point 22.....	110
Table 5-3: Parameters for measured and optimal condenser airflow and subcooling temperature difference for point 8	113
Table 5-4: Parameters for point 40 for Case 1 (V_{z_m} and V_{o_m}), Case 2 (V_{z_m} and V_{o_opt}) and Case 3 (V_{z_opt} and V_{o_opt})	115
Table 5-5: Parameters for point 8 for Case 1 (V_{z_m} and V_{o_m}), Case 2 (V_{z_m} and V_{o_opt}) and Case 3 (V_{z_opt} and V_{o_opt})	117
Table A-1: Standard operation data for “Mr. Slim” [29].....	131
Table C- 1: Measured data [20]	145

List of Symbols

Symbol	Description	Unit
English letter symbols		
A	area	m ²
C	fluid capacity rate	W/K
C	constant	-
c _p	specific heat at constant pressure	J/(kgK)
c _v	specific heat at constant volume	J/(kgK)
D	effective or actual displacement	m ³
d	pipe diameter	m
E	pipe roughness	m
f	compressor shaft speed	Hz
f	friction factor	-
G	mass velocity	kg/(m ² s)
g	acceleration due to gravity	m/s ²
h	convective heat transfer coefficient	W/(m ² K)
h	specific enthalpy	kJ/kg
J	power	W
KW	compressor power	W
k	compression exponent for ideal gas undergoing isentropic compression	-
k	thermal conductivity	W/mK
L	heat exchanger pipe length	m
M	molar mass	kg/kmol
m	mass flow rate	kg/s
N	number of measurement points	-
N	number of heat exchanger pipe rows	-
NTU	number of transfer units	-
n	compression exponent	-
n _s	compression exponent for real gas undergoing isentropic compression	-
n _t	compression exponent for ideal gas undergoing isothermal compression	-
P	pressure	Pa
RMS	square root of arithmetic mean of the squared residuals	
r	pipe radius	m
Q	heat rate	W
s	entropy	J/(kgK)
p.UA	constant evaporator UA value	W/K
p.UA _c	constant condenser UA value	W/K
p.x _{oil}	constant mass fraction of oil	kg _{oil} /kg
T	temperature	K
t	heat exchanger pipe thickness	m
U	overall heat transfer coefficient	W/(m ² K)
UA	heat exchanger UA value	W/K
V	volumetric airflow	m ³ /s

v	specific volume	m ³ /kg
w	fan speed	rpm
w	mass fraction	kg/kg
w	speed	m/s
x	vapor quality	kg _v /kg
y	heat exchanger area percentage devoted to desuperheating, subcooling, evaporation, or condensation	-
Z	resistance factor	-

Greek letter symbols

Δ	difference	-
ε	cross-flow effectiveness	-
η	efficiency	-
ψ	mole fraction	kmol/kg
ρ	density	kg/m ³
μ	dynamic viscosity	Ns/m ²

Subscripts

air	air
as	assumed
c	whole condenser
c1	condenser inlet
c2	beginning of condensing region in condenser
c3	end of condensing region in condenser
c4	condenser outlet
calc	calculated
comp	compressor
comp_in	compressor inlet
comp_out	compressor outlet
cp	condensing region of condenser
csh	desuperheating region of condenser
d	discharge pipe
discharge	compressor discharge state
fg	refers to change from saturated liquid to saturated vapor
fin	fin
e	whole evaporator
e1	evaporator inlet
e1	end of evaporating region in evaporator
e3	evaporator outlet
ep	evaporating region of evaporator
esh	desuperheating region of evaporator
ex	external
in	internal
liq	evaporator inlet and condenser outlet state
liq	liquid
log m	logarithmic mean

m	measured
max	maximum
min	minimum
mix	refrigerant and oil mixture
o	outside
o	oil
out	outside
ref	refrigerant
s	suction pipe
s	surface
sc	subcooling region of condenser
sph	single phase
suction	compressor suction state
tph	two phase
v	volumetric
z	zone

Chapter 1: Introduction

In the United States, buildings consume around 40% of the total energy and more than 70% of electricity. The second and third largest consumers of electricity in commercial buildings are cooling and ventilation systems, as shown in Figure 1-1.

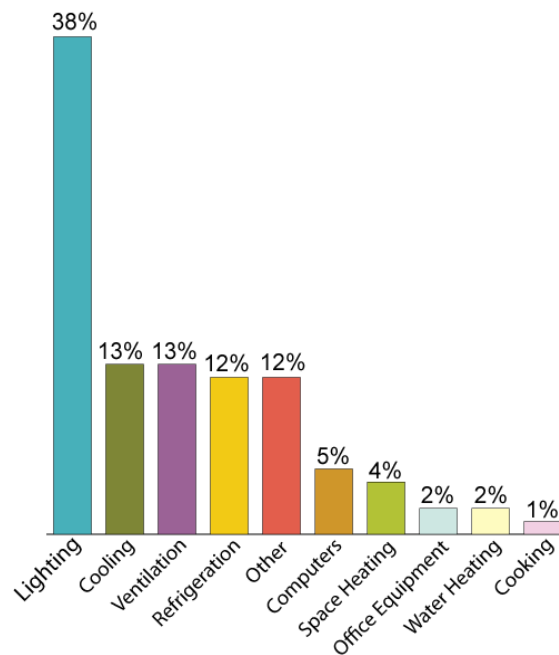


Figure 1-1: Use of electricity in commercial buildings [35]

To reduce the amount of energy for cooling, improvements in the equipment efficiency and the cooling process efficiency are essential. In the last few decades, important studies have been conducted related to the improvement of the cooling equipment energy efficiency and the assessment of equipment behavior. However, not many studies have proposed and analyzed different combinations of cooling technologies. One of the most interesting proposals on a combined cooling system has been provided by Armstrong et al. [1, 2]. Since the major part of the electricity for cooling is used for the compression process, the main idea behind Armstrong's work is to reduce the energy for compression by decreasing the condensing temperature and increasing the evaporating temperature. This system reduces the pressure rise across the compressor and it is therefore termed "low-lift cooling." However, although the pressure rise reduction decreases the compressor energy consumption, it would normally

increase the transport energy consumption (energy for fans and pumps) and hence, needs to be carefully balanced.

The first component of the low-lift cooling chiller is a variable-speed drive motor (VSD) for the compressor and auxiliary fans and pumps. The VSD offers a wide range of operating possibilities to efficiently balance compressor and transport energy, and is a crucial component for the low-lift cooling. The second important component is hydronic radiant cooling (RCS) that can be imbedded in any part of the building structure (e.g. floors, ceiling, walls). Although most U.S. buildings have all-air system for both cooling and heating, numerous studies have shown that water systems usually require less energy for the same cooling or heating effect. First, when compared with air, water has around 3500 times larger $\rho_{\text{air}} * c_{p,\text{air}}$ product, meaning that water systems can significantly reduce the amount of transport energy. Second, in hydronic radiant cooling, the whole floor or ceiling area acts as a cooling area. Because the exchanged heat is proportional to the heat transfer area and temperature difference, then due to the large floor or ceiling area the temperature difference between the zone and chilled water can be smaller, and the chilled water temperature can be higher compared to other systems. Higher chilled water temperature enables higher evaporating temperature and pressure, which then lowers the compressor pressure rise and power consumption. The third component, thermal energy storage (TES) is the component that has great advantage for the climates with the significant outside temperature differences between day and night. In these climates, cooling energy can be stored during nights when the condensing temperature and pressure can be lower due to the lower outside temperature. In climates where large temperature differences are not the case, thermal storage can still be beneficial economically, if the price of electricity is lower during the night. The last component is the dedicated outside air system (DOAS) that delivers fresh, dehumidified air to each zone. That way, water is used to remove zone sensible loads and air just to provide fresh air and to remove latent loads, which are in most cases smaller than sensible loads. Further, enthalpy recovery is more economical in DOAS than in all air systems.

While different studies have shown the benefits of each separate component of this system, there is no other research that combines them together and analyzes the combined system benefits. Armstrong has developed a computer simulation of the combined system and analyzed what the possible annual energy consumption savings for the building are, compared to a typical VAV system with a two-speed chiller, and given different combinations of low-lift cooling system components (VS, RCS, TES, DOS). The analysis for five different U.S. climates and three building types (low-performance, mid-performance and high-performance) has shown that possible energy savings range from 30 to 70 %, depending on the climate and

the building envelope, when all four components are included. The annual energy consumption for a mid-performance building is shown in Figure 1-2:

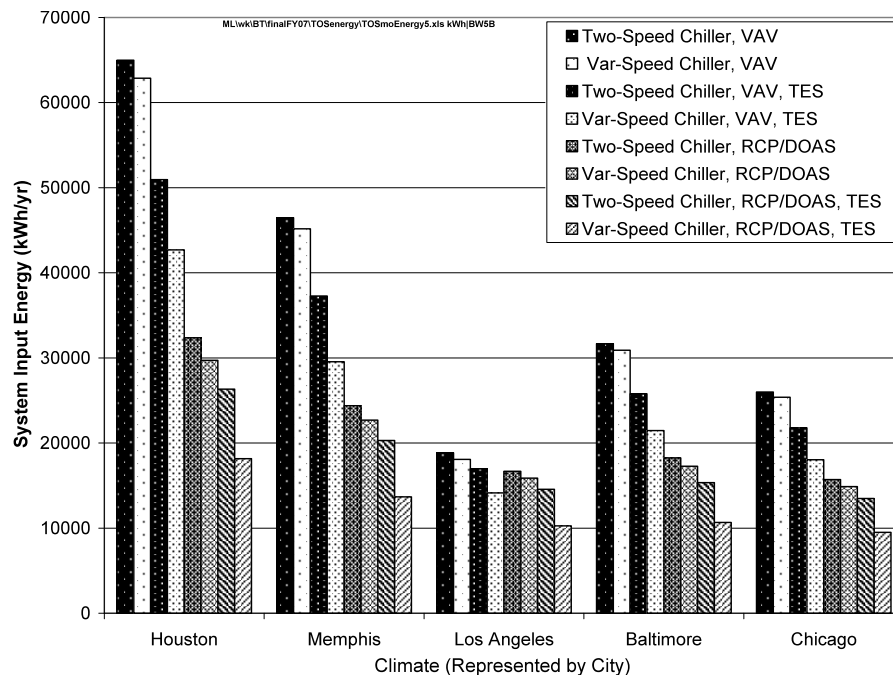


Figure 1-2: Results of mid-performance building annual energy simulations for different chiller-distribution-thermal-storage system configurations in five climates [2]

In addition to Armstrong's computer analysis, the combined system has been implemented in a test rooms in Abu Dhabi and at MIT, and the experimental data from both test rooms are currently being collected. Although experimental data will be used for more realistic system analysis, computer modeling is still an invaluable tool for fast system performance analysis, parameter influence analysis and potential improvement decisions.

Armstrong's computer model has the sub-models of each low-lift cooling component, with the heat pump model being the most important one. However, the model does not include some very important parts of the heat pump modeling: the pressure drop inside the heat pump and the variable heat transfer coefficients in the heat exchangers. It also does not include the desuperheating process in the evaporator or the subcooling process in the condenser. In order to perform more accurate analysis of the low-lift cooling technology an improved model is needed.

The heat pump model (HPM) described in Chapter 3 is based on Armstrong's existing model, but is significantly changed and extended to describe more realistic behavior. The HPM

consists of three component sub-models, each describing the steady-state performance of the evaporator, condenser and compressor. This modular approach enables further development of each component independent from the other parts, and the replacement of one component sub-model with a different one. An idealized expansion valve has been modeled, which accurately models the real steady-state throttling process in cases where the valve is positioned at the evaporator inlet¹. The developed model includes the pressure drops and heat transfer coefficients that vary with refrigerant and transport fluid flow rates. Furthermore, the model includes desuperheating in the evaporator and subcooling in the condenser. Modeling of subcooling is especially important since it enables one to analyze the influence of subcooling on the heat pump process efficiency. The lubricant influence is taken into account for the evaporator and condenser pressure drop calculations and also in the compressor heat balance calculations. The HPM has the possibility of including or neglecting different options mentioned above; for example, it can range from the simplest model variation with a constant heat exchanger conductance, without pressure drop calculations, evaporator desuperheating or condenser subcooling to the most complex model variation where all those options are included. Different variations of the model can be used to analyze how each option or combination of options influences the overall heat pump performance, result accuracy and computational time.

Chapter 4 outlines the model validation process using experimental data from Mitsubishi's MUZ09NA variable-speed heat pump [29]. After the heat pump data have been measured by Gayeski [20] over the range of operating conditions, all relevant variables are compared with the simulation model. The parameters measured on the refrigerant-side are the evaporator inlet and outlet temperature and pressure, compressor outlet temperature and pressure and condenser outlet temperature. For the air-side, the evaporator and condenser airflow temperature differences and condenser airflow versus fan speed characteristics are measured. The compressor power, cooling rate and condenser power versus speed characteristic are also measured. The evaporator fan speed remained constant through the measurements and hence, the evaporator flow versus speed and power versus speed characteristic were not measured. Due to the modular approach to computer modeling, it was possible to analyze first each component separately and then to compare the performance of the whole system with

¹ The literature on modeling of transient heat pump operations contains many analyses, models and inventions addressing transient response. However, electronic expansion valves with micro-processor-based control, which are expected to dominate the future market, much as electronic fuel injection dominates the automotive market in developed countries, largely eliminate problems of transient response.

measured data. The component-by-component validation was especially important since the model is organized in a way that the outputs from one component are the inputs to the following component, meaning that the errors from each component can easily progress through the system. For the system validation, the measured data used as the input parameters to the model were: cooling rate, zone and outside temperature, evaporator and condenser airflow rate, evaporator desuperheating temperature difference and condenser subcooling temperature difference. All important model output parameters, with heat pump power consumption being the most important one, were then compared against experimental data.

Chapter 5 explains the process of finding the heat pump optimal operating point using the HMP whose organization and validation are presented in Chapters 3 and 4, respectively. The heat pump consumes power for the compressor, evaporator fan and condenser fan. The optimal operating point is the point for which the total fan and compressor power consumption is a minimum for the given evaporator load, zone temperature, and outside temperature. Currently, the optimal point is found using the grid search approach and the future work plan is to implement one of the MATLAB built-in optimizing functions. With the total power consumption being the optimization objective, the optimizing parameters can be the condenser fan speed, evaporator fan speed, subcooling temperature difference, and any combination of these parameters, including all of them. The parameters that are not chosen as the optimizing parameters need to be specified as the inputs to the optimizer, together with the cooling rate, zone and outside temperature and evaporator desuperheating. Because the model offers flexibility in choosing between different models options (desuperheating, subcooling, pressure drop, constant heat exchanger conductance), it is possible to analyze how the optimal variables and objective function change depending on the chosen options.

Chapter 6 gives the conclusion about the work presented in this thesis and plans about future work. At this stage, the evaporator and condenser fan are modeled using the curve fit to measured data, and the plan is to modeled them using fan laws. Also, in addition to air-to-air heat pump, the model will have the possibility to simulate chiller performance, which means that the evaporator sub-model needs to be expanded to model the water-to-refrigerant heat exchange. The heat pump optimization will be changed from the grid search algorithm to some faster method, like perhaps a gradient-based method. Finally, the algorithm for free-cooling mode will be implemented, since free-cooling can be very important for cooling energy reduction.

Chapter 2: Literature review

Ever since the development of different heat pump simulation models began in the late 1970's, simulation models have become more and more popular and widely used in research. They are important tools for heat pump manufacturers because they enable the analysis of different parameter variations before the real prototype is made. Although they cannot describe the real product performance completely accurately, simulation models are very useful for new product decision-making. Additionally, these models are very important for the development of new HVAC technologies, for which a system performance analysis is most often required before commercial production and implementation starts. For these reasons, computer simulations are irreplaceable. They are, for now, the fastest and cheapest tools for that type of analysis.

Among the models found in literature, there are two main paths for heat pump simulations. The first approach, more often found in literature, is using experimental data for a specific heat pump type. These simulations can accurately predict heat pump performances if all the necessary input data are accurately measured. However, in most cases, especially for the new technology analysis, experimental data cannot be collected since the system does not exist in reality, or long and expensive measurements are required. In addition to that, models developed from experimental data are usually valid only for a specific heat pump type and limited range of operating conditions, for which experimental data are known. The second approach to modeling is using the first principles and input variables that can be collected from the manufacturer's data. This approach is not necessarily more accurate than the first approach, but enables the analysis of different heat pump types and wider range of operating conditions.

One of the first models developed using the first principles approach was Hiller's air-to-air heat pump model [22]. The main heat pump components (evaporator, compressor, condenser and expansion valve) are modeled at a very detailed level, including parameters such as real gas properties, pressure drops, moisture removal on the evaporator, effect of the oil circulation on the capacity, check for liquid line flashing and check for an excessive compressor discharge temperature. Because the main purpose of his model was to analyze how the compressor capacity control can improve the heat pump performance, a relatively complex compressor sub-model considered many of the phenomena that influence the compression process. The computer model was compared with the Carrier unitary heat pump system and,

among other results, the reported heat pump COP accuracy was within 4 – 6%, depending on the operating temperatures. Hiller’s elaborate model, in addition to being a great starting tool for understanding the influence of different parameters on overall heat pump performance, also served as a starting point for many first principle models that came afterwards.

Probably the best known and most widely used air-to-air, steady-state heat pump model today is the DOE/ORNL heat pump model (Mark VI) [11]. Ellison, et al. [15, 16] started with the development of the first principles model just two years after Hiller’s heat pump model. They appreciated the structure of Hiller’s model and used many of his routines, but found that the model was in most cases troublesome to use due to the large number of parameters that were difficult to obtain from the manufacturer. Their objective was to maintain the structure of Hiller’s model, but to make it easier to use with the known manufacturer’s data. Since then, the model was enhanced by several researchers and is available for web usage. It offers a great level of detail and is continually improved. However, because the model is not open-source and is used online, it is impossible for one to make changes to the model or to combine it with other simulation models. The authors have mentioned that the possible future improvements will go in the direction of making it in “fully modular fashion so that the user can simulate different system configurations (alternative sources/sinks, desiccant systems, alternative refrigeration cycles, manufacturer-specific algorithms, etc.)” and also “having the model serve as an equipment module within a building simulation code.”

Domanski and Didion’s [12] air-to-air heat pump model includes the sub-models of the heat exchangers, compressor, capillarity tube, four-way valve, connecting tubes and accumulator. According to authors, “the basic assumption for the compressor simulation is that the highly dynamic compression process results in steady vapor flow condition through the compressor.” Further, the compressor is divided into five internal parts and the heat transfer and pressure drop are calculated for each part separately. Although the compressor sub-model is not as complex as Hiller’s, it still requires a relatively large number of input compressor data compared with the more simplified volumetric efficiency compressor sub-model used in most heat pump models found in the literature. The required compressor data are five heat transfer parameters at five different locations, four pressure drop parameters, compressor effective clearance, polytropic efficiency based on the manufacturer’s bench test and compressor motor RPM and electric efficiency versus load characteristics. For the heat exchangers, both single-phase-to-air and two-phase-to-air heat transfers are modeled using a tube-by-tube approach where the heat transfer coefficient correlations are applied to each tube separately. The heat exchanger sub-model also distinguishes between the single-phase and two-phase refrigerant

pressure drop. The expanding device sub-model is developed for the capillarity tube type, and it allows the refrigerant flow in the capillary tube to be liquid only, two-phase only or both liquid and two-phase state. Domanski and Didion have also modeled the accumulator that stores the refrigerant if the evaporation is incomplete. The heat pump model is validated using the laboratory test data for the wide range of operating conditions for both heating and cooling mode. The reported maximum errors are 2.2% for the capacity, 3.8% for power and 5.1% for COP.

Domasceno et al. [14] have compared Domanski and Didion's heat pump model, the model of Ellison et al. (Mark III version was developed at that time) and a third heat pump model developed by Nguyen and Goldschmidt [30, 31] and updated by Domasceno and Goldschmidt [13]. For all three models the compressor sub-model was developed for the reciprocating type compressor, but modeled in different ways. Domanski and Didion compressor sub-model required the largest number of design parameters. In the Mark III model the user could provide either specific compressor design parameters or use a compressor map-based sub-model. The Nguyen et al. model used only a map-based approach. The heat exchangers for all three models are calculated using ε -NTU method, but while Domanski and Didion calculated tube-by-tube heat transfer, the other two models separated the heat exchangers into two-phase and single-phase refrigerant regions. The comparison between the models was preformed for the 3-ton split heat pump system and for the range of operating conditions in heating and cooling mode. According to the results shown in Table 2-1 Domasceno et al. gave slight preference to Domanski and Didion and Mark III over the Nguyen et al. model. The Domanski and Didion model was the most accurate, but in the same time the most time-consuming model. The authors also reported that although both models gave satisfactory capacity and COP predictions, they failed to predict the refrigerant temperature and pressure distribution.

	Heating mode (8 °C)		Cooling (35 °C)	
	Capacity	COP	Capacity	COP
Domanski and Didion	+15.5	+7.1	+3.0	+7.5
Mark III	+6.5	-9.5	+10.5	+8.0
Nguyen et al.	+19.5	-2.5	+13.0	+8.0

Table 2-1: Summary of predicted capacity and COP discrepancies based on comparisons against actual test data [14]

The main objective for Jeter's et al. heat pump model [25] was to compare the performance and seasonal energy requirements of a variable-speed drive heat pump against a constant-speed drive heat pump for heating mode. Their results also show the sensitivity of COP to compressor frequency and ambient air temperature. The compressor sub-model assumes the polytropic compression in the variable-speed positive-displacement compressor using the volumetric efficiency approach, and values for the motor mechanical efficiency and compressor electrical efficiency. The authors also take into account heating of the refrigerant as it passes over the motor and the pressure drops at the inlet and outlet valves. The expansion device is modeled as a simple capillarity tube. The air-to-air heat exchangers are divided into smaller elements where each element receives the entire refrigerant flow, but only a fraction of the airflow. The ϵ -NTU method is then used for each element, assuming a cross-flow heat exchanger and constant UA_c and UA_e values through each element. The fans are modeled by applying the fan laws for airflow versus speed and power versus speed. Jeters et al. recognize the need for a more complex model that would describe how an external heat transfer coefficient changes for different airflows and also more detailed approach for the fan performance.

Braun et al. have presented the model for a centrifugal chiller with a variable-speed control [7], where the compressor sub-model is developed using the compressor impeller geometry, momentum balance on the impeller and energy balance. In addition to a single-stage compressor, a two-stage compressor with an economizer is modeled. The evaporator and condenser are assumed to be flooded shell-and-tube-type heat exchangers in which only evaporation or condensation can occur (no desuperheating or subcooling). Different from most heat pump models that are using the ϵ -NTU method, the logarithmic mean temperature difference method is applied. The model is compared against the performance data for a 19.3 MW variable-speed centrifugal chiller, and the reported results have shown good agreement for the power consumption, except at low values for which the model underestimated measurements.

Another interesting first principles model is the steady-state heat pump model recently developed by Hui Jin [26]. The model simulates air-to-water and water-to-water heat pump types with the purpose of enabling easier system performance analysis. The model is validated using the catalog data for three different heat pumps. In this work the author offers a comprehensive literature review for up-to-date heat pump models. Jin also recognizes the lack of models that are not only able to describe more general heat pump types using a first principles approach to avoid expensive and time-consuming measurements, but also the model

that requires only parameters that can be easily collected from manufacturer catalogs. Jin's model is based on a parameter estimation; it uses multi-variable optimization and manufacturer catalog data to find system parameters representing the electro-mechanical power losses, piston displacement, clearance factor, electro-mechanical efficiency, desuperheat that occurs before refrigerant enters the compressor, and evaporator and condenser UA values. After the parameters are estimated, the inputs for each operating point are the load and source's side water temperatures and mass flow rates, while the outputs are the cooling capacity and power consumption. The model assumes no pressure drop in the evaporator, condenser or heat pump pipes, no desuperheating effect in the evaporator or condenser and no subcooling effect in the condenser. The expanding device has not been modeled. Instead, the evaporator outlet state is assumed to be saturated vapor and the mass flow rate is calculated from the compressor sub-model. According to Jin, although this is a good representation for a thermostatic expansion valve, the model might not be accurate with other expansion devices.

Fu et al. have developed the steady-state screw chiller model, with and without an economizer [19]. The compressor is modeled using a simplified volumetric efficiency approach for the mass flow rate calculations while the compressor power is calculated as the work for polytropic compression divided by the product of given constant values for indicated, motor and mechanical efficiency. The heat exchangers are divided into regions – two for the evaporator (evaporating and desuperheating region) and one for the condenser (condensing region), and the logarithmic mean temperature difference method is then applied for each of the regions. The expansion valve is modeled using the assumption about the constant enthalpy across the valve. The model is validated using experimental data from seven screw liquid chiller specifications “obtained from the statistic mean values of a great deal of products”. It is reported that the predicted values were within $\pm 10\%$ of the experimental data.

Iu's heat pump model [23], intended to be a design tool for manufacturers, has a unique heat exchanger circuiting algorithm that allows modeling of heat exchanger with various circuit patterns. The compressor refrigerant mass flow rate and power are modeled using the bi-cubic characteristics from the ARI standard [3] and the compressor outlet state is calculated from the compressor heat balance. Because the compressor manufacturer specifies the polynomial coefficients for a specific range of operating conditions and for fixed suction desuperheat, it is not certain how reliable predicted values are for other conditions. The author used the corrections developed by Dabiri and Rice (1981) and Mullen et al. (1998) in the mass flow and power calculations for the conditions other than the rated. For the heat exchanger, a tube-by-tube segmentation is applied and each segment is treated as a single-flow cross-tube heat

exchanger for which the ϵ -NTU method is applied. The expansion device sub-model is developed for two configurations: a short tube orifice and a thermal expansion valve. The heat pump model takes into account pressure drops in the filter dryer and between the expansion valve and the evaporator caused by the distributor that has a function to distribute the refrigerant equally to each evaporator pipe. The model has been compared against experimental data on the component and system level. On the component level, the mass flow rate, power consumption and capacity have been evaluated, and reported errors are within $\pm 5\%$. On the system level, predicted COP was within $\pm 0.5\%$ compared to the experimental data.

Bertsch and Groll have done research on air-source heat pumps for heating and cooling for northern U.S. climates [6]. The challenge that those heat pump applications face is very low ambient temperature in winter. Low ambient temperatures cause low suction pressure and high pressure ratios, which then results in extremely high compressor discharge temperatures and power consumption. Bertsch and Groll were interested in which among the cascade cycle, two-stage cycle with intercooling and two-stage cycle with economizing will perform best for the air-source heat pump operating at low outdoor temperatures. Separate steady-state sub-models for each component were developed, which allowed them to simulate all three cycles using the same component sub-models. The compressor is modeled using the ANSI/ARI standard and the compressor heat loss is calculated with a fixed heat loss factor. The ϵ -NTU method is applied for the air-source evaporator and water-cooled condenser calculations, for which the heat transfer characteristics need to be known. Assumptions for the heat exchangers were a fixed amount of subcooling on the condenser and the usage of dry air (meaning no frost buildup on the evaporator). Bertsch and Groll recognize that the second assumption results in an over-prediction of the heating capacity and system efficiency; however, since they were interested in comparing three different systems, they believe that this over prediction is similar for all three systems and does not influence the comparison results significantly. In the models, the pressure drops and heat losses in refrigerant lines are neglected.

Armstrong has used a somewhat similar model to Jin's in the low-lift cooling technology performance analysis [1]. For the given cooling rate and zone and ambient temperatures, the model optimizes the heat pump cooling cycle by finding the minimal total power used. The optimization of the speed control using a detailed component-based model is the first of its kind to the best of our knowledge. The compressor sub-model is developed using a volumetric efficiency approach and assuming polytrophic compression. In the volumetric efficiency calculations, the pressure drop on the suction valve is taken into account as a function of effective valve free area, shaft speed and inlet density. The heat exchanger heat balances are

calculated applying the ϵ -NTU method, similarly to models mentioned before. The model also includes the possibility for economizer mode (free-cooling), if the discharge pressure is lower than the suction pressure. The model has already been implemented and used as a part of a larger building simulation model [2], which shows it is suitable and robust enough for implementation with other systems. However, similar to Jin's model, Armstrong does not include some important parts of the heat pump modeling such as the pressure drop inside the heat pump and variable heat transfer coefficients in the heat exchangers. He does not include either the desuperheating process in the evaporator, or the subcooling process in the condenser.

From the discussion above, it can be seen that although the steady-state heat pump model development has started a long time ago and many models can be found in literature, there is still a need for a the model that will accurately simulate and optimize not just commercially available heat pumps, but also heat pumps with much broader range of operating conditions than currently available. For a model that will be implemented as a part of a larger building simulation, it is essential to have balance between detailed, time-consuming models on one side and over simplified models on the other side. Hiller's and Iu's model are the examples of the complex and very accurate but also more time-consuming heat pump models. Additionally, those models require some input data that are usually hard to find in manufacturer catalogs and, hence, are probably more suitable as manufacturer's tools. A more simplified model that represents a very good starting point for an open-source, modular approach, first principles model that can be easily changed and implemented as a part of some other simulation model is Armstrong's model. Nevertheless, it requires the implementation of additional phenomena important for the heat pump performance (e.g. subcooling, desuperheating, pressure drop, and variable heat transfer coefficients) and analysis that would show the sensitivity of the overall energy consumption on those phenomena.

Chapter 3: Heat pump model

The heat pump cooling cycle is reviewed at the beginning of this chapter with the purpose of having a better understanding of the heat pump computer model. The main parts of any heat pump are an evaporator, a compressor, a condenser and an expansion valve. The purpose of the evaporator is to exchange heat between air (or water) that we want to cool on one side, and a refrigerant used as a working fluid on the other side. Transfer of heat from the air to the refrigerant at low pressure and at a temperature lower than the temperature of air causes evaporation of the refrigerant and a decrease in air temperature. The heat received by the refrigerant needs to be released to the environment; however, the environment is usually at a temperature higher than the refrigerant temperature at the end of evaporation (e.g. during a hot summer day). According to the Second Law of Thermodynamics, it is not possible to transfer heat from the medium of lower temperature to the medium of higher temperature. Hence, before heat can be rejected to the environment the refrigerant needs to be brought at a temperature higher than the temperature of the cooling fluid (ambient air or water in case we have a water cooled system). The process of raising the refrigerant temperature and pressure occurs in a compressor. After compression, the refrigerant enters a condenser and heat collected in both the evaporator and the compressor is transferred from the refrigerant to the cooling fluid. The last component in the cycle is an expansion valve whose purpose is to control the flow of refrigerant from a high condensing pressure to a low evaporating pressure. The heat pump cycle performance is usually evaluated using a Coefficient of Performance (COP). For the cooling process, the COP is defined as the ratio of the evaporator load (cooling rate) to the total power used during the process, where the total power is calculated as the sum of the power for compression, evaporator fan power and the condenser fan power.

The HPM presented in this thesis simulates the steady-state performance of the heat pump cycle explained above. Since the model will be implemented as part of the larger low-lift cooling technology simulation model, a balance between simplicity and accuracy is very important. The model needs to be simple enough to provide results in the shortest possible time, but it also needs to include all of the relevant processes in the heat pump. The great advantage of computer simulations is that they allow one to analyze different possibilities in a relatively short time. For example, one might be interested in how different processes in the heat pump influence overall performance, e.g. what is the difference in the performance between the

process with zero subcooling and the process with few degrees subcooling in the condenser. Because answers are not always obvious, the model is developed to facilitate an analysis about the influence of different processes in the heat pump using different options. The options are desuperheating in the evaporator, subcooling in the condenser, variable or constant heat transfer coefficients and pressure drops. This way, HPM can range from the simplest model with constant heat transfer coefficients, no pressure drop and no desuperheating in the evaporator or subcooling in the condenser, to the more realistic model where all the options are included. Also, every combination in between is possible; however, one should be aware that there is always a tradeoff between model accuracy and computational time.

Another, perhaps greater, advantage is the possibility of exploring the heat pump performance under operating conditions that are not typical of current practice. This allows detailed analysis of the low-lift cooling technology, or some other new technology for which commercially available performance data and analysis cannot be found.

The HPM is written in MATLAB™, and the software Refprop™ [32] is used for calculations of working fluid (R410a) properties. The model consists of four loops with the first three loops being the component sub-models. The evaporator, the compressor and the condenser component are modeled separately using energy balance equations and also some empirical and semi-empirical correlations. The expansion valve is modeled as an idealized device, i.e. it is assumed to exactly maintain a desired desuperheating at the end of evaporator. Thus, a second important assumption is an ideal adiabatic process in the expansion valve, which implies that the enthalpy at the evaporator inlet is equal to the enthalpy at the condenser outlet. This assumption is valid when the thermal expansion valve is close to the evaporator inlet, which is not true for most mini-split systems but is true for the low-lift applications of interest. The fourth loop in the model is the main solver loop, explained more thoroughly later in the chapter.

The variable heat transfer coefficients and the pressure drops in the components and in the connecting suction and discharge pipes have been modeled using correlations explained at the end of the chapter. The liquid line pressure drop has not been modeled since it is much smaller than the vapor line pressure drops and is part of the idealized expansion valve model.

The schematic of the heat pump cooling cycle is shown in Figure 3-1, and the cycle in T-s diagram can be seen in Figure 3-2. The points marked on the figures correspond to the subscripts used in model equations and also later in the code, e.g. the subscript e_1 corresponds to evaporator inlet conditions and c_3 corresponds to conditions in the condenser where condensation finishes (before subcooling).

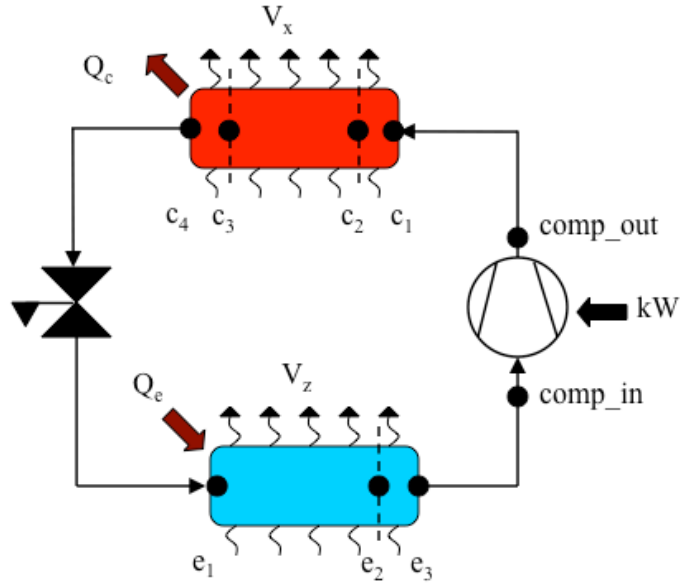


Figure 3-1: Schematic of the heat pump cooling cycle

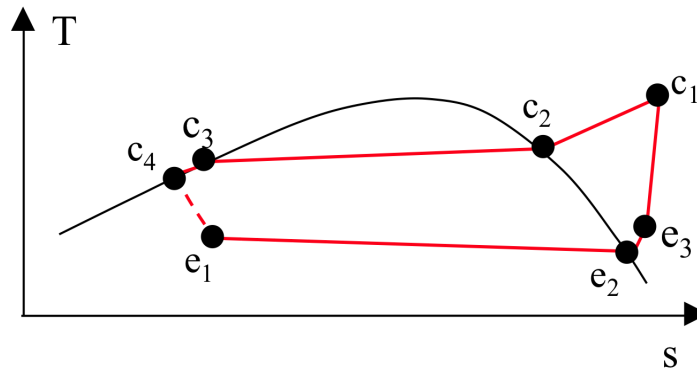


Figure 3-2: T-s diagram of the heat pump cooling cycle

3.1. Evaporator sub-model

The evaporator sub-model is developed for a finned tube heat exchanger used to cool the air in a room. Modeling of different types of heat exchangers (e.g. cooling of water) is also possible if the evaporator geometry and the heat transfer coefficient correlations are modified. The evaporator is divided into two regions: the evaporating region and desuperheating region. If the given desuperheating temperature difference ΔT_{esh} is zero, the whole evaporator is calculated as the evaporating region. Condensation of water on the evaporator external surfaces

does not occur in the machine used to provide validation data, nor has it been taken into account in this stage of model development.

The steady-state evaporator behavior is modeled using the NTU method [5] and the following energy balance equations:

a) Evaporating region:

$$Q_{ep} = m_{ref} * (h_{e2} - h_{liq}) \quad (1)$$

$$Q_{ep} = \epsilon_{ep} * C_{ep} * (T_z - T_{e1}) \quad (2)$$

where

$$C_{ep} = y_{ep} * V_z * \rho_{air} * c_{p,air} \quad (3)$$

$$\epsilon_{ep} = 1 - \exp\left[-(UA_{ep}) / C_{ep}\right] \quad (4)$$

b) Desuperheating region:

$$Q_{esh} = m_{ref} * (h_{e3} - h_{e2}) \quad (5)$$

$$Q_{esh} = \epsilon_{esh} * C_{esh_min} * (T_z - T_{e2}) \quad (6)$$

where

$$C_{esh_min} = \text{the smaller of } y_{esh} * V_z * \rho_{air} * c_{p,air} \text{ and } y_{esh} * V_z * \rho_{air} * \frac{h_{e3} - h_{e2}}{T_{e3} - T_{e2}} \quad (7)$$

$$C_{esh_max} = \text{the larger of } y_{esh} * V_z * \rho_{air} * c_{p,air} \text{ and } y_{esh} * V_z * \rho_{air} * \frac{h_{e3} - h_{e2}}{T_{e3} - T_{e2}} \quad (8)$$

The heat exchanger thermal effectiveness, which represents the ratio between the actual and the ideal (for a heat exchanger with an infinite area) heat transfer rate is calculated for the desuperheating region using the correlation for a cross-flow heat exchanger with both hot and cold stream unmixed [28]:

$$\epsilon_{esh} = 1 - \exp\left\{\frac{1}{\frac{C_{esh_min}}{C_{esh_max}} * NTU_{esh}^{-0.22}} * \left\{\exp\left[(-NTU_{esh}) * \frac{C_{esh_min}}{C_{esh_max}} * NTU_{esh}^{-0.22}\right]\right\}\right\} \quad (9)$$

$$NTU_{esh} = \frac{UA_{esh}}{C_{esh_min}} \quad (10)$$

Correlations used to calculate the product of the overall heat transfer coefficient and heat exchanger area for the evaporating region UA_{ep} and the desuperheating region UA_{esh} are discussed in part 4.5.

c) Total heat removed by the evaporator:

$$Q_e = Q_{ep} + Q_{esh} \quad (11)$$

The evaporator sub-model input parameters are:

- cooling rate – Q_e
- evaporator airflow rate – V_z
- enthalpy at the evaporator inlet – h_{liq}
- desuperheating temperature difference at the evaporator outlet – ΔT_{esh}
- zone (room) air temperature – T_z
- evaporator geometry (tube diameters, areas, fin thickness, etc.)

The main output variables from the evaporator sub-model are:

- refrigerant mass flow rate – m_{ref}
- temperatures in the evaporator – T_{e1}, T_{e2}, T_{e3}
- compressor inlet pressure – P_{comp_in}
- fan power – J_e

All input parameters, except the enthalpy at the evaporator inlet h_{liq} , are given as the inputs to the main solver loop and remain constant during the iteration process for the particular heat pump operating point. The enthalpy at the evaporator inlet changes depending on the state at the condenser outlet and is iterated in the main solver loop. The main solver loop is explained in part 3.4.

Because the main purpose of the model is to analyze the heat pump performance and power usage for different operating conditions, it is important to model power versus speed and speed versus airflow dependence for both the evaporator and the condenser fan. The fan power-speed dependence is for simple analysis usually described using a cubic function whereas for

speed-airflow dependence linear function is used. In order to determine the coefficients of the linear function, data for at least two experimental points are needed; for the cubic function three points are the required minimum. During the measurements, the condenser airflow, fan speed and power were varied; the evaporator side fan speed, however remained relatively constant and the evaporator airflow rate and power have been measured only for one operating point. For the condenser fan the functionalities have been determined from experimental data. Because one point was not enough to describe the evaporator fan performance, condenser functionalities have been scaled to match the values for the measured evaporator point.

Five fan speeds and corresponding airflow rates have been measured for the condenser fan and values in between have been calculated using a linear interpolation (Figure 3-3). For the evaporator, the same speed-airflow dependence is assumed.

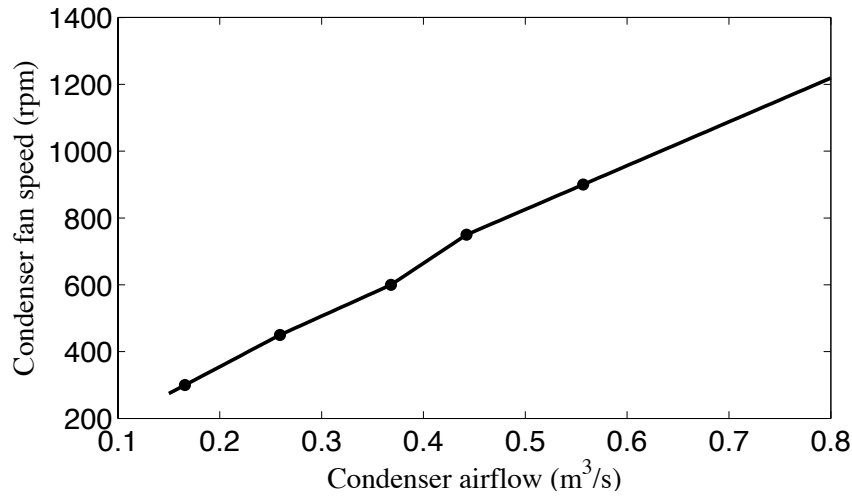


Figure 3-3: Condenser fan speed vs. airflow dependence

Power – speed dependence is described using cubic functions:

$$J_e = C_3 * w_e^3 + C_2 * w_e^2 + C_1 * w_e + C_{e0} \quad (12)$$

$$J_e = C_3 * w_e^3 + C_2 * w_e^2 + C_1 * w_e + C_{e0} \quad (13)$$

Constants C_{e0} , C_1 , C_2 and C_3 have been calculated for the condenser fan using MATLAB™ curve fit function on the condenser fan experimental data. For the evaporator fan C_{e0} has been replaced with a new constant C_{e0} calculated to match the measured point, and the other coefficients remained the same. Condenser fan power versus airflow dependence can be seen in Figure 3-4 and in the same figure values for the only measured point on the evaporator are shown with +. Figure 3-4 shows matched evaporator fan power versus airflow dependence.

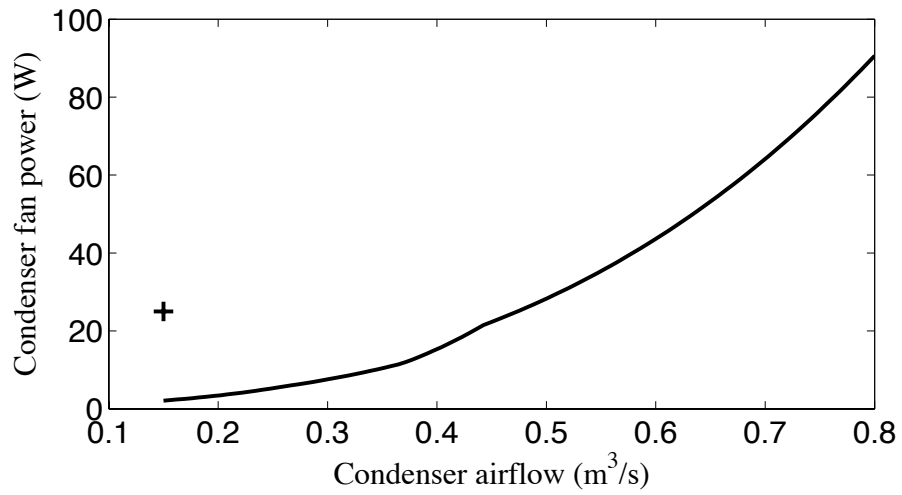


Figure 3-4: Condenser fan power vs. airflow

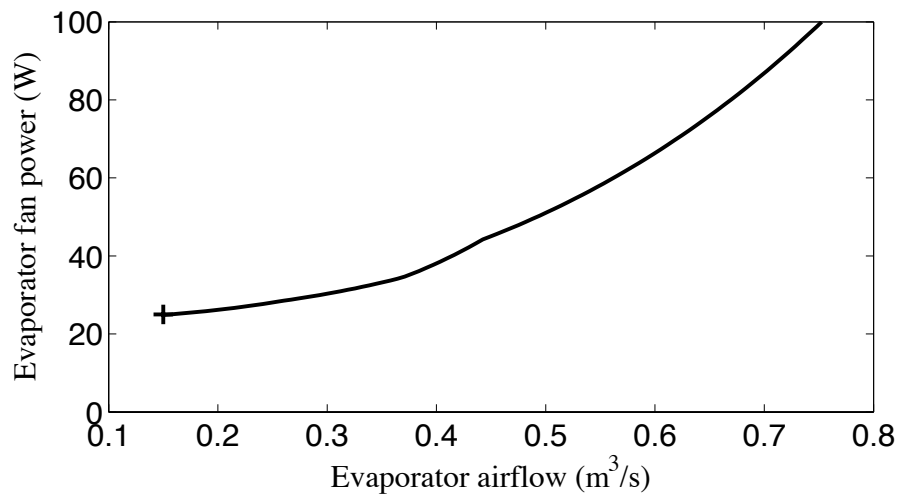
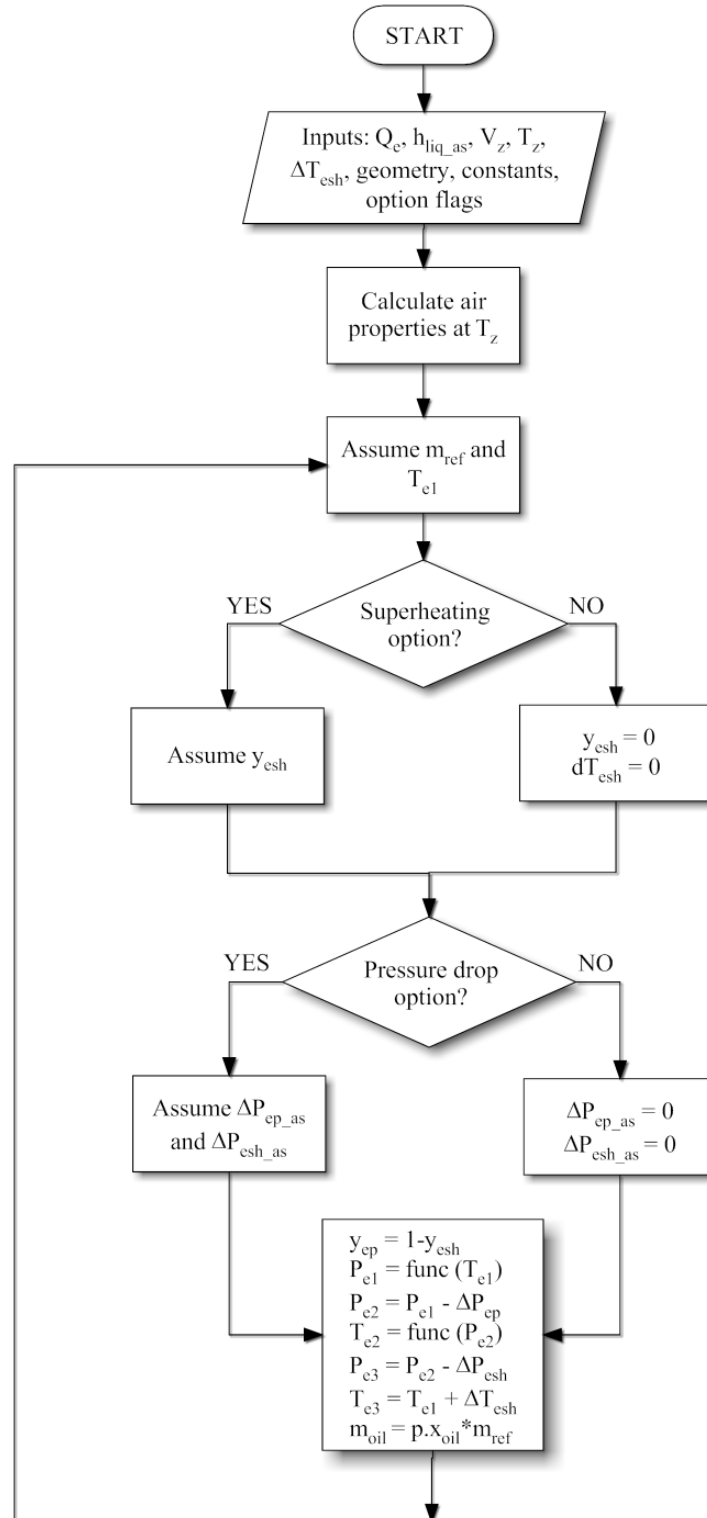


Figure 3-5: Approximated evaporator fan power vs. airflow dependence

The flow chart for the evaporator sub-model is shown in Figure 3-6:



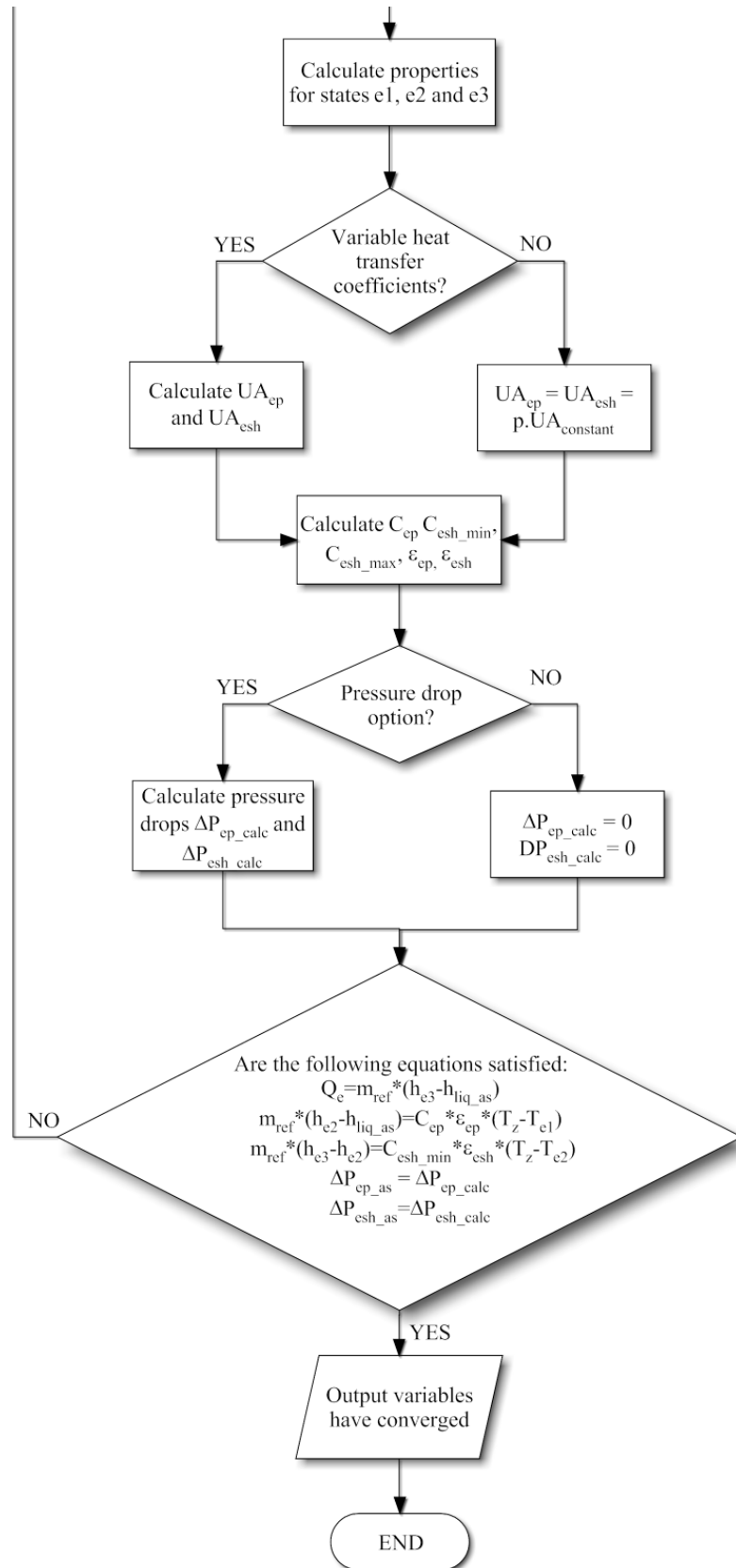


Figure 3-6: Evaporator sub-model flow chart

3.2. Compressor sub-model

The compressor is a component that can have a large impact on the system energy efficiency since the majority of the cooling cycle input power is used for compression. There are many processes and parameters that affect the compression process and one may therefore expect the form of the model to depend on the compressor type. Although numerous compressor sub-models can be found in the literature, they usually represent one of the two extremes between detailed, complicated models on one side, and very simple, limited models on the other side. Models that analyze the majority of important parameters and describe the compression process for the particular type of compressor rather accurately require great level of detailed parameters, usually hard to define. Also, they increase the simulation time tremendously. On the other side, there are relatively simple models, most often developed as semi-empirical models for constant-speed compressors. The disadvantage is that they require experimental data in order to calculate particular model constants and the calculated constants are valid just for a particular speed. Moreover, they do not take into account some phenomena important in different types of compressors, which can have large impact on result accuracy. The HPM was envisioned as a sufficiently accurate, as well as fast analysis tool for the variable-speed drive compressor. However, since the objective of this thesis was not to develop a new compressor sub-model, it was necessary to implement one of the existing simple models.

The objective for the compressor sub-model is to calculate the shaft speed, input power and outlet temperature for the given refrigerant mass flow rate, inlet temperature, inlet pressure and outlet pressure. The compression process is usually described using the polytropic model for which:

$$P_{\text{comp_in}} * (v_{\text{compr_in}})^n = P_{\text{comp_out}} * (v_{\text{compr_out}})^n \quad (14)$$

The polytropic exponent n depends on the compression process and refrigerant properties, and for some specific processes it can be calculated as:

- the ideal gas undergoing isothermal compression:

$$n = n_t = 1 \quad (15)$$

- the ideal gas undergoing isentropic compression:

$$n = k = \frac{c_p}{c_v} \quad (16)$$

- real gas undergoing isentropic compression:

$$n = n_s = \frac{\ln \frac{P_{\text{comp_out}}}{P_{\text{comp_in}}}}{\ln \frac{\rho \{P_{\text{comp_out}}, s_{\text{comp_in}}\}}{\rho_{\text{comp_in}}}} \quad (17)$$

Because the real compression process is more complex than these special processes, exponent n is usually calculated using measured data. The polytropic exponent affects both the volumetric efficiency (mass flow model) and the isentropic efficiency (power model).

Two very important phenomena occur during compression and influence the compressor performance: the pressure drop at the suction and discharge valve, and the re-expansion of the mixture in the clearance volume. For reciprocating compressors, both of these processes are usually modeled using the relatively simple volumetric efficiency model. The volumetric efficiency η_v represents the ratio of the actual refrigerant flow rate delivered in a compression cycle to the refrigerant flow rate that could fill the swept volume of the cylinder.

The relation between the refrigerant mass flow rate and the compressor shaft speed is for the volumetric efficiency model:

$$m_{\text{ref}} = D * f * \rho_{\text{comp_in}} * \eta_v \quad (18)$$

In order to find the model that will give good agreement with experimental data, four existing volumetric efficiency models have been compared. Although two [24, 27] out of four models have been developed for constant speed compressors and would require different set of constants for each speed, only one set of constants is calculated for each model. The constants are calculated using 82 measured points subjected to nonlinear regression. The best fit for the constants is assumed to be the one that minimizes the square root of the arithmetic mean of the squared residuals (RMS):

$$\text{RMS} = \sqrt{\frac{\sum \left(\frac{f_m - f_{\text{calc}}}{f_m} \right)^2}{N_m}} \quad (19)$$

a) The first model is developed by Jähnig, Reindl and Klein for the reciprocating compressor type [24]. The minimum of four data point is required for the constant calculations; however, the model is developed for the constant-speed compressor. That means

that the one set of constants determined using different shaft speeds experimental data might not give good agreements over the whole range of operating conditions.

$$m_{ref} = C_1 * f * \rho_{comp_in} * \eta_v \quad (20)$$

where

$$\eta_v = 1 - C_2 * \left[\left(\frac{P_{comp_out}}{P_{suction}} \right)^{1/k} - 1 \right] \quad (21)$$

$$P_{suction} = P_{comp_in} * (1 - C_3) \quad (22)$$

The model takes into account the pressure drop on the suction valve, but not the pressure drop on the discharge valve since the authors found the latter has a little effect on the mass flow rate calculations for the experimental data they were using. The exponent for an ideal gas k can be calculated from Equation (16).

b) The second comparison model has been developed by Kim and Bullard for reciprocating and rotary compressors [27]:

$$m_{ref} = C_1 * f * \rho_{comp_in} * \eta_v \quad (23)$$

$$\eta_v = 1 - C_2 * \left[\frac{\rho \{ P_{comp_out}, s_{comp_in} \}}{\rho_{comp_in}} - 1 \right] \quad (24)$$

c) An interesting addition in the model suggested by Armstrong [4] is the term that accounts for back leakage losses:

$$m_{ref} = \left[C_1 * f * \eta_v - C_3 * (P_{comp_out} - P_{comp_in}) \right] * \rho_{comp_in} \quad (25)$$

$$\eta_v = 1 - C_2 * \left[\left(\frac{P_{comp_out}}{P_{comp_in}} \right)^{1/n_s} - 1 \right] \quad (26)$$

where the isentropic exponent for a real gas n_s is calculated using Equation (17).

d) The last model, developed by Willingham [36], has an important advantage that it has been developed for a variable-speed compressor for which the pressure drop on the suction and discharge valve varies with the compressor speed:

$$m_{ref} = C_1 * f * \rho_{comp_in} * \eta_v \quad (27)$$

where

$$\eta_v = 1 - C_2 * \left[\left(\frac{P_{discharge}}{P_{suction}} \right)^{1/n} - 1 \right] \quad (28)$$

$$P_{suction} = P_{comp_in} - C_3 * \rho_{comp_in} * f^2 \quad (29)$$

$$P_{discharge} = P_{comp_out} - C_4 * \rho_{comp_out} * f^2 \quad (30)$$

$$n = n_s = \frac{\ln \frac{P_{discharge}}{P_{suction}}}{\ln \frac{\rho_{discharge}}{\rho_{suction}}} \quad (31)$$

The comparison results for all four models are shown in the table:

	Model 1	Model 2	Model 3	Model 4
C_1	$9.00*10^{-6}$	$9.07*10^{-6}$	$10.63*10^{-6}$	$9.67*10^{-6}$
C_2	$6.11*10^{-2}$	$4.85*10^{-2}$	$5.73*10^{-2}$	$2.89*10^{-2}$
C_3	0	-	$3.40*10^{-5}$	0
C_4	-	-	-	$2.68*10^{-2}$
RMS	6.77 %	6.55 %	2.70 %	4.90 %

Table 3-1: Coefficients and RMS errors for four different models

It is important to recognize physical meaning of the constants in the volumetric efficiency model. In all the models, the constant C_1 represents a piston displacement volume (thus C_1*f is ideal displacement rate) and the constant C_2 represents the clearance factor, which is the ratio of the clearance volume to the piston displacement volume. In model 3, C_3 represents an effective free-area (divided by viscosity) for back-leakage and in model 4, C_4 represents a discharge valve flow resistance.

It can be seen that the third model developed by Armstrong shows the best agreement with the measured data. In addition to that, Equation (17) is used in Armstrong's model to calculate isentropic exponent, meaning that one does not need to know the compressor outlet temperature in order to calculate the mass flow rate. This is useful for the HPM since the outlet temperature will be calculated later in the compressor sub-model from the energy balance

equation. As a result of everything mentioned above, the third model has been chosen for the compressor mass flow rate model.

The power model used for the compressor sub-model was developed by Jähnig, Reindl and Klein [24]. It calculates electrical power supplied to the motor (KW) introducing the combined efficiency parameter, η_{comb} . The combined efficiency represents the ratio of the estimated work required for a polytrophic compression process to the total power supplied to the motor. It includes the electric motor efficiency and all other inefficiencies that occur inside the compressor, such as frictional effects:

$$KW * \eta_{comb} = m_{ref} * \frac{k}{k-1} * \frac{P_{comp_in}}{\rho_{comp_in}} * \left[\left(\frac{P_{comp_out}}{P_{suction}} \right)^{\frac{k-1}{k}} - 1 \right] \quad (32)$$

where

$$P_{suction} = P_{comp_in} * (1 - C_3) \quad (33)$$

$$\eta_{comb} = C_5 + C_6 * \exp(C_7 * P_{comp_in}) \quad (34)$$

In Equation (33) the constant C_3 found in the mass flow rate model has been used. The constant C_3 being equal to zero (Table 3-1) implies that the suction pressure is equal to the pressure at the compressor inlet for the compressor power calculation. This is consistent with the model used for the mass flow rate calculation, although the models are not developed by the same author. The change has been made to the power model presented by Jähnig at el.: P_{comp_in} in the correlation for combined efficiency has been replaced by the pressure ratio P_{comp_out}/P_{comp_in} . After making that replacement, the RMS value decreased from 14.5% to 5%.

C_5	0.865
C_6	0.009
C_7	0.619
RMS	5.03 %

Table 3-2: Coefficients and RMS error for power model

The temperature at the compressor outlet is determined from the energy balance equation, neglecting the losses from the compressor to environment. These losses are small for the well-insulated compressor used in the test rig. A jacket loss correction can easily be applied for

uninsulated compressors by estimating the portions of the jacket exposed internally to suction and discharge conditions.

The compressor energy input is used for the refrigerant enthalpy rise, and for heating of the circulating compressor oil:

$$KW = Q_{\text{comp}} + Q_{\text{oil}} \quad (35)$$

where

$$Q_{\text{comp}} = m_{\text{ref}} * (h_{\text{comp_out}} - h_{\text{comp_in}}) \quad (36)$$

$$Q_{\text{oil}} = m_{\text{oil}} * c_{\text{oil}} (T_{\text{comp_out}} - T_{\text{comp_in}}) \quad (37)$$

The oil mass flow rate has been taken as 4% of the refrigerant mass flow rate and that fraction remains constant for all calculations where oil is included.

The input parameters for the compressor sub-model are:

- refrigerant mass flow rate – m_{ref} ,
- temperature at the compressor inlet – $T_{\text{comp_in}}$ ($= T_{e3}$)
- pressure at the compressor inlet – $P_{\text{comp_in}}$
- pressure at the compressor outlet – $P_{\text{comp_out}}$

The outputs from the compressor sub-model are:

- compressor shaft speed – f
- compressor input power – KW
- temperature at the compressor outlet – $T_{\text{comp_out}}$

While the first three input variables are calculated from the evaporator sub-model, the pressure at the compressor outlet is iterated in the main solver loop, as described in section 4.4.

The flow chart for the compressor sub-model is shown in Figure 3-7:

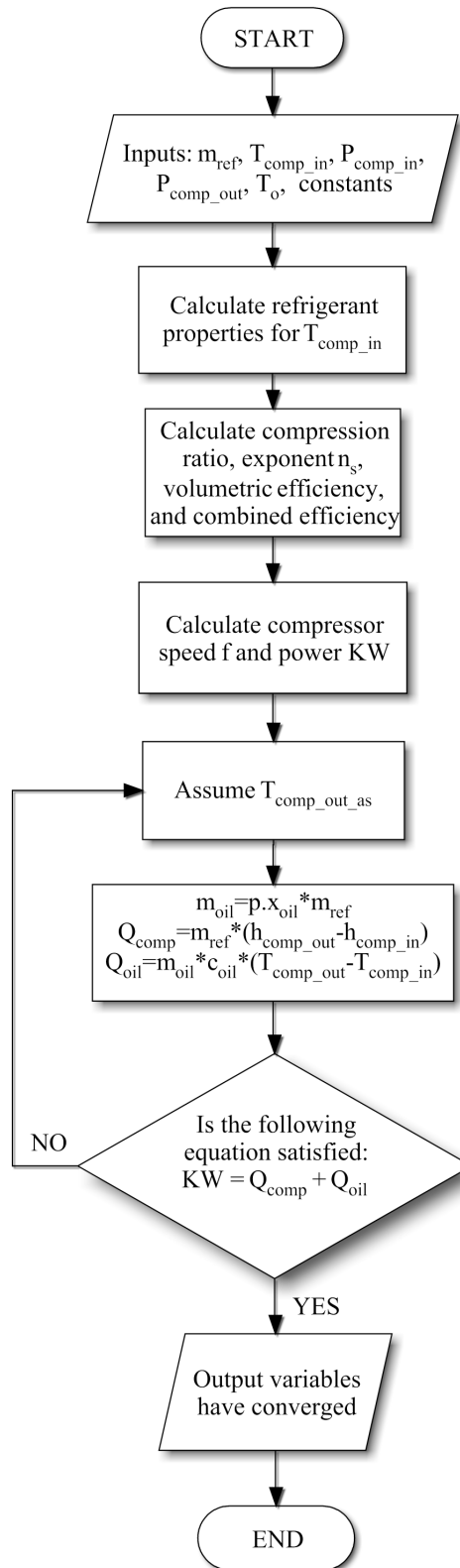


Figure 3-7: Compressor sub-model flow chart

3.3. Condenser sub-model

The condenser sub-model is developed for a finned tube heat exchanger cooled with air, as is the evaporator sub-model. The only difference for the condenser is that it is divided into three regions: the desuperheating, condensing and subcooling region. If the given subcooling temperature difference ΔT_{sc} is zero, the condenser is divided into two regions: the desuperheating and condensing region.

The steady-state condenser behavior is modeled using NTU method [5] and the following energy balance equations:

a) Desuperheating region:

$$Q_{csh} = m_{ref} * (h_{c1} - h_{c2}) \quad (38)$$

$$Q_{csh} = \epsilon_{csh} * C_{csh_min} * (T_{c1} - T_o) \quad (39)$$

where

$$C_{csh_min} = \text{the smaller of } y_{csh} * V_o * \rho_{air} * c_{p,air} \text{ and } y_{csh} * V_o * \rho_{air} * \frac{h_{c1} - h_{c2}}{T_{c1} - T_{c2}} \quad (40)$$

$$C_{csh_max} = \text{the larger of } y_{csh} * V_o * \rho_{air} * c_{p,air} \text{ and } y_{csh} * V_o * \rho_{air} * \frac{h_{c1} - h_{c2}}{T_{c1} - T_{c2}} \quad (41)$$

The thermal effectiveness ϵ_{csh} for the desuperheating region is calculated using the correlation for a cross-flow heat exchanger with both streams unmixed [28]:

$$\epsilon_{csh} = 1 - \exp \left\{ \frac{1}{\frac{C_{csh_min}}{C_{csh_max}} * NTU_{csh}^{-0.22}} * \left\{ \exp \left[(-NTU_{csh}) * \frac{C_{csh_min}}{C_{csh_max}} * NTU_{csh}^{-0.22} \right] \right\} \right\} \quad (42)$$

$$NTU_{csh} = \frac{UA_{csh}}{C_{csh_min}} \quad (43)$$

b) Condensing region:

$$Q_{cp} = m_{ref} * (h_{c2} - h_{c3}) \quad (44)$$

$$Q_{cp} = \epsilon_{cp} * C_{cp} * (T_{c2} - T_o) \quad (45)$$

where

$$C_{cp} = y_{cp} * V_o * \rho_{air} * c_{p,air} \quad (46)$$

$$\epsilon_{cp} = 1 - \exp \left[\left(-UA_{cp} \right) / C_{cp} \right] \quad (47)$$

c) Subcooling region:

$$Q_{sc} = m_{ref} * (h_{c3} - h_{c4}) \quad (48)$$

$$Q_{sc} = C_{sc_min} * (T_{c3} - T_o) \quad (49)$$

where

$$C_{sc_min} = \text{the smaller of } y_{sc} * V_o * \rho_{air} * c_{p,air} \text{ and } y_{sc} * V_o * \rho_{air} * \frac{h_{c3} - h_{c4}}{T_{c3} - T_{c4}} \quad (50)$$

$$C_{sc_max} = \text{the larger of } y_{sc} * V_o * \rho_{air} * c_{p,air} \text{ and } y_{sc} * V_o * \rho_{air} * \frac{h_{c3} - h_{c4}}{T_{c3} - T_{c4}} \quad (51)$$

The heat exchanger thermal effectiveness ϵ_{sc} for the subcooling region is calculated using the same correlation as for the desuperheating region:

$$\epsilon_{sc} = 1 - \exp \left\{ \frac{1}{\frac{C_{sc_min}}{C_{sc_max}} * NTU_{sc}^{-0.22}} * \left\{ \exp \left[\left(-NTU_{sc} \right) * \frac{C_{sc_min}}{C_{sc_max}} * NTU_{sc}^{-0.22} \right] \right\} \right\} \quad (52)$$

$$NTU_{sc} = \frac{UA_{sc}}{C_{sc_min}} \quad (53)$$

The correlations used to calculate the product of the overall heat transfer coefficient and heat exchanger area for the desuperheating region UA_{csh} , the condensing region UA_{cp} and the subcooling region UA_{sc} of the condenser are discussed in part 4.5.

d) Total heat removed at the condenser:

$$Q_c = Q_{csh} + Q_{cp} + Q_{sc} \quad (54)$$

The condenser sub-model input parameters are:

- refrigerant mass flow rate – m_{ref}
- temperature at the condenser inlet – T_{c1} ($= T_{comp_out}$)
- subcooling temperature difference at the condenser outlet – ΔT_{sc}
- condenser airflow rate – V_o
- ambient air temperature – T_o
- condenser geometry (tube diameters, areas, fin thickness...)

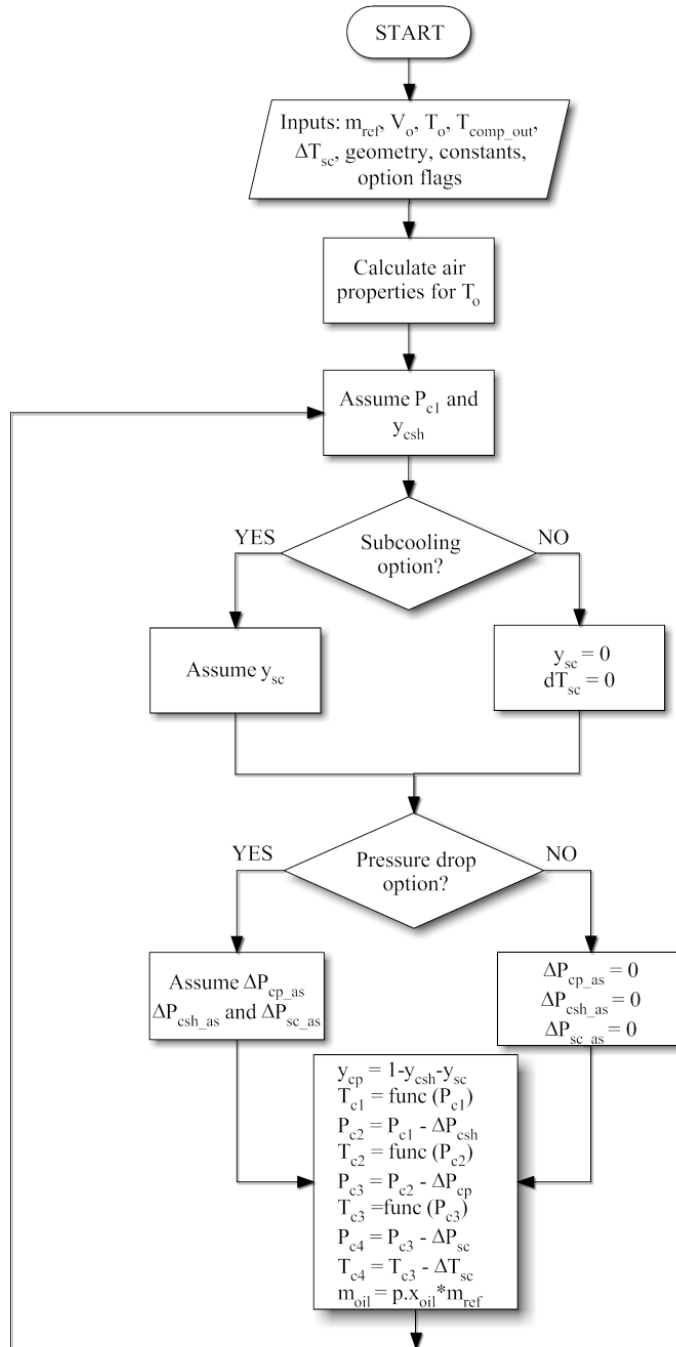
The main output variables from the condenser sub-model are:

- total heat exchanged on the condenser – Q_c
- temperatures in the condenser – $T_{c1}, T_{c2}, T_{c3}, T_{c4}$
- pressure at the condenser inlet – P_{c1}
- fan power – J_c

The refrigerant mass flow rate and the temperature at the condenser inlet are parameters calculated in the evaporator and compressor sub-model. All other input parameters are given as the inputs to the main solver loop and remain constant during the iteration process for a particular heat pump operating point.

The condenser fan power is calculated from the speed-airflow and speed-power relations explained in part 3.1

The flow chart for the condenser sub-model is shown in Figure 3-8:



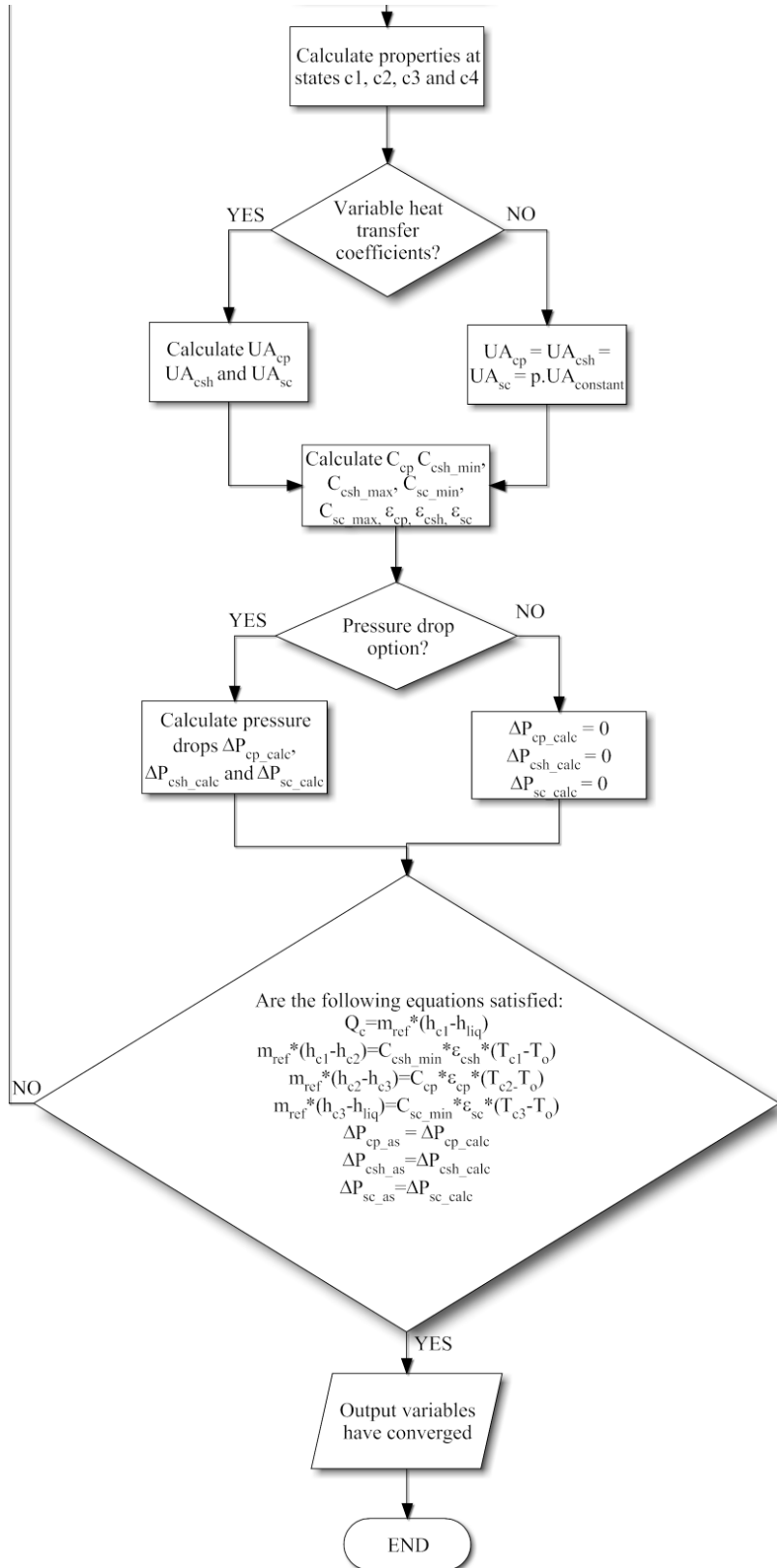


Figure 3-8: Condenser sub-model flow chart

3.4. Whole system model

The main model consists of three separate sub-models that define the evaporator, compressor and condenser steady-state behavior. The system model first calls the evaporator sub-model, then the compressor sub-model, and at the end the condenser sub-model. Between the evaporator and compressor sub-model the suction line pressure drop has been calculated and between the compressor and condenser sub-model the discharge line pressure drop has been calculated. The process in the suction and discharge line are assumed to be isothermal, meaning that the temperature at the evaporator outlet is equal to the temperature at compressor inlet and the temperature at compressor outlet is equal to the temperature at condenser inlet:

$$T_{e3} = T_{comp_in} \quad (55)$$

$$T_{comp_out} = T_{c1} \quad (56)$$

An idealized expansion valve has been modeled, which accurately models the real steady-state throttling process in cases where the valve is positioned at the evaporator inlet. It is assumed that the expansion valve delivers the exact refrigerant mass flow rate for the given desuperheating at the evaporator outlet to be achieved and that the enthalpy at the compressor outlet is equal to the enthalpy at the evaporator inlet:

$$h_{e1} = h_{c4} = h_{liq} \quad (57)$$

The input parameters for the main model loop are:

- cooling rate – Q_e
- evaporator airflow rate – V_z
- condenser airflow rate – V_o
- zone (room) air temperature – T_z
- ambient air temperature – T_o
- desuperheating temperature difference at the evaporator outlet – ΔT_{esh}
- subcooling temperature difference at the condenser outlet – ΔT_{sc}
- geometry (tube diameters, areas, fin thickness...)
- option flags (evaporator desuperheating on/off, subcooling on/off, pressure drop on/off, variable heat transfer coefficient on/off)
- constants (compressor constants, oil fraction, fin and tube thermal conductance parameters...)

Outputs of the main model are:

- temperatures in the condenser – $T_{c1}, T_{c2}, T_{c3}, T_{c4}$
- temperatures in the evaporator – T_{e1}, T_{e2}, T_{e3}
- compressor shaft speed – f
- compressor inlet and outlet pressures – $P_{comp_in}, P_{comp_out}$
- evaporator and condenser fan speeds – w_e, w_c
- COP

Two variables are assumed at the beginning and iterated during the simulation. The first variable is the enthalpy of the refrigerant at the condenser outlet h_{liq_as} . This value is used in the evaporator sub-model, since we are making an assumption that the enthalpy at the condenser outlet is equal to the enthalpy at the evaporator inlet. The second assumed variable is the pressure at the compressor outlet $P_{comp_out_as}$, which is the input in the compressor sub-model for the compressor shaft speed and power calculation. Two conditions used for the iteration of these two variables are:

1. The enthalpy assumed at the evaporator inlet needs to be equal to the calculated enthalpy of the liquid at the condenser outlet calculated from the condenser sub-model.

$$h_{liq_as} = h_{liq} \quad (58)$$

2. The pressure assumed at the compressor outlet needs to be equal to the calculated pressure at the condenser inlet decreased for the pressure drop in the discharge line.

$$P_{comp_out_as} = P_{c1} - \Delta P_d \quad (59)$$

The main model structure can be seen in Figure 3-9:

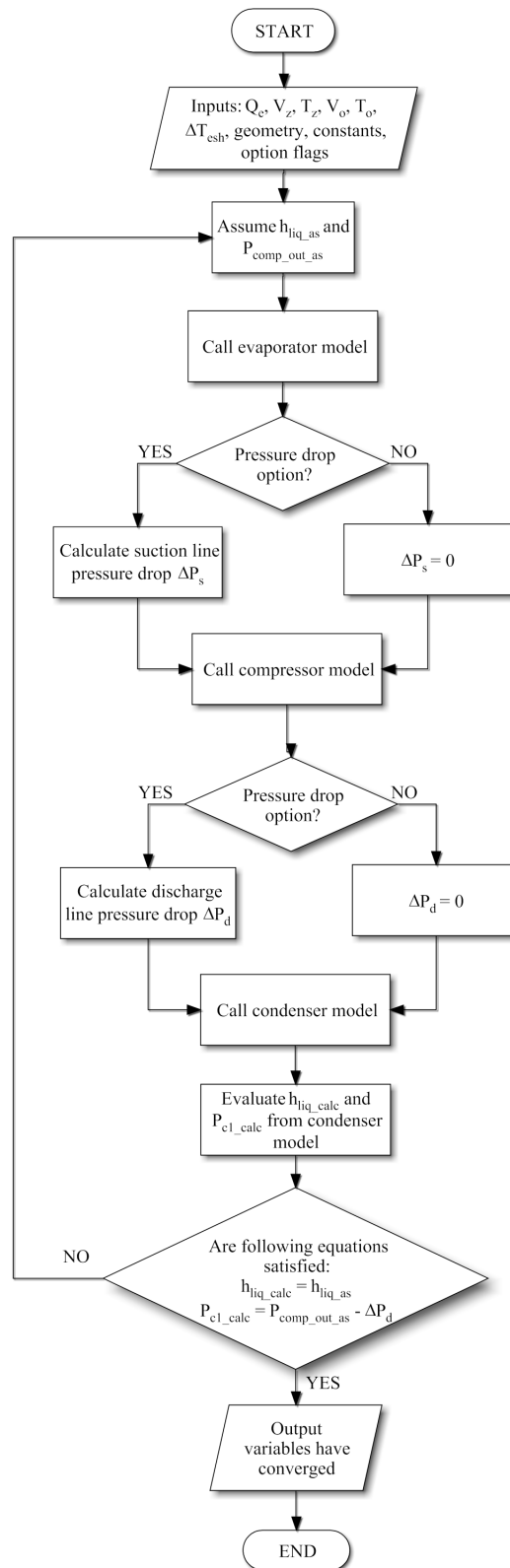


Figure 3-9: Whole system solver flow diagram

The schematic of the whole system solver is given in Figure 3-10. For simplification purposes, pressure drops are not included in this schematic. After the condenser outlet enthalpy and compressor outlet pressure are assumed, the evaporator sub-model is called. For the given cooling load, zone temperature, desuperheating, evaporator airflow and assumed evaporator inlet enthalpy, the evaporator sub-model calculates the refrigerant mass flow rate, temperatures and pressure required to satisfy the evaporator energy balance equations. After the evaporator sub-model calculation, the compressor inlet state and refrigerant mass flow rate are known variables, which are then used in the compressor sub-model. Since the compressor outlet pressure is also required to calculate the compressor shaft speed, power and outlet temperature, that pressure is assumed and then iterated through the process. At the end, the condenser sub-model is called with the refrigerant mass flow rate (from the evaporator sub-model), condenser inlet temperature (from the compressor sub-model), condenser airflow rate, outside temperature and subcooling as the inputs. The condenser temperatures, pressures and exchanged heat are calculated from the condenser energy balance equations. The calculated condenser pressure and outlet enthalpy are used to check whether the assumed values are equal to the calculated values; if not, the whole calculation procedure starts from the beginning with an improved estimate of the pressure and enthalpy.

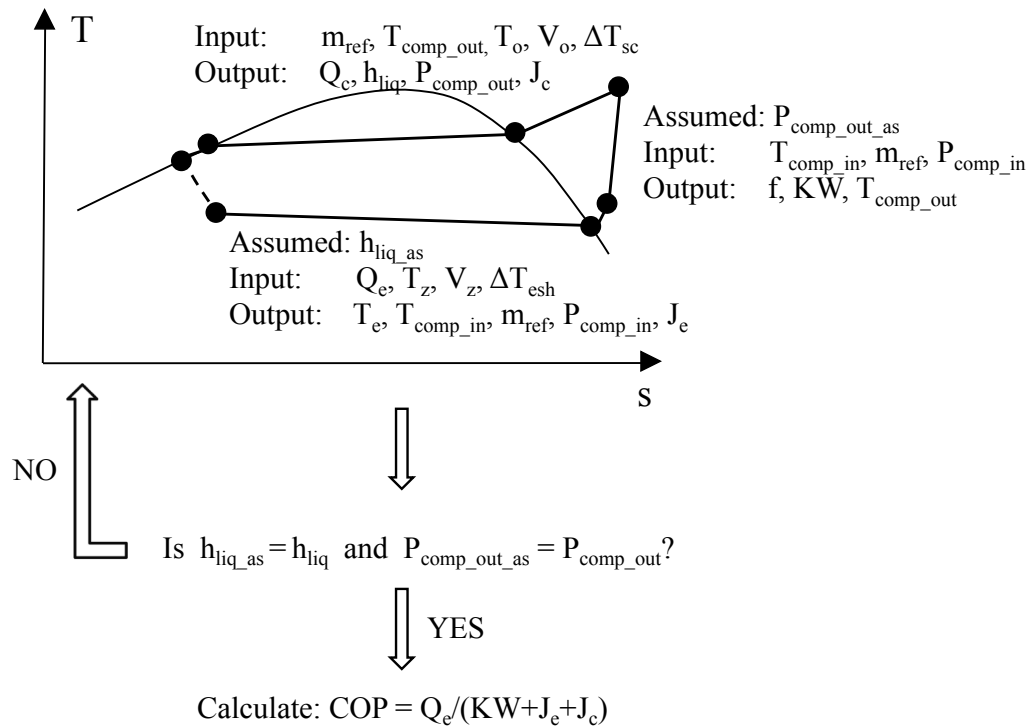


Figure 3-10: Whole system solver schematic

For the whole heat pump system, and neglecting the heat and pressure losses, the sum of the cooling rate and compressor power needs to be equal to the heat released from the condenser to the environment. This condition is automatically satisfied if the cycle is closed, which for the HPM means if the assumed pressure and enthalpy are equal to the calculated values. The proof for that is given in following equations, neglecting the heat and pressure losses between different components:

$$Q_e = m_{\text{ref}} * (h_{e3} - h_{\text{liq}}) \quad (60)$$

$$KW = m_{\text{ref}} * (h_{\text{comp_out}} - h_{\text{comp_in}}) = m_{\text{ref}} * (h_{c1} - h_{e3}) \quad (61)$$

$$Q_c = m_{\text{ref}} * (h_{c1} - h_{\text{liq}}) \quad (62)$$

$$\begin{aligned} Q_e + KW &= m_{\text{ref}} * (h_{e3} - h_{\text{liq}}) + m_{\text{ref}} * (h_{c1} - h_{e3}) = \\ &= m_{\text{ref}} * (h_{c1} - h_{\text{liq}}) = Q_c \end{aligned} \quad (63)$$

In addition to the HPM structure described above, there was also an intention to have a similar model but with the evaporating and condensing temperatures being the inputs and the airflow rates being the outputs from the main solver loop. With the evaporating and condensing temperatures as inputs, the evaporating and condensing pressure are also defined, which can simplify the iterating process by reducing the number of variables that are iterated in the main loop. In the current model, with the airflows as the inputs, the condensing pressure is calculated in the condenser sub-model from energy balance equations. Since the compressor sub-model requires the compressor outlet pressure (same as the condensing pressure if no pressure drop) as the input, and the compressor sub-model is called before the condenser sub-model, the compressor outlet pressure needs to be iterated throughout the process. The advantage of the model variation without the pressure drops and with the evaporating and condensing temperatures given as the HPM inputs, is that the condensing pressure does not need to be iterated since it is related to the condensing temperature. In the model variation where the temperatures are given as the inputs, but the pressure drops are taken into account (the condensing pressure is not equal to the compressor outlet pressure), the discharge pipe pressure drop would require an iteration process. Iterating the pressure drop instead of the compressor outlet pressure is again much faster since the pressure drop can be guessed quite close to the

final one, and the changes in the pressured drop do not influence the whole process as much as the changes in the compressor outlet pressure. Despite the mentioned benefits for the whole system iteration loop, this code structure has shown to be more time-consuming than the originally proposed model due to longer evaporator and condenser sub-model computational time. From Figure 3-11 it can be seen that the thermal effectiveness is quite sensitive to the NTU value and thermal capacitance changes, which both strongly depend on the airflow. Hence, if the airflow is iterated throughout the process, the effectiveness can change significantly from one iteration to another, which then slows down the iteration process. If on the other hand, the airflows are given as inputs and temperatures are iterated, the iteration process progresses much faster since NTU and effectiveness do not change much through the iteration.

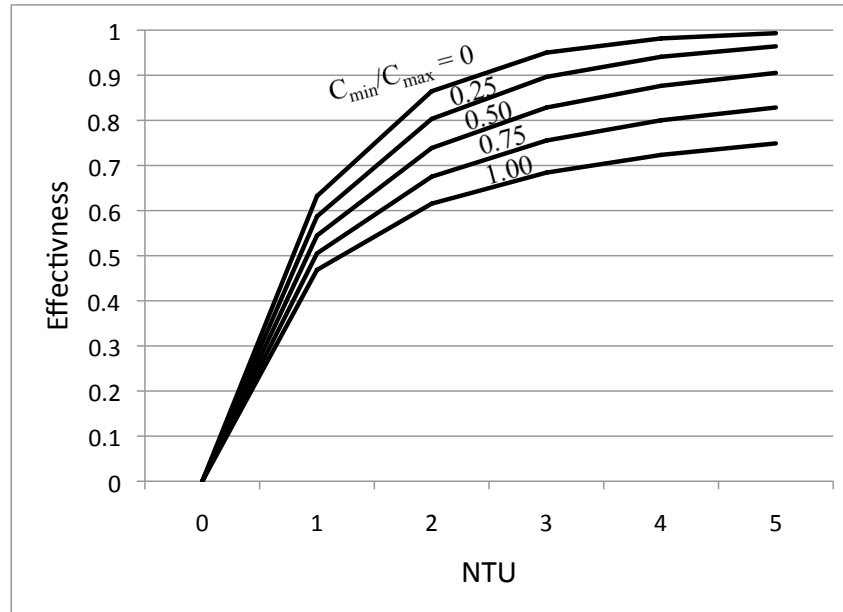


Figure 3-11: Effectiveness of cross-flow exchanger with both fluids unmixed

3.5. Heat transfer coefficient correlations

The heat transfer coefficients for the evaporator and condenser are modeled as the functions of the refrigerant flow rate, airflow rate and heat exchanger geometry. Since both the evaporator and condenser are modeled as finned tube heat exchangers cooled by air, the product of heat conductance and the heat exchanger area, UA , is calculated using:

$$\frac{1}{UA} = \frac{1}{\eta_s * h_{ex} * A_{ex}} + \frac{t}{k * A_m} + \frac{1}{h_{in} * A_{in}} \quad (64)$$

The surface efficiency η_s is the surface-area-adjusted fin efficiency [28] given by:

$$\eta_s = 1 - \frac{A_{fin}}{A_{fin} + A_{ex}} * (1 - \eta_{fin}) \quad (65)$$

The fin efficiency is calculated by the Schmidt method for continuous-plate fins [28]:

$$\eta_{fin} = \frac{\tanh(m * r_{out} * \phi)}{m * r_{out} * \phi} \quad (66)$$

$$m = \frac{2 * h_{ex}}{k * y} \quad (67)$$

$$\phi = \left(\frac{R_{equiv}}{r_{out}} - 1 \right) * \left[1 + 0.35 * \ln \left(\frac{R_{equiv}}{r_{out}} \right) \right] \quad (68)$$

$$\frac{R_{equiv}}{r_{out}} = 1.28 * \psi * (\beta - 0.2)^{0.5} \quad (69)$$

$$\psi = \frac{M}{r_{out}} \quad (70)$$

$$\beta = \frac{L}{M} \quad (71)$$

M and L are defined in Figure 3-12 , where L is always selected to be greater than or equal to M .

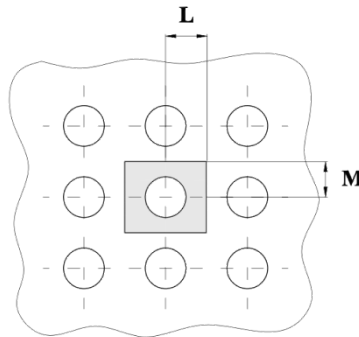


Figure 3-12: Rectangular tube array [28]

The external heat transfer coefficient is calculated using Webb and Gray correlations for a plate finned-tube heat exchanger [21]. First, the j-factor for four pipe rows in the airflow direction is calculated and then a multiplier accounts for the heat exchanger geometry with N pipe rows instead of four. The “characteristic length” for Re number is the outside tube diameter.

$$h_{ex} = St * c_p * \rho_{air} * w_{air} \quad (72)$$

where

$$St = \frac{j_N}{Pr^{2/3}} \quad (73)$$

$$\frac{j_N}{j_4} = 0.991 * \left[2.24 * Re^{-0.092} * \left(\frac{N}{4} \right)^{-0.031} \right]^{0.607 * (4-N)} \quad (74)$$

$$j_4 = 0.14 * Re^{-0.328} * \left(\frac{S_v}{S_h} \right)^{-0.502} * \left(\frac{S_d}{d_{out}} \right)^{0.0312} \quad (75)$$

Equation (75) calculates the j-factor for four rows of tubes in a heat exchanger. For a smaller number of tubes, the correction is made using Equation (74).

The air velocity w_{air} is calculated from the airflow rate and heat exchanger minimum flow area (area between fins, perpendicular to airflow direction). The geometry parameters are defined in Figure 3-12:

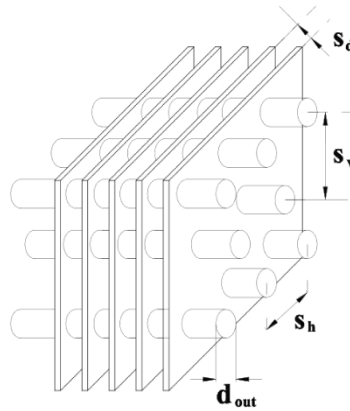


Figure 3-13: Heat exchanger geometry

The internal heat transfer coefficient for a single phase fluid is calculated using forced-convection correlations from ASHRAE Fundamentals [5]:

$$\text{for laminar flow: } Nu = \frac{h_{in} * d_{in}}{k} = 1.86 * \left(\frac{Re * Pr}{L / d_{in}} \right)^{1/3} * \left(\frac{\mu}{\mu_s} \right)^{0.14} \quad (76)$$

$$\text{for turbulent flow: } Nu = \frac{h_{in} * d_{in}}{k} = 0.023 * Re^{4/5} * Pr^x \quad (77)$$

where $x = 0.4$ if the air temperature is higher than the refrigerant temperature (in the evaporator) and $x = 0.3$ if the air temperature is lower (condenser).

The internal heat transfer coefficient for evaporation is calculated using Pierre's correlation for complete evaporation [28]:

$$Nu = \frac{h_{in} * d_{in}}{k_{liq}} = 0.0082 * \left[\left(\frac{G_{ref} * d_{in}}{\mu_{liq}} \right)^2 * \frac{(x_{out} - x_{in}) * h_{fg}}{L * g} \right]^{0.5} \quad (78)$$

where

$$G_{ref} = \frac{m_{ref}}{d_{in}^2 * \pi / 4} \quad (79)$$

The internal heat transfer coefficient for condensation is calculated from correlations for the film condensation which is the dominant mode inside the horizontal tubes [28]:

$$Nu_{liq} = \frac{h_{in} * d_{in}}{k_{liq}} = 13.8 * (Pr_{liq})^{1/3} * \left(\frac{h_{fg}}{c_{p,liq} * (T_{sat} - T_{wall})} \right)^{1/6} * \left[\frac{d_{in} * G_{ref} * \left(\frac{\rho_{liq}}{\rho_{vap}} \right)^{1/2}}{\mu_{liq}} \right]^{0.2} \quad (80)$$

where T_{wall} is the pipe wall surface temperature.

Equation (80) is valid for:

$$\frac{d_{in} * G_{ref}}{\mu_{liq}} < 5,000 \text{ and } \frac{d_{in} * G_{ref}}{\mu_{liq}} * \left(\frac{\rho_{liq}}{\rho_{vap}} \right)^{1/2} < 20,000 \quad (81)$$

When

$$10,000 < \frac{d_{in} * G_{ref}}{\mu_{liq}} * \left(\frac{\rho_{liq}}{\rho_{vap}} \right)^{1/2} < 100,000 \quad (82)$$

Equation (83) is valid:

$$\text{Nu}_{\text{liq}} = \frac{h * d_{\text{in}}}{k_{\text{liq}}} = 0.1 * \left(\frac{c_{p,\text{liq}} * \mu_{\text{liq}}}{k_{\text{liq}}} \right)^{1/3} * (\text{Pr}_{\text{liq}})^{1/3} \left(\frac{h_{\text{fg}}}{c_{p,\text{liq}} * (T_{\text{sat}} - T_{\text{wall}})} \right)^{1/6} * \left[\frac{d_{\text{in}} * G_{\text{ref}}}{\mu_l} * \left(\frac{\rho_{\text{liq}}}{\rho_{\text{vap}}} \right)^{1/2} \right]^{2/3} \quad (83)$$

The evaporator is divided into two regions, the evaporating and desuperheating region, and the UA value is calculated, during simulation, separately for each region. The external heat transfer coefficient and the surface efficiency are equal for both regions, but the internal heat transfer coefficients are different. The areas for each region are calculated as:

$$A_{\text{ep}} = y_{\text{ep}} * A_e = y_{\text{ep}} * d_e * \pi * L_e \quad (84)$$

$$A_{\text{esh}} = y_{\text{esh}} * A_e = y_{\text{esh}} * d_e * \pi * L_e \quad (85)$$

where y_{ep} and y_{esh} represent the fraction of the total evaporator area devoted to evaporation and desuperheating, respectively, and those fractions are calculated during the iteration process in the evaporator sub-models.

The condenser UA values are calculated in regions, as for the evaporator, except that the condenser has three (desuperheating, condensing and subcooling) instead of two regions.

3.6. Pressure drop correlations

The pressure drops inside the heat pump have been modeled for the evaporator, condenser, suction pipe, and discharge pipe. The pressure drop for the liquid line has not been modeled because of the assumptions explained before. The pressure drop is calculated separately for single-phase and two-phase flow. Single-phase flow occurs in the evaporator desuperheating region, condenser desuperheating region, condenser subcooling region, suction pipe and discharge pipe, while two-phase flow develops in the evaporating region of the evaporator and condensing region of the condenser. The length of each evaporator region is calculated as the fraction of the total evaporator pipe length:

$$L_{\text{ep}} = y_{\text{ep}} * L_e \quad (86)$$

$$L_{\text{esh}} = y_{\text{esh}} * L_e \quad (87)$$

The condenser pipe lengths are evaluated in an analogous manner.

Pressure drops for single-phase flow are calculated from Darcy-Weisbach equation [5]:

$$\Delta p_{\text{sph}} = \left(f * \frac{L}{d_{\text{in}}} + \sum Z \right) * \frac{G_{\text{ref}}^2}{2 * \rho_{\text{ref}}} \quad (88)$$

where the resistance factor Z accounts for local pressure drops (U-turns, valves). The friction factor is calculated from Colebrook equation [5]:

$$\frac{1}{\sqrt{f}} = 1.74 - 2 * \log \left(\frac{2 * E}{d_{\text{in}}} + \frac{18.7}{\text{Re} * \sqrt{f}} \right) \quad (89)$$

Pressure drops for two-phase flow are modeled using pressure drop correlations developed by Choi, Kadzierski and Domanski [10]. The pressure drop correlations are the improved version of relatively older Pierre's model, which is still often used because of its simplicity and validity. The pressure drop for two-phase flow is not simple to calculate since it depends on many factors, such as vapor quality, oil influence, the type of the refrigerant etc. Several semi-empirical models can be found in the literature, where most of them suggest to divide a heat exchanger into several smaller sections and then to calculate the local pressure drop for each of those sections. For Pierre's model, only the refrigerant properties at the beginning and the end of two-phase process are needed. The model was originally developed for an evaporator and it includes the oil influence for refrigerant/lubricant mixtures. Several authors reported very good agreement between the model and the different sets of measurements, even for pressure drop in a condenser. The foregoing properties give the model great advantage over more complicated models, especially for the calculations that are expected to be fast.

In the HPM, the oil mass flow rate has been taken as 4% of the refrigerant mass flow rate, same as in the compressor sub-model. The pressure drop due to friction and acceleration in the pipes is calculated as:

$$\Delta p_{\text{tp},f+a} = \left[\frac{f * L * (v_{\text{out}} - v_{\text{in}})}{d_{\text{in}}} + (v_{\text{out}} - v_{\text{in}}) \right] * G^2 \quad (90)$$

where:

$$f = 0.00506 * \text{Re}_{\text{liq}}^{-0.0951} * K_f^{0.1554} \quad (91)$$

$$\text{Re}_{\text{liq}} = \frac{G * d_{\text{in}}}{\mu_{\text{mix}}} \quad (92)$$

$$K_f = \frac{\Delta x * h_{fg}}{L * g} \quad (93)$$

Modifications have been made to accommodate the influence of oil on vapor quality and liquid Reynolds number:

$$x = \frac{G_{ref,vap}}{G_{ref,vap} + G_{ref,liq} + G_{oil}} \quad (94)$$

$$\ln \mu_{mix} = \xi_{ref} * \ln \mu_{ref} + \xi_{oil} * \ln \mu_{oil} \quad (95)$$

where:

$$\xi_i = \frac{M_i^{0.58} * \psi_i}{\sum_j M_j^{0.58} * \psi_j} \quad (96)$$

$$\psi_{oil} = \frac{\overline{w_{oil}} * \frac{M_{ref}}{M_{oil}}}{1 - \overline{w_{oil}} + \overline{w_{oil}} * \frac{M_{ref}}{M_{oil}}} \quad (97)$$

$$\psi_{ref} = 1 - \psi_{oil} \quad (98)$$

The lubricant mass fraction w_{oil} should be linearly averaged over the length of the tube:

$$\overline{w_{oil}} = \frac{w_{oil,in} + w_{oil,out}}{2} \quad (99)$$

where for the lubricant mass fraction calculation only the liquid state refrigerant is considered:

$$w_{oil} = \frac{m_{oil}}{m_{oil} + m_{ref,liq}} \quad (100)$$

The model developed by Choi, Kadzierski and Domanski does not investigate the loss due to the flow turn in the 180 degrees return bends. However, in Pierre's original model that loss is accounted for using the resistance factor Z of the magnitude 0.7 to 1.0, where the higher value represents the case where oil is presented.

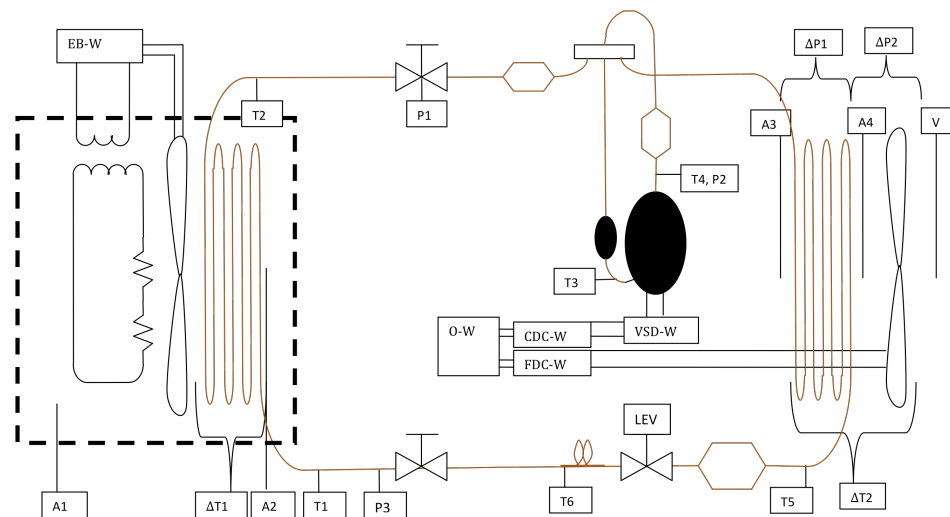
$$\Delta p_{tph,U-turn} = \sum Z * \frac{G_{ref}^2}{2 * \rho_{ref}} \quad (101)$$

The total pressure drop in the HPM for two-phase flow is then calculated as:

$$\Delta p_{tph,f+a} = \Delta p_{tph,f+a} + \Delta p_{tph,U-turn} \quad (102)$$

Chapter 4: Heat pump model validation

The Mitsubishi heat pump “Mr. Slim”[®] is used to validate the accuracy of the heat pump model. The Mitsubishi heat pump type is MSZ-A09NA with refrigerant R410a as a working fluid and a rotary-piston type compressor. More detailed data about the heat pump can be found in the service manual [29]. The real heat pump has been instrumented with sensors that measure relevant temperatures, pressures, evaporator fan power, condenser fan power, compressor power and evaporator cooling rate. The test stand schematic with the sensor placement is shown in Figure 4-1.



	Code	Description		Description
T1	T_{e1}	Evaporator inlet refrigerant temperature	CDC-W	DC compressor power
T2	T_{e2}	Evaporator outlet refrigerant temperature	A1	Evaporator box air temperature
A2	T_z	Evaporator inlet air temperature	ΔT1	Evaporator air temperature difference
EB-W		Evaporator box power	A4	Condenser air outlet temperature
T3	$T_{comp\ in}$	Compressor suction refrigerant temperature	ΔT2	Condenser air temperature difference
T4	$T_{comp\ out}$	Compressor discharge refrigerant temp.	ΔP1	Condenser HX pressure drop
P1	$P_{comp\ in}$	Suction pressure	ΔP2	Condenser fan pressure rise
P2	$P_{comp\ out}$	Discharge pressure	O-W	Outdoor unit power
C-W	KW	3-phase compressor power	T6	Expansion valve refrigerant temperature
T5	T_{c4}	Condenser outlet refrigerant temperature	P3	Expansion valve pressure
A3	T_o	Condenser air inlet temperature	V	Flow traverse measurement
FDC-W		DC condenser fan power	P3	Expansion valve pressure

Figure 4-1: Schematic of the heat pump test stand [20]








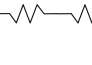
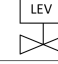
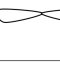

	Refrigerant muffler		Capillary tube
	Strainer		Stop valve
	Compressor with filter/dryer		Variat
	Heat exchanger		Resistance heater
	Expansion valve		Fan
	4-way valve		

Figure 4-2: Components of the heat pump test stand [20]

During operation, the zone and ambient temperature, compressor speed, condenser fan speed and cooling rate were varied, while the evaporator fan speed remained constant. From 86 experimental operating points, 4 are discovered to be outliers²; hence the data for 82 points are used for model validation. The detailed data for each point can be found in Appendix C.

The comparisons between the heat pump model outputs and the experimental observations have been made at the component level (for evaporator, compressor and condenser) and also at the system level. Certain experimentally measured parameters have served as the heat pump model inputs and the other parameters served as the responses that the model is supposed to accurately predict. The results of the comparison are shown in the graphs in sections 4.1. – 4.4. for each important output variable and each experimental point separately.

In the graphs, the absolute error is defined as:

$$\text{Absolute error} = X_m - X_{\text{calc}} \quad (103)$$

² For one point the airflow was not measured. Two points have the difference between the evaporating and airflow temperature 18 °C for Q_e/V_z ratio 10, while all other points have temperature difference 10 °C (Figure 4-5). The fourth point has large differences between the mass flow rates calculated from the evaporator, compressor and condenser energy balance equations for the same point.

the relative error is defined as:

$$\text{Relative error} = \frac{X_m - X_{\text{calc.}}}{X_m} * 100 \quad (104)$$

and the RMS is calculated using Equation (19):

$$\text{RMS} = \sqrt{\frac{\sum \left(\frac{f_m - f_{\text{calc}}}{f_m} \right)^2}{N_m}} \quad (19)$$

Four model variations have been compared to determine how several local phenomena influence the system performance. The difference between the model variations is whether they assume evaporator desuperheating, condenser subcooling, the pressure drop inside the heat pump and constant or variable heat transfer coefficients. One color in the graphs corresponds to each variation (Table 4-1).

	Desuperheating	Subcooling	Variable or	Pressure	Color
Model 1 (M1)	No	No	Constant	No	Blue
Model 2 (M2)	Yes	Yes	Constant	No	Green
Model 3 (M3)	Yes	Yes	Variable	No	Yellow
Model 4 (M4)	Yes	Yes	Variable	Yes	Red

Table 4-1: Overview of the 4 compared models

If one is not familiar with the heat exchanger geometry details needed for the UA value calculations and hence, decides to use constant heat transfer coefficients, there are two possibilities to estimate UA value. The first is to use experimental data and the second is to use data specified by the manufacturer. Most manufacturers will publish detailed data only for one, standard operation point, which usually will not give very accurate UA value estimate. However, because experimental data are rarely available, the second approach is used most often. The constant UA value calculations are explained in more detail in Appendix A, and the estimated constant evaporator and condenser UA values are 220 W/K and 830 W/K respectively. The airside thermal capacitance and heat exchanger effectiveness are determined for constant UA values and given airflow rates using the procedure explained in sections 3.1. and 3.3.

4.1. Evaporator sub-model validation

For the evaporator validation, the heat exchanger geometry and experimental data have been used as the input parameters, and then the model outputs and experimental data have been compared.

The experimental data used as the evaporator sub-model inputs are:

- cooling rate – Q_{e_m}
- evaporator airflow rate – V_{z_m}
- enthalpy at the evaporator inlet – h_{liq_m}
- zone (room) air temperature – T_{z_m}
- desuperheating temperature difference – $\Delta T_{esh_m} (T_{e3_m} - T_{e1_m})$

The important evaporator sub-model output variables are:

- refrigerant mass flow rate – m_{ref}
- evaporator inlet temperature – T_{e1}
- evaporator outlet temperature – T_{e3}
- evaporator inlet pressure – P_{e1}
- compressor inlet pressure – P_{comp_in}

For M1, M2 and M3 the compressor inlet pressure is equal to the evaporator outlet pressure. For M4 the suction line pressure drop ΔP_s is determined and the compressor inlet pressure is calculated as:

$$P_{comp_in} = P_{e3} - \Delta P_s \quad (105)$$

Since the evaporator sub-model outputs are used as the compressor sub-model inlets, the errors in the evaporator parameters prediction might cause large errors in the compressor parameters predictions. For the compressor sub-model, the mass flow rate and compressor inlet state are given input parameters and from Equation (18) the compressor shaft speed is calculated as:

$$f = \frac{m_{ref}}{D * \rho_{comp_in} * \eta_V} \quad (106)$$

and compressor power from Equation (32) as:

$$KW * \eta_{comb} = m_{ref} * \frac{k}{k-1} * \frac{P_{comp_in}}{\rho_{comp_in}} * \left[\left(\frac{P_{comp_out}}{P_{suction}} \right)^{\frac{k-1}{k}} - 1 \right] \quad (32)$$

Hence, the refrigerant mass flow rate and suction density have crucial influence on the shaft frequency and compressor power prediction, but most importantly, the crucial influence on the COP value, the most important heat pump parameter.

The two most important evaporator output parameters for the energy consumption analysis are the refrigerant mass flow rate and compressor inlet pressure. Because they have crucial influence on the compressor power consumption, the largest power consumption fraction, it is important that HPM predicts them as accurate as possible.

For further analysis it is useful to recognize which experimental data are more reliable. The refrigerant temperatures, air temperatures, suction pressure, evaporator inlet pressure and cooling rate have been measured directly, so one would expect they are most reliable.

Because the vapor fraction at the evaporator inlet has not been measured, the evaporator inlet enthalpy is calculated using the assumption that the condenser outlet and evaporator inlet enthalpies are equal, which is the same assumption as the one in HPM. To calculate the enthalpy at the condenser outlet, the temperature and pressure need to be measured. Since only temperature is measured, another assumption is that the pressure at the condenser outlet is equal to the pressure measured after the compressor. The refrigerant at the condenser outlet is in liquid state and its enthalpy will depend much more on the temperature than on the pressure. The first assumption (that the enthalpies are equal) will however introduce more inaccuracy since there will be some enthalpy losses between the condenser and evaporator due to heat exchange and friction.

The refrigerant mass flow rate has been calculated from the measured cooling rate and the evaporator enthalpy difference. It is mentioned before that the evaporator inlet enthalpy is probably slightly overestimated due to enthalpy losses in the liquid line. The evaporator outlet enthalpy is calculated from the outlet temperature and the pressure measured between the evaporator and the compressor. The evaporator outlet enthalpy would in reality be somewhat lower since the pressure at the evaporator outlet would be slightly higher than at the middle of the suction pipe where it is measured (for R410a and evaporating conditions, between two points with the same temperature the point with higher pressure will have lower enthalpy than the point with lower pressure). We can argue that the resulting enthalpy difference error and

corresponding mass flow rate error probably will not be large since both calculated enthalpies are slightly overestimated.

The evaporator airflow rate is calculated from the measured cooling rate and the air temperature difference. The average temperature difference is susceptible to non-uniform air temperature distribution and errors in the cooling rate measurements.

The results of the evaporator sub-model comparison can be seen in Figure 4-3 through Figure 4-10.

First, the evaporator inlet temperature comparison is presented since the errors in this temperature can have a crucial impact on many other variables (shown later in the chapter). It can be seen from Figure 4-3 that the model variations M3 and M4 (for which the UA values are calculated rather than assumed to be constant) show much better agreement with the measured data. The model variations M1 and M2 where the constant UA values are calculated from manufacturer's standard operating point data, did not give very good predictions for the heat pump evaporating temperatures.

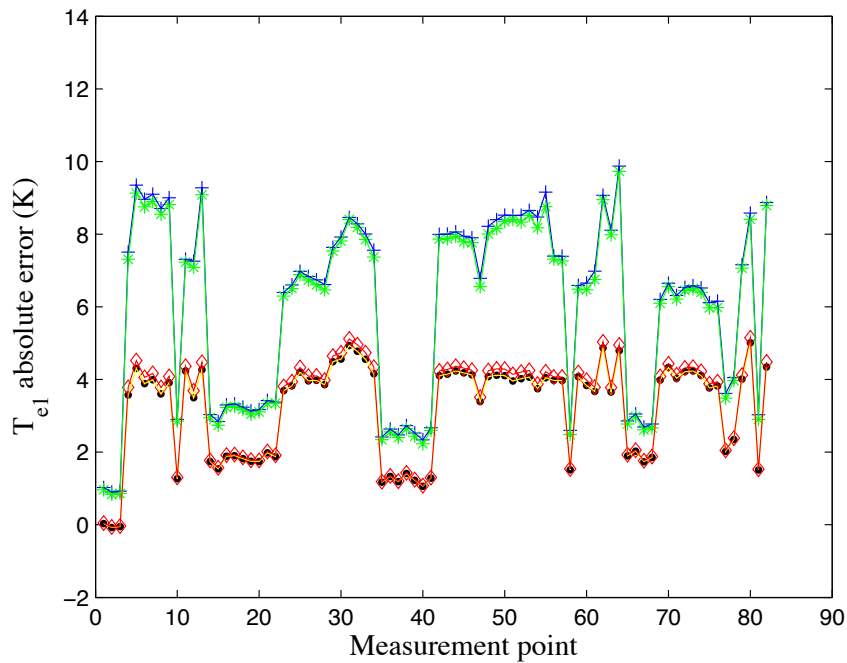


Figure 4-3: Evaporator inlet temperature absolute error

The specific structure in the absolute temperature errors can be explained if one plots the cooling rate to airflow ratio for each measurement point (Figure 4-4). Both the temperature absolute errors and cooling rate to airflow ratio show very similar trend, where the high temperature errors occur for high ratios.

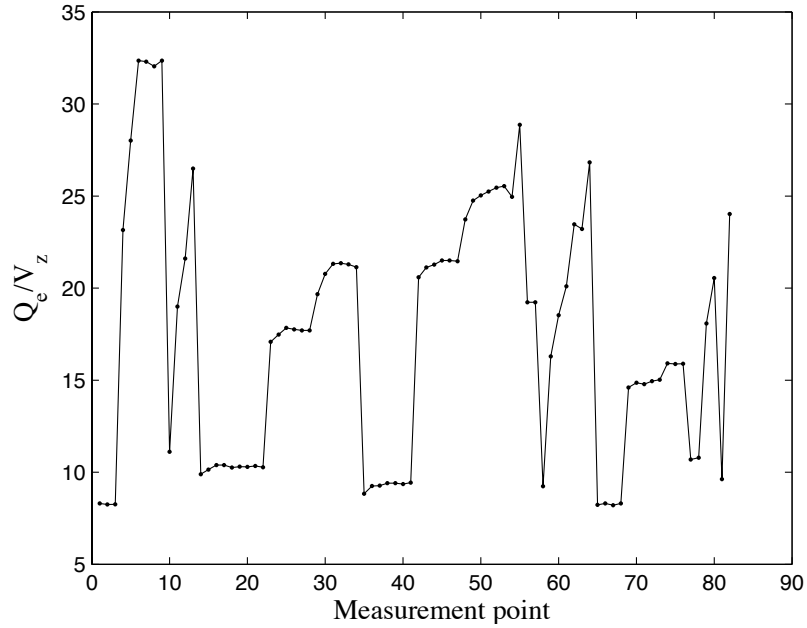


Figure 4-4: Cooling rate to airflow ratio for each measurement point

Figure 4-5 shows the measured and calculated temperature difference between the refrigerant evaporating temperature and air temperature. Again, when presented as the function of the cooling rate to airflow ratio, it can be seen that for the small ratios only a small discrepancy between the measured and predicted values exists. For larger ratios, the trend is equal for the both the measured and predicted case, but the systematic absolute error occurs.

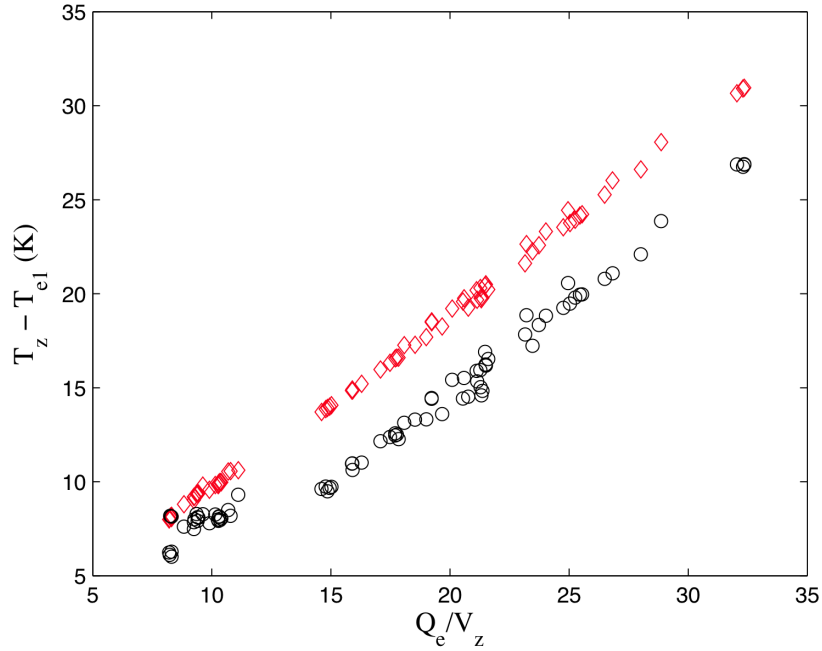


Figure 4-5: Temperature difference between the refrigerant evaporating temperature and zone temperature as a function of Q_e/V_z ; red are the calculated and black are the measured values

The evaporating temperature is calculated using Equation (2), so the error can occur due to the error in the cooling rate measurements, the airflow calculations from the measured data or the HPM evaporator thermal effectiveness calculations. The last is again the function of the airflow and calculated UA value.

It is mentioned before that the cooling rate is measured directly, so it is probably the least possible reason for the error.

If the thermal effectiveness causes the errors, for better agreement with the measured data the UA value should be higher, resulting in a higher thermal effectiveness. There are a few possible reasons for the error in UA value. First, the geometry for the “Mr. Slim” evaporator is difficult to describe and is more complicated than the one assumed for the external heat transfer coefficient and surface efficiency calculations. The internal heat transfer coefficient calculated for the evaporating region can also cause errors because the model uses the very simple Pierre’s correlation to describe relatively complex processes in the evaporator. A more accurate calculation would be to divide the evaporator into several segments and to calculate the internal heat transfer coefficient for each of them. The next possible cause is the evaporator area, which might be inaccurately measured due to the complicated evaporator geometry. Most importantly, the water condensation on the evaporator external areas has not been taken into account, which leads to more errors in UA value. As mentioned before, to decrease the evaporating temperature

errors, the UA value should be higher, leading to higher thermal effectiveness. The analysis is made with the constant thermal effectiveness value of 0.95 to determine whether a high effectiveness value would improve the results (Figure 4-6). Although resulting in a slightly better estimate, the thermal effectiveness increase did not improve the calculated temperature difference completely. Hence, it is probably safe to conclude that the errors in UA value cause some percentage of errors, but are not the only reason for the errors in evaporating temperature calculations.

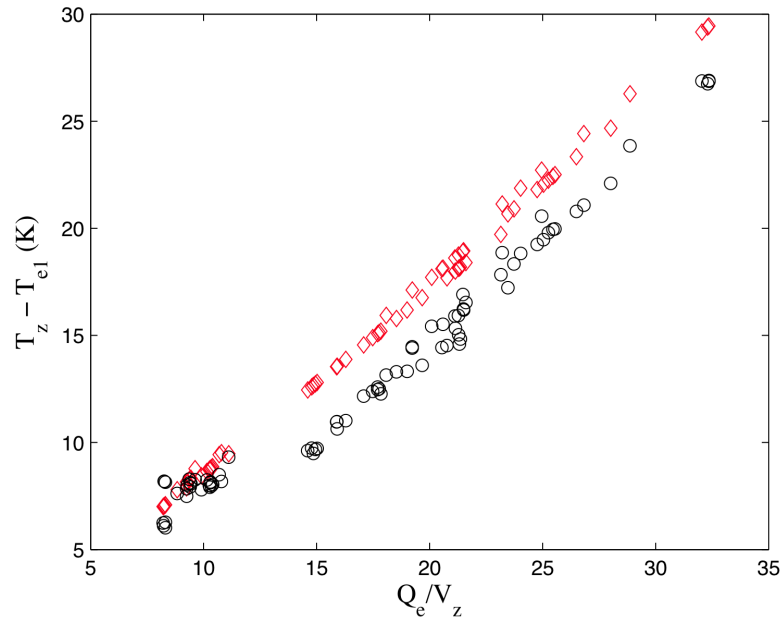


Figure 4-6: Temperature difference if the evaporating region thermal effectiveness is set to constant value of 0.95

The third possible reason behind the errors is the airflow rate value, and the analysis has shown that with 20% large airflow rate than the one calculated for the measurements, the calculated temperature difference shows very good agreement with the experimental data. Because the scope of this research was not to evaluate the errors in the measured data, the possibility for the systematic 20% error in evaporator airflow rate will not be analyzed.

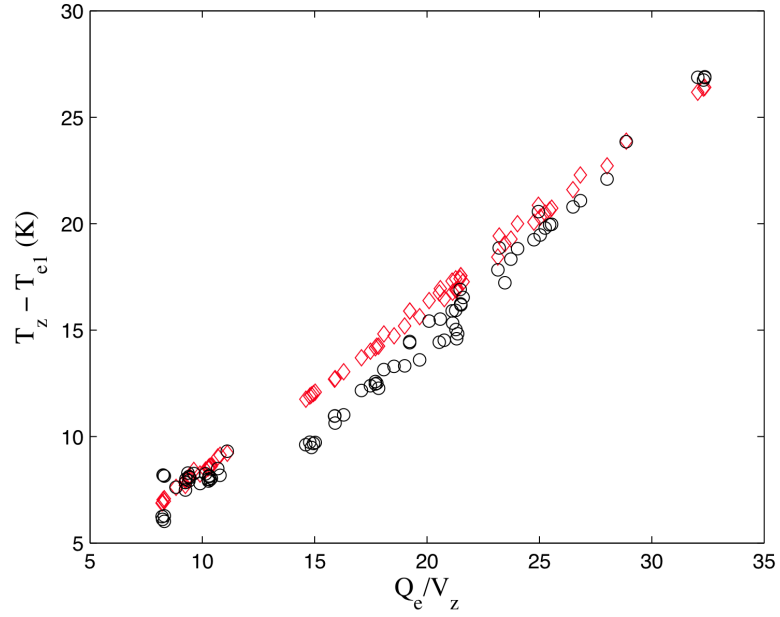


Figure 4-7: Temperature difference if the evaporator airflow is 20% larger than the measured values

Because the evaporator outlet temperature is determined from the calculated inlet temperature and given desuperheating temperature difference, the errors in the outlet temperatures are completely influenced by the inlet temperature errors. The largest errors in the outlet temperature can be seen for the simplest model variation M1 (blue), which does not take into account evaporator desuperheating.

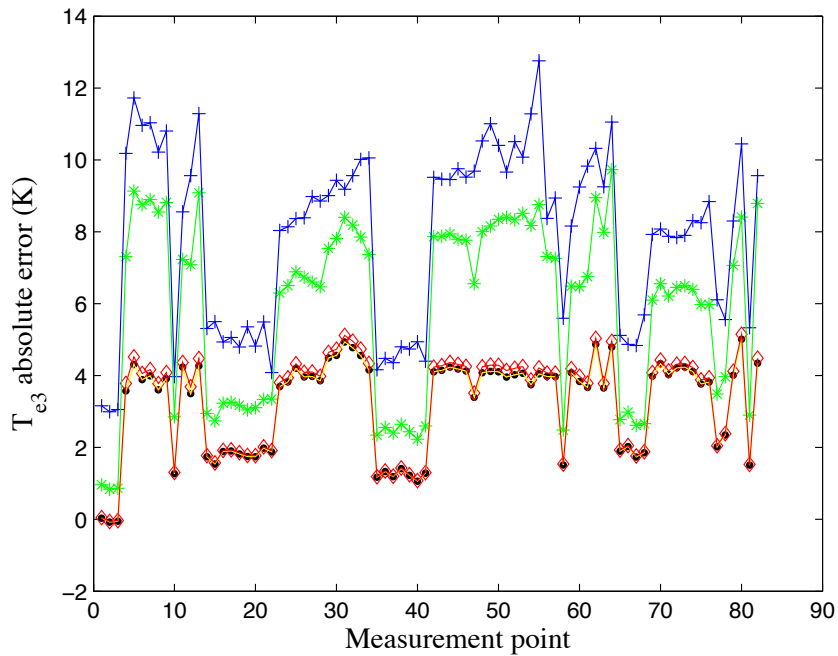


Figure 4-8: Evaporator outlet temperature absolute error

As pressure is a function of temperature for a saturated refrigerant state, the evaporator inlet pressure errors show exactly the same behavior as the inlet temperature errors:

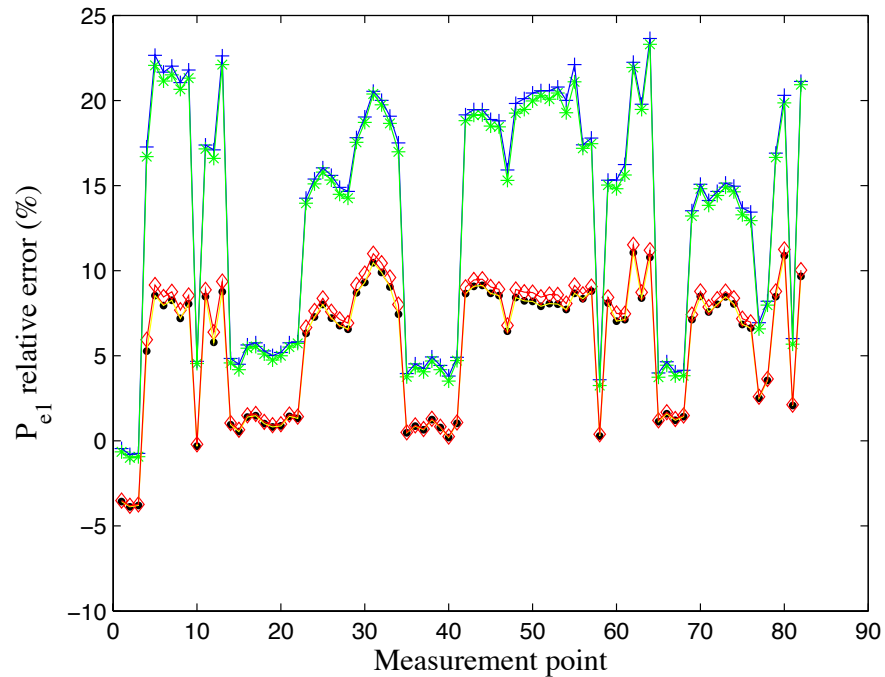


Figure 4-9: Evaporator inlet pressure relative error

Although the compressor inlet pressures for variations M1 and M2 seem to show the best agreement with the measured data (Figure 4-10), it is also the result of the large evaporating temperature errors. If M1 and M2 would predict the temperatures closer to the measured ones, the pressure errors would behave similar to the M3's errors because none of those three models take pressure drop into account. The evaporator inlet pressures for M3 were under-predicted for a majority of points (Figure 4-9), since the predicted inlet temperatures were lower than the measured temperatures. The compressor inlet pressure comparison for M3 shows the opposite behavior where the predicted pressure is higher than the measured. This over-prediction occurs because the pressure drops in the evaporator are not taken into account. Moreover, the errors would be even larger if the evaporator inlet pressures have not been under-predicted. At a first glance it seems that M4, which includes the refrigerant side pressure drop, gives the most unreliable results for the compressor inlet pressure. This happens because a few degrees error in the evaporating temperature causes significant errors in the compressor inlet pressure. The error in pressure occurs, first, because the evaporating pressure is the function of the evaporating temperature, and the errors in evaporating temperatures will cause larger relative errors in evaporating pressures. Second, the calculated evaporator pressure drop increases for lower

evaporating temperatures due to lower density, so again, the small errors in the evaporating temperature can result in large evaporator pressure drop errors and compressor inlet pressure errors. The sensitivity of the pressure errors to the evaporating temperature errors can be seen from Figure 4-3, Figure 4-9 and Figure 4-10. Although M4 shows only about 4 K maximum absolute error (about 1.5% relative error) in the evaporating temperature, it causes about 10% relative error in the evaporating pressure and additional errors in the evaporator pressure drop that at the end result in 15-25% error in the compressor inlet pressure.

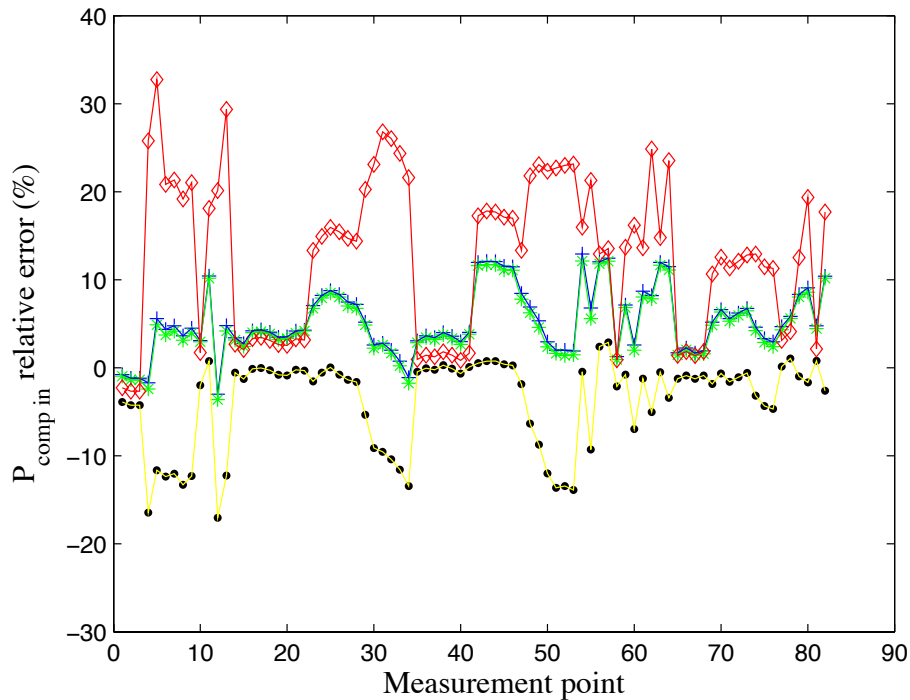


Figure 4-10: Compressor inlet pressure relative error

The refrigerant mass flow rate is calculated from the cooling rate and evaporator enthalpy difference. Because both the cooling rate and inlet enthalpy are the same for all four models (inputs from measured data), the mass flow rate errors are only related to the evaporator outlet enthalpy errors. All models tend to over-predict the refrigerant mass flow rate, but since the mass flow rate was not directly measured during the experimental work (it was calculated from the cooling rate and enthalpy differences) the mass flow rate errors should be analyzed more as a comparison between the different models than as the exact error values. The model M1 shows the largest mass flow rate errors, which is expected since the large under-prediction in the evaporator outlet temperature leads to the enthalpy under-prediction, and finally to the mass flow rate over-prediction. Although M3 and M4 show very small differences in the evaporator

outlet temperature, the enthalpy differences and corresponding mass flow rate errors are significantly different between the models due to the differences in the evaporator outlet pressures.

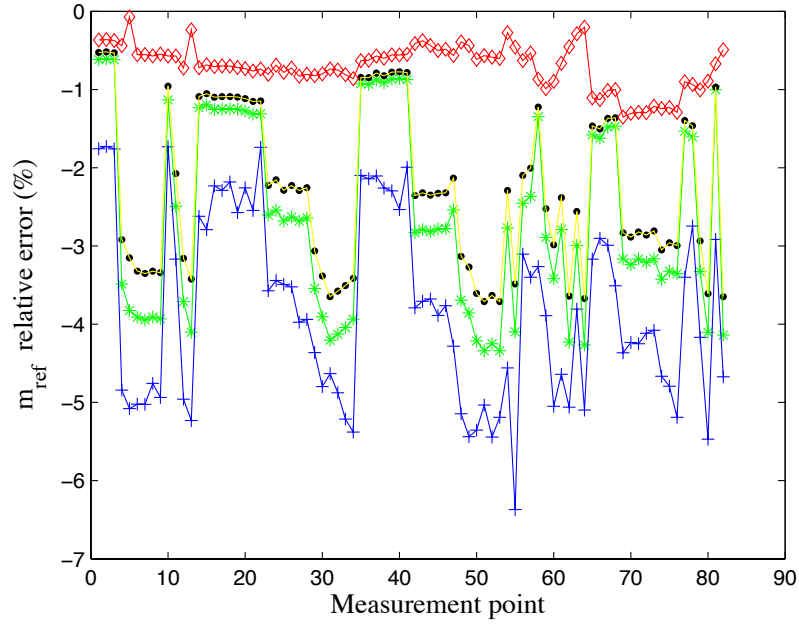


Figure 4-11: Refrigerant mass flow rate relative error

It can be seen from Table 4-2 that errors for the refrigerant mass flow rate, the evaporator temperatures and evaporator inlet pressures show significantly better results for M4 (red) than for simpler models M1 (blue) and M2 (green). Between models M3 and M4, model M4 have a notable improvement in the mass flow rate predictions. However, M4 shows the largest errors in the compressor inlet pressure due to the errors in the evaporating temperature, which can have an important impact on the compressor power.

	RMS (%)				
	m_{ref}	T_{e1}	T_{e3}	P_{e1}	P_{comp_in}
M1	3.99	2.35	2.95	15.24	6.39
M2	2.89	2.30	2.29	14.90	6.07
M3	2.49	1.24	1.24	6.78	6.30
M4	0.75	1.29	1.28	7.12	15.52

Table 4-2: Evaporator RMS errors for output variables for 4 different model variations

In order to show how the smaller evaporating temperature errors influence the final results, the new comparison is performed for the evaporator airflows 20% higher than the measured. It is shown in Figure 4-7 that this correction will result in better temperature prediction for M3 and M4. For M1 and M2, the UA value is taken as constant and it does not depend on the airflow increase. However, because the airflow change will influence the thermal capacitance C_{ep} , the M1's and M2's evaporating temperatures will also change for higher airflows. In Figure 4-12 – Figure 4-14, the models M3 and M4 show respectable accuracy in the evaporator temperatures and inlet pressure prediction, while the M1's and M2's predictions are still far from the measurements.

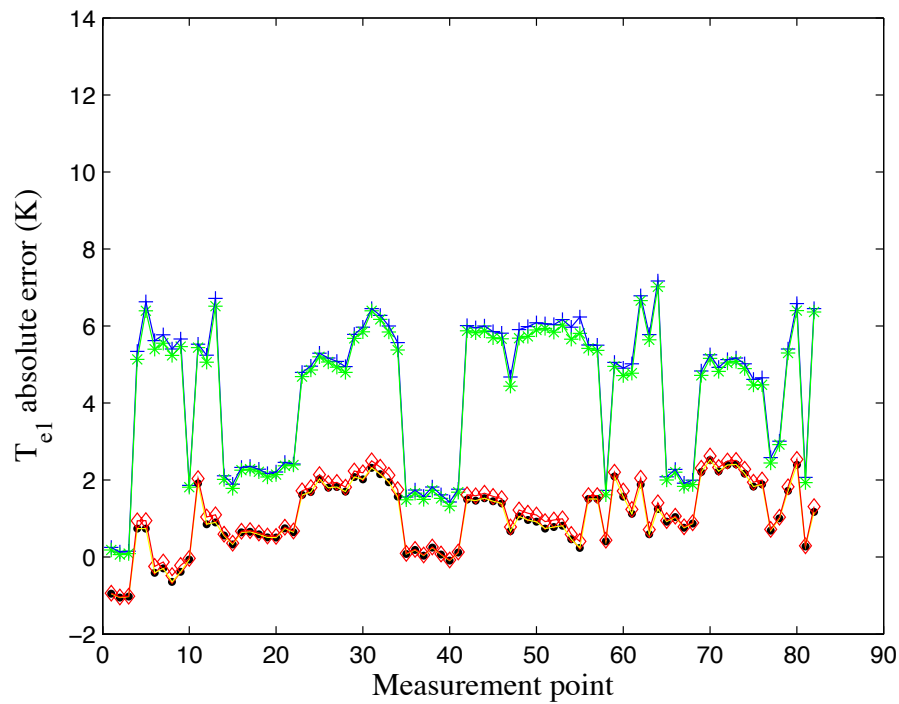


Figure 4-12: Evaporator inlet temperature absolute error for 20% larger evaporator airflow than the measured values

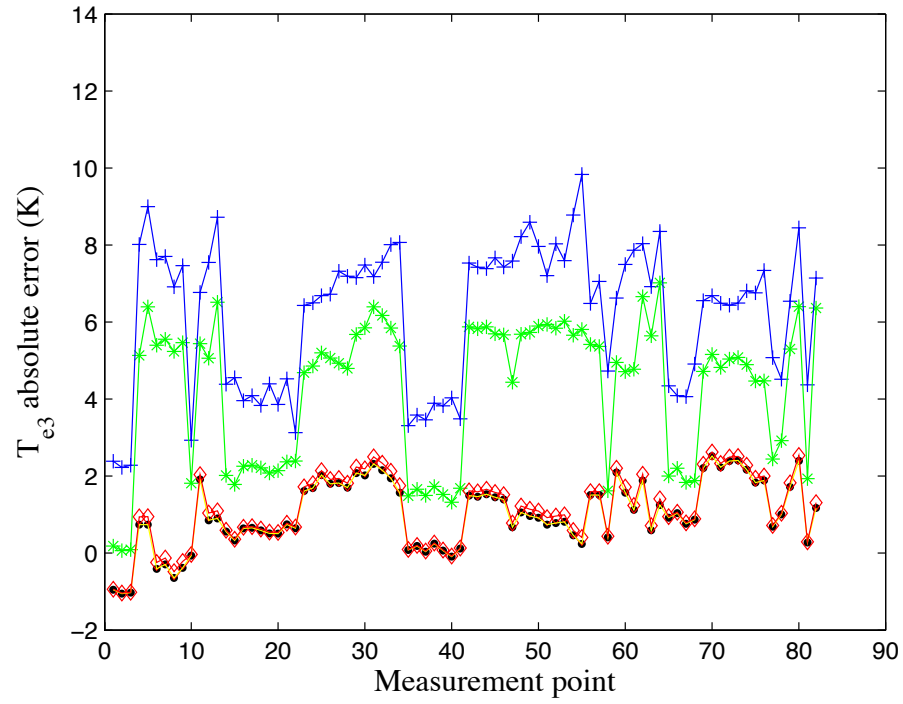


Figure 4-13: Evaporator outlet temperature absolute error for 20% larger evaporator airflow than the measured values

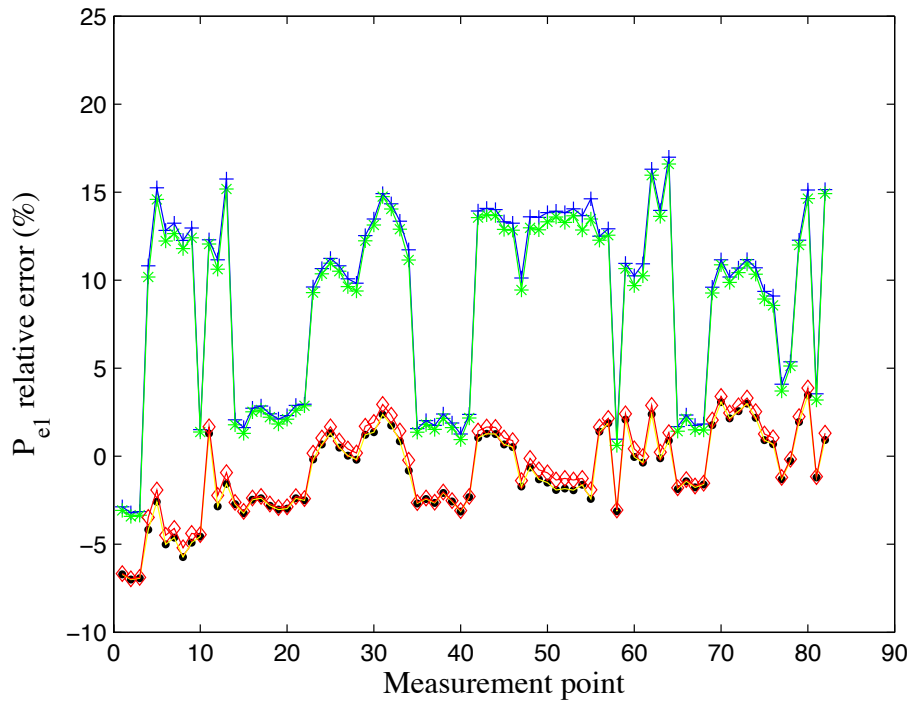


Figure 4-14: Evaporator inlet pressure relative error for 20% larger evaporator airflow than the measured values

Figure 4-15 shows that M4 gives much better agreement with the measured compressor inlet pressure than the model M3 (yellow), which does not include the pressure drop calculation. The calculated compressor inlet pressure is still slightly under-predicted for many points in M4, but that is the result of the errors in the evaporating temperature. Although it looks as if M1 and M2 give good results for the compressor inlet pressure, it is purely the result of the large evaporating temperatures errors. If the temperature errors were lower, the compressor inlet values would be close to M3's results (yellow), suggesting the significantly compressor inlet pressure over-prediction.

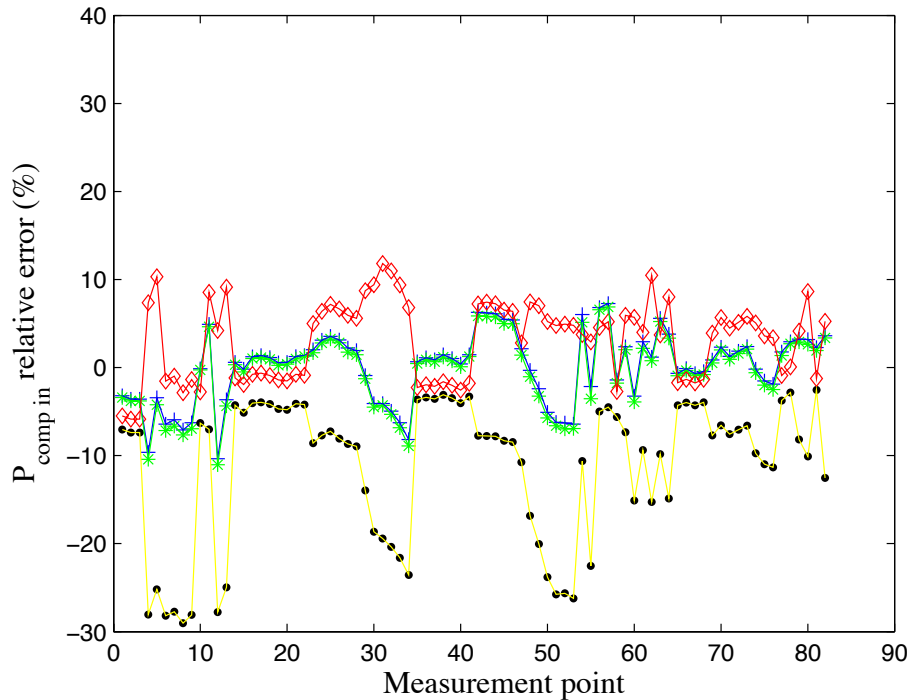


Figure 4-15: Compressor inlet pressure relative error for 20% larger evaporator airflow than the measured values

From the mass flow rate comparisons in Figure 4-16 it can be seen that the mass flow rate errors did not change much. Although the 20% evaporator airflow increase resulted in the evaporating temperature increase (raises the enthalpy), it also resulted in the pressure increase, which has the opposite effect (lowers the enthalpy). Hence, the combination of these two effects has not resulted in a large evaporator outlet enthalpy change and the corresponding mass flow rate change.

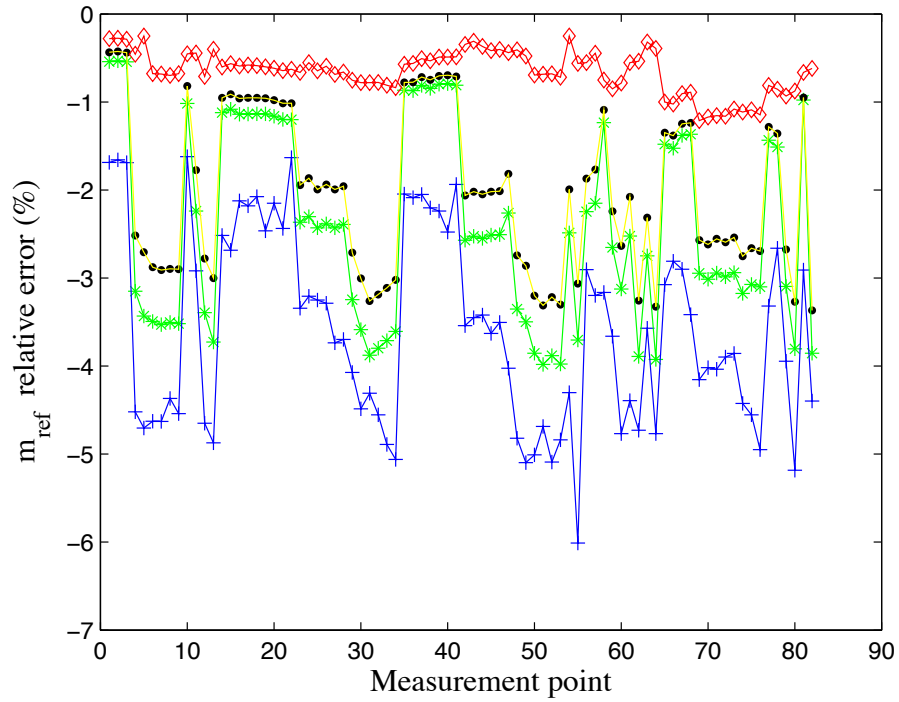


Figure 4-16: Refrigerant mass flow rate relative error for 20% larger evaporator airflow than the measured values

The RMS errors for the comparison in which the evaporator airflow is increased from the measured airflow by 20% are shown in Table 4-3.

	RMS (%)				
	m_{ref}	T_{el}	T_{e2}	P_{el}	P_{comp_in}
M1	3.75	1.70	2.31	10.42	3.98
M2	2.65	1.66	1.65	10.06	4.09
M3	2.21	0.48	0.48	2.61	13.80
M4	0.69	0.51	0.51	2.57	5.41

Table 4-3: RMS errors for 20% larger evaporator airflow than the measured values

4.2. Compressor sub-model validation

A variable-speed compressor enables efficient part-load operation of the heat pump and is one of the main characteristics of the low-lift cooling technology. The measurements performed on “Mr. Slim” for different compressor speeds, pressure ratios and inlet conditions, and related observations can be found in Appendix C.

The compressor validation process is performed the same way as the evaporator validation process, by taking one set the experimental data as the HPM inputs and comparing the model outputs with the other set of the experimental data. Armstrong’s model has been chosen among several mass flow rate models described in section 3.2. The power model developed by Jähnig et al. has been used in slightly changed form.

The experimental data used as the inputs to the compressor sub-model are:

- refrigerant mass flow rate – m_{ref_m}
- compressor inlet temperature – $T_{comp_in_m}$
- compressor inlet pressure – $P_{comp_in_m}$
- compressor outlet pressure – $P_{comp_out_m}$

The compressor output variables that have been compared with experimental data are:

- compressor shaft speed – f
- compressor power – KW
- compressor outlet temperature – T_{comp_out}

In the experimental data, the directly measured parameters are the compressor inlet and outlet pressure, shaft frequency, power and outlet temperature. The compressor inlet temperature was also directly measured, but it was later discovered that there are some errors related to this measurement. Hence, the assumption is made that the compressor inlet temperature is equal to the measured evaporator outlet temperature, which is the same assumption as in HPM.

While the four model variations are compared for the evaporator and condenser (M1-M4), the compressor sub-model is the same for all those variations and the comparison between the calculated and measured data is shown in the Figure 4-17 – Figure 4-19. It can be seen from the compressor speed comparison in Figure 4-17 that the relative errors range between -3 and

3%, except for 6 points that are out of these limits (6-9, 42 and 62). For these 6 points no obvious reason is found for large discrepancies between the measured and calculated speeds. The transposed compressor sub-model, with the compressor speed as the sub-model input and the mass flow rate as the output was also analyzed, although it is not part of the heat pump model. The analysis has again shown $\pm 3\%$ relative errors for the majority of points (the same points, 6-9, 42 and 62, do not fall into these limits).

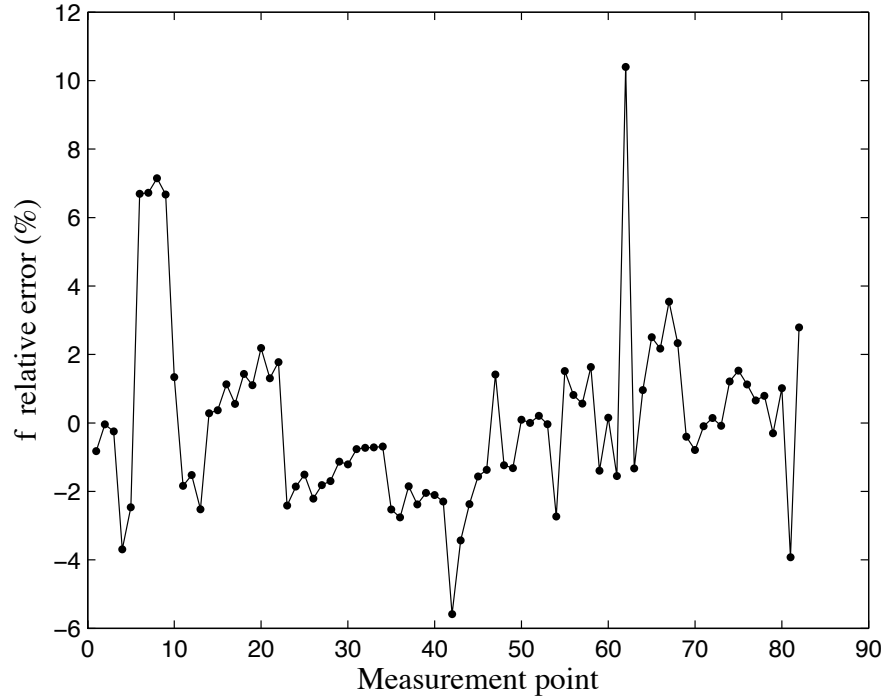


Figure 4-17: Compressor shaft speed relative error

For the majority of points the compressor power model shows acceptable accuracy, which is very important for the heat pump COP predictions. The power errors that stand out are for the points 1 – 3 and 65 – 68 for which the compressor power is small (100 – 400 W) and hence, the small absolute errors result in large relative errors. Except for these outliers, the errors are larger for the same points that show larger errors for the compressor shaft speed, points 6 – 9 and 42.

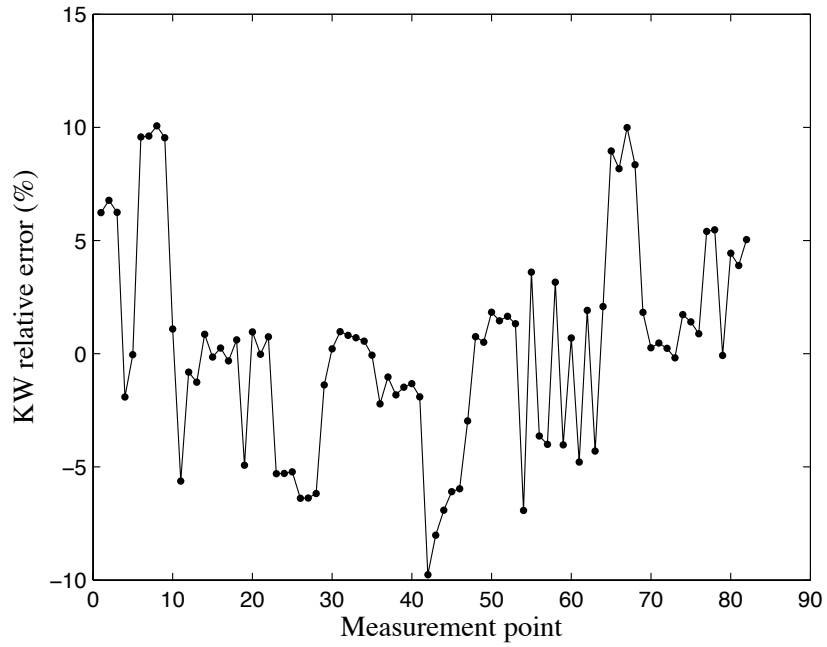


Figure 4-18: Compressor power relative error

The HPM tends to over-predict the compressor outlet temperatures by as much as 8 K, which can be the consequence of neglecting the compressor heat losses or assuming too low lubricant oil fraction. The errors in the measured temperature or pressure can also influence the calculated inlet and outlet enthalpy errors and cause errors in the calculated outlet temperature.

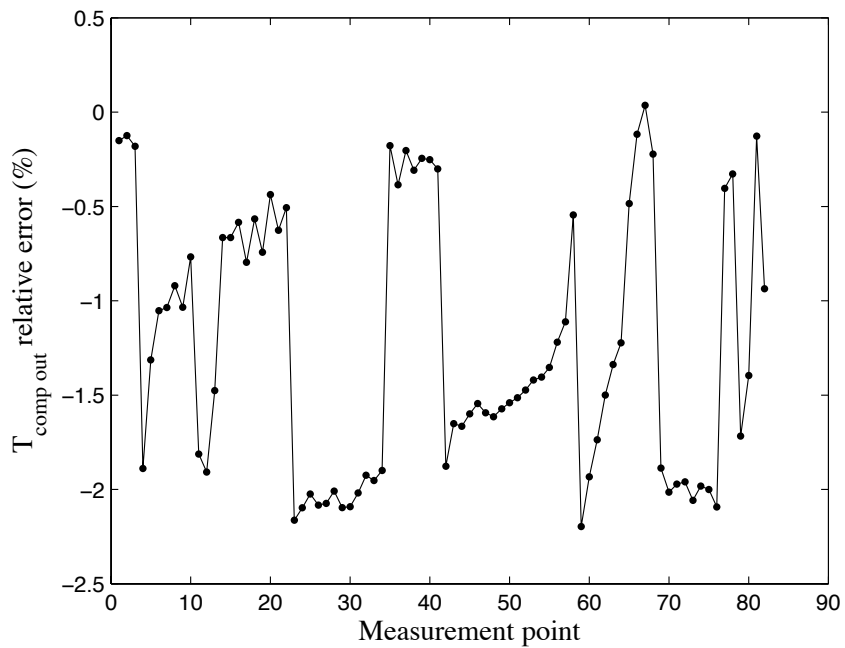


Figure 4-19: Discharge temperature relative error

The compressor comparison RMS errors are shown in Table 4-4. The compressor power, the most important output variable for the energy consumption analysis, shows a relative error of $\pm 5\%$ for the majority of points. Although it is important to predict this variable as accurately as possible, it is much to expect lower errors from in-situ (as opposed to test stand) measurements and with the simple compressor model as used in HPM.

RMS (%)		
f	Power	T_{comp_out}
2.58	4.55	1.42

Table 4-4: Compressor RMS errors for the compressor sub-model output variables

4.3. Condenser sub-model validation

For the condenser validation, four model variations (M1-M4) are analyzed the same way as for the evaporator sub-model.

The experimental data used as the model input parameters are:

- refrigerant mass flow rate – m_{ref_m}
- condenser inlet temperature (compressor outlet temperature) – $T_{comp_out_m}$
- condenser airflow rate – V_{o_m}
- outside air temperature – T_{o_m}
- subcooling temperature difference – ΔT_{sc_m}

The main condenser output variables that have been compared with the experimental data are:

- heat exchanged by the condenser – Q_c
- compressor outlet pressure – P_{comp_out}
- condenser outlet temperature – T_{c4}
- condenser outlet enthalpy – h_{liq}

For M1- M3 the compressor outlet pressure is equal to the condenser inlet pressure. For M4, the discharge line pressure drop ΔP_{dp} is determined and the compressor outlet pressure is calculated as:

$$P_{\text{comp_out}} = P_{c1} + \Delta P_{dp} \quad (107)$$

The important output parameters are the condenser outlet enthalpy and compressor outlet pressure. The pressure is relevant because it influences the compressor power consumption, and the outlet enthalpy is the important input to the evaporator sub-model.

Among the measured data, the compressor outlet pressure, condenser inlet and outlet temperatures and air temperatures have been measured directly, so one would expect they are most reliable. The enthalpy at the condenser outlet is calculated from the measured condenser outlet temperature and the assumption that the pressure at the condenser outlet is equal to the pressure measured after the compressor outlet. Since the liquid state properties depend much more on the temperature than on the pressure, the calculated outlet enthalpy most probably shows accurate values. The condenser heat is calculated from the refrigerant mass flow rate and condenser enthalpy differences, so those two variables are possible source of inaccuracies. The subcooling temperature difference is calculated from the measured condenser outlet temperature and the approximated condensing temperature, where the average condensing temperature is approximated making the assumption that the condensing pressure is equal to the pressure measured after the compressor.

Results of the condenser comparison for M1 - M4 are shown in Figure 4-20 – Figure 4-25. The condensing temperature has a big impact on the condensing pressure and compressor outlet pressure, which then influences the compressor power. The larger errors for M1 and M2 shown in Figure 4-20 are the consequence of the condenser constant UA value over-prediction (constant UA value is determined from the manufacturer's data for the standard operation point).

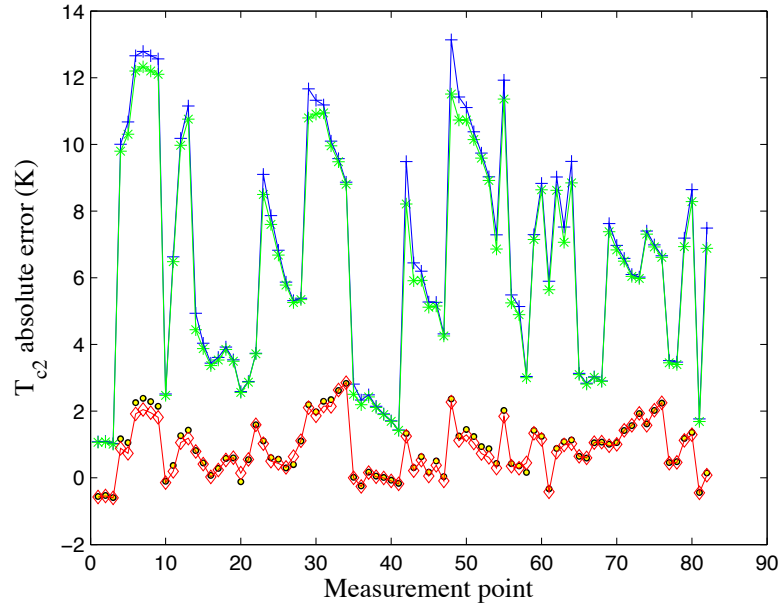


Figure 4-20: Condensing temperature relative error

Figure 4-21 shows the measured and calculated temperature differences between the refrigerant condensing temperature and outside air temperature for M3 and M4. When presented as a function of the condenser heat to air flow ratio, it can be seen that, different from the evaporator model, the calculated values for the condenser show good agreement with measured data.

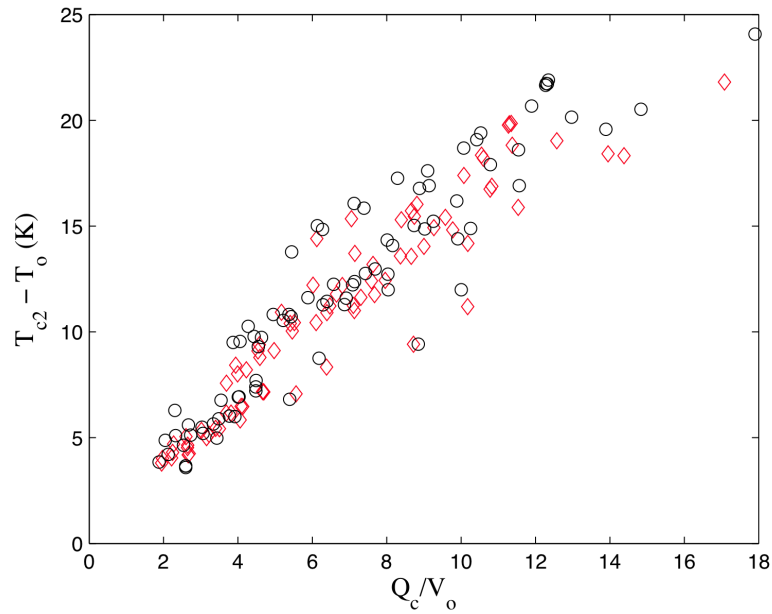


Figure 4-21: Temperature difference between the refrigerant evaporating temperature and zone temperature as a function of Q_c/V_o ; red are the calculated and black are the measured values

The measured subcooling temperature differences are the input to the condenser model. Because they are equal for M2 – M4, one would expect that the condenser outlet temperature errors will behave exactly the same as the condensing temperature errors. However, because the condensing temperatures for M2 were significantly lower than the measured temperatures for the majority of points, the measured subcooling was larger than physically possible for M2. For example, if the measured case is $T_o = 20\text{ }^{\circ}\text{C}$ and $T_c = 35\text{ }^{\circ}\text{C}$, it is possible to have $10\text{ }^{\circ}\text{C}$ subcooling. However, with the under-predicted $T_c = 28\text{ }^{\circ}\text{C}$, $10\text{ }^{\circ}\text{C}$ subcooling would not be physically feasible. The compressor sub-model solves this situation by changing the subcooling input from $10\text{ }^{\circ}\text{C}$ to what is physically feasible, (0.5 K above outside temperature is used as default in the code). Because of this unavoidable correction, the condenser outlet temperature errors show a somewhat different trend than the condensing temperature errors for M2.

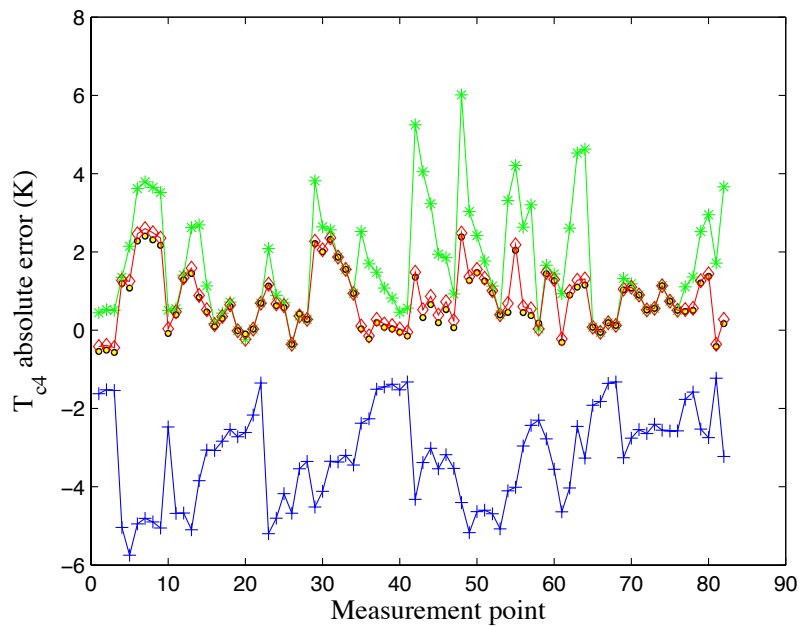


Figure 4-22: Condenser outlet temperature absolute error

The condenser outlet temperature most strongly influences the outlet enthalpy because the enthalpy is much more affected by the temperature than the pressure for the refrigerant liquid state. That can be seen in Figure 4-23, where the outlet enthalpy errors follow the same trend as the outlet temperature errors. Since the condenser outlet enthalpy is the input to the evaporator sub-model, the errors in the condenser outlet temperature can progress through the HPM.

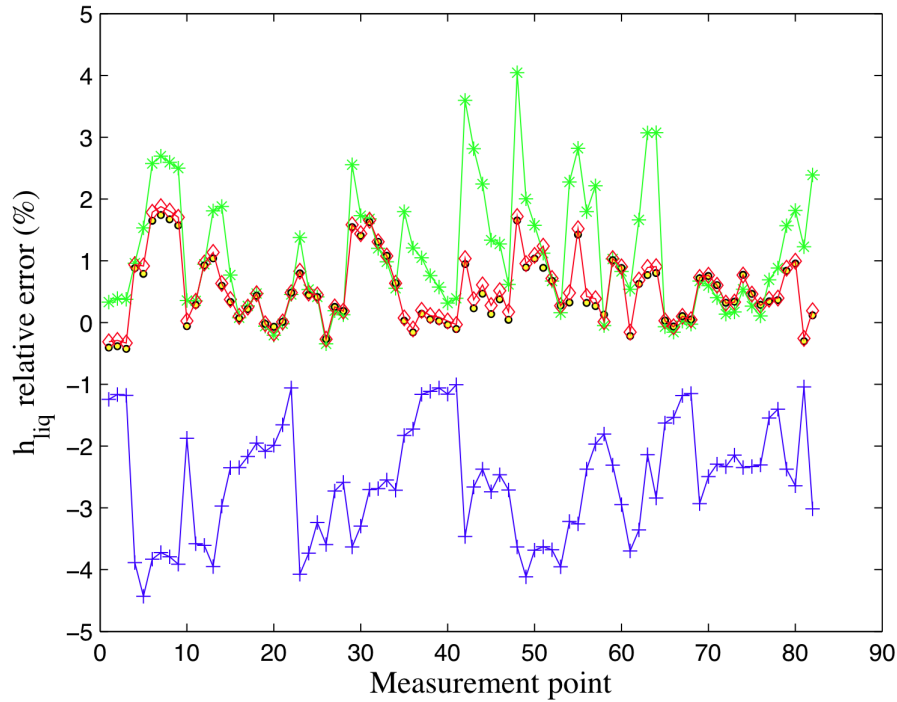


Figure 4-23: Condenser outlet enthalpy relative error

The errors in the predicted compressor outlet pressures for M3 and M4 are not as different as they were for the compressor inlet pressure (calculated from the evaporator sub-model). The first reason is the significantly lower condenser pressure drop than the evaporator pressure drop, due to larger densities. Also, the condensing pressure is higher than the evaporating pressure, so the pressure drop accounts for a much lower percentage of the total condensing pressure. For example, the calculated condenser pressure drop has an order of magnitude 10 – 60 kPa, which is approximately 1.5% of the condensing pressure, whereas the evaporating pressure has an order of magnitude 10 – 200 kPa, which is approximately 1 – 20% of the evaporating pressure. M1 and M2 show large errors in the pressure due to the errors in the condensing temperature, and these pressure errors can significantly influence the rest of the heat pump variables, especially the compressor speed and power consumption.

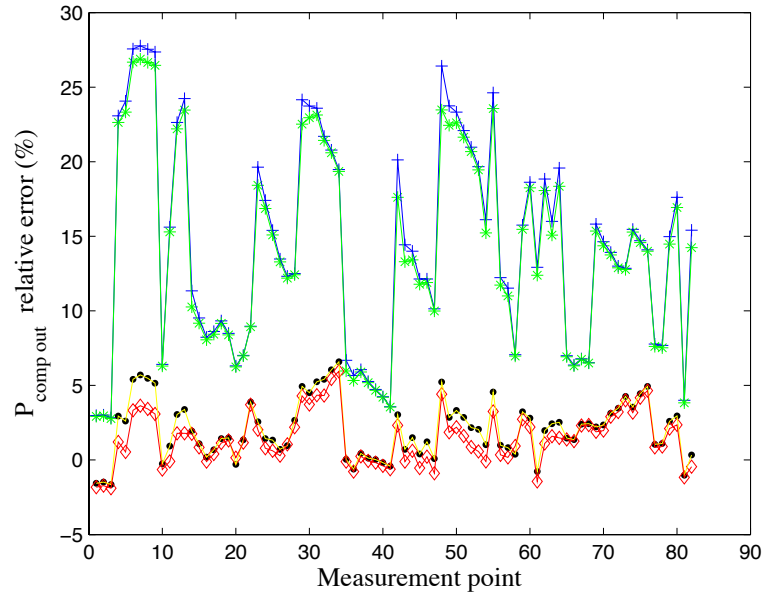


Figure 4-24: Compressor outlet pressure relative error

The condenser heat errors are influenced by the errors in the condenser outlet enthalpy and inlet pressure since the condenser heat is calculated from the mass flow rate and enthalpy differences (the mass flow rate and inlet temperature were inputs taken from the measurements). However, the condenser heat was not directly measured during experimental work but was determined from the airflow rate and air temperature differences, which has probably caused some errors in the condenser heat values (in measured data).

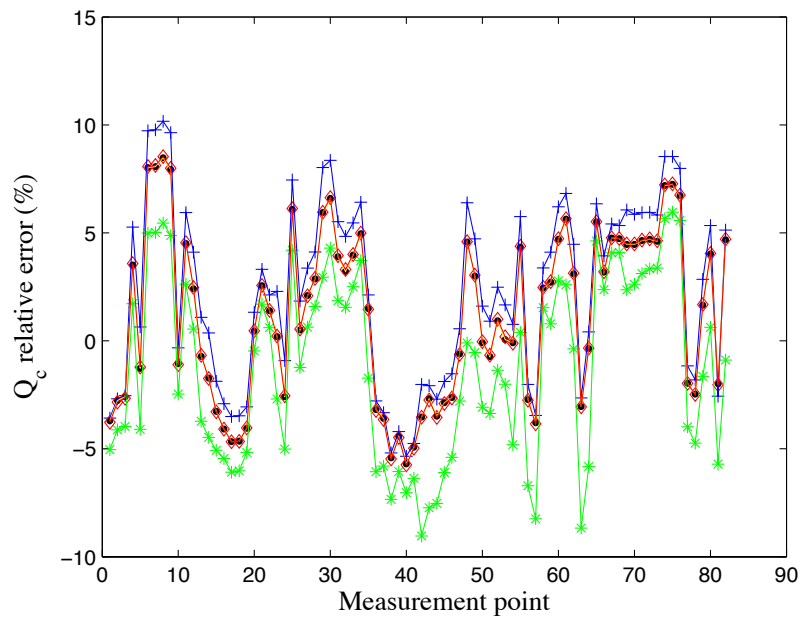


Figure 4-25: Condenser heat relative error

From the RMS errors in Table 4-5 it can be seen that there is almost no difference between M3 and M4 for the condenser parameters and the main reason are small pressure drops relative to the condensing pressure. The models M1 and M2 have significant errors in pressure and enthalpy predictions, and those errors will affect both the evaporator and compressor sub-model calculations.

	RMS (%)				
	Q_c	$P_{\text{comp_out}}$	T_{c2}	T_{c4}	h_{c4}
M1	4.80	15.95	2.31	1.12	2.74
M2	4.40	15.39	2.22	0.71	1.48
M3	4.08	2.86	0.39	0.34	0.74
M4	4.11	2.30	0.36	0.36	0.79

Table 4-5: Condenser RMS errors for output variables for 4 different models

4.4. System validation

The system model presented in Chapter 3 consists of the evaporator, compressor and condenser sub-models called in that order. For M4, which includes the pressure drop calculation, the suction line and discharge line pressured drops have been calculated between the evaporator and compressor sub-model and compressor and condenser sub-model. The system model convergence criterion is that the condenser outlet enthalpy and evaporator inlet enthalpies are equal and also that the assumed compressor inlet pressure is equal to the calculated condenser pressure decreased for the discharge pipe pressure drop. Heat losses or heat gains through suction and discharge pipes are assumed negligible, meaning that the evaporator outlet temperature is equal to the compressor inlet temperature and the compressor outlet temperature is equal to the condenser inlet temperature.

The measured values used as the system model input parameters are:

- cooling rate – Q_{e_m}
- evaporator airflow rate – V_{z_m}
- condenser airflow rate – V_{o_m}
- zone (room) air temperature – T_{z_m}

- ambient air temperature – T_{o_m}
- desuperheating temperature difference at the evaporator outlet – ΔT_{esh_m}
- subcooling temperature difference at the condenser outlet – ΔT_{sc_m}

The relevant output parameters compared with the measured data are:

- refrigerant mass flow rate – m_{ref}
- temperatures at the evaporator inlet and outlet – T_{e1}, T_{e3}
- pressure at the evaporator inlet – P_{e1}
- pressure at the compressor inlet and outlet – $P_{comp_in}, P_{comp_out}$
- compressor shaft speed – f
- compressor power – KW
- heat exchanged on the condenser – Q_c
- temperatures at the condenser inlet and outlet – T_{c1}, T_{c4}
- temperature at end of desuperheating region – T_{c2} ,
- enthalpy at condenser outlet – h_{liq}
- COP

For the whole model simulation, the evaporator temperatures and pressures errors are the same as in the evaporator sub-model validation section since the input cooling rate, airflow and zone temperature are the same (Figure 4-26 – Figure 4-29).

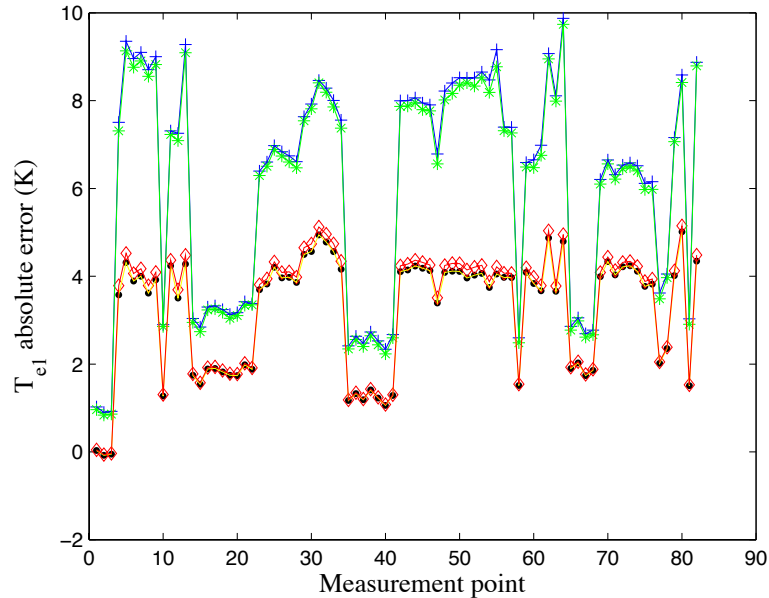


Figure 4-26: Evaporator inlet temperature absolute error

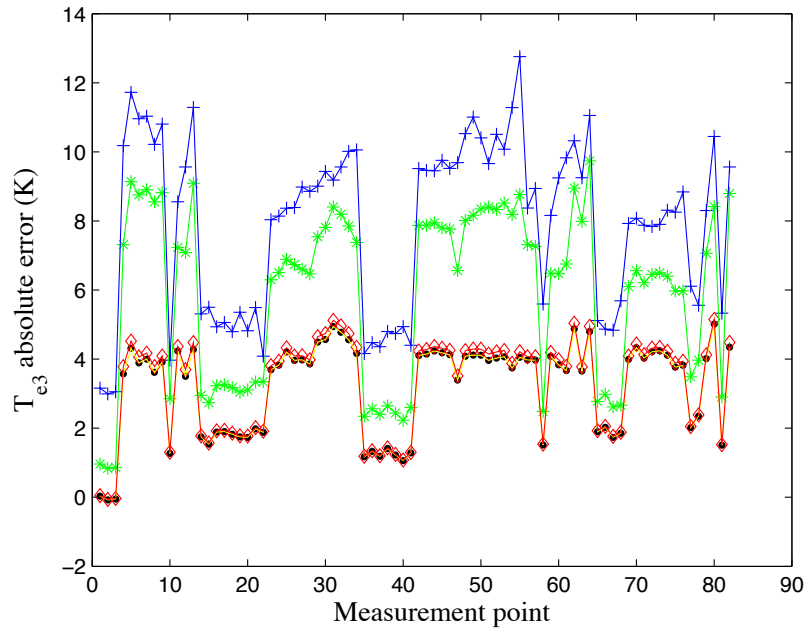


Figure 4-27: Evaporator outlet temperature absolute error

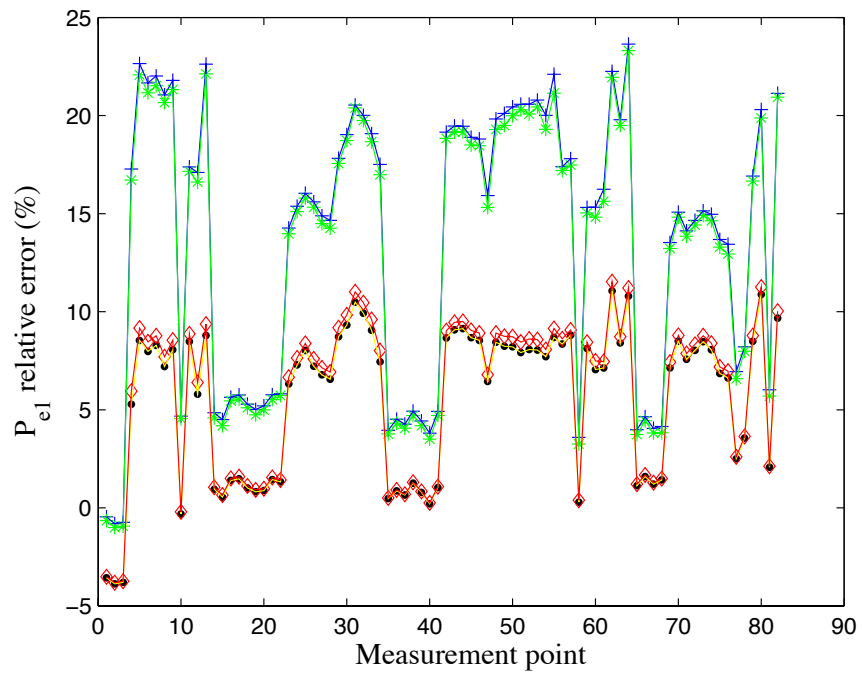


Figure 4-28: Evaporator inlet pressure relative error

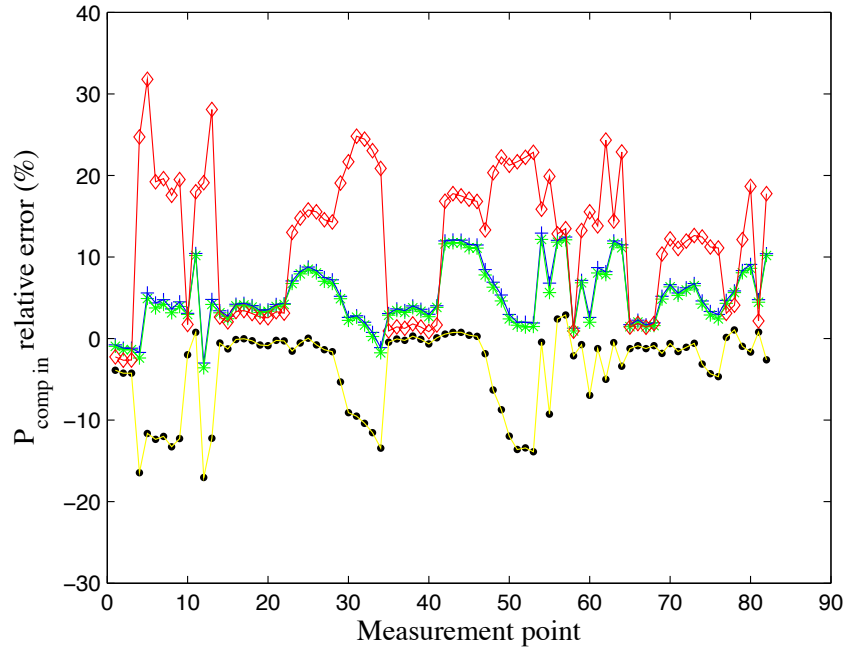


Figure 4-29: Compressor inlet pressure relative error

The mass flow rate errors (Figure 4-30) are different than for the evaporator sub-model because of the errors in the condenser outlet enthalpy (Figure 4-31). For the evaporator validation, the refrigerant mass flow rate was slightly over-predicted for M4 and much more over-predicted for M2 – M4. For the whole model validation, the predicted condenser outlet enthalpy (same as evaporator inlet enthalpy) is slightly lower than the measured value for M2, M3 and M4, which causes the increase in the evaporator enthalpy difference and decrease in mass flow rate. The end result are smaller errors in mass flow rate for M2, M3 and M4, but it is important to note that the smaller errors are purely due to the errors in condenser outlet enthalpy. The mass flow rate errors for M1 are even larger than for the evaporator validation, again due to the enthalpy errors that have an opposite trend for M1 (tend to over-predict the enthalpy). The enthalpy errors shown in Figure 4-31 are the result of the condenser outlet temperature errors shown later on in Figure 4-39.

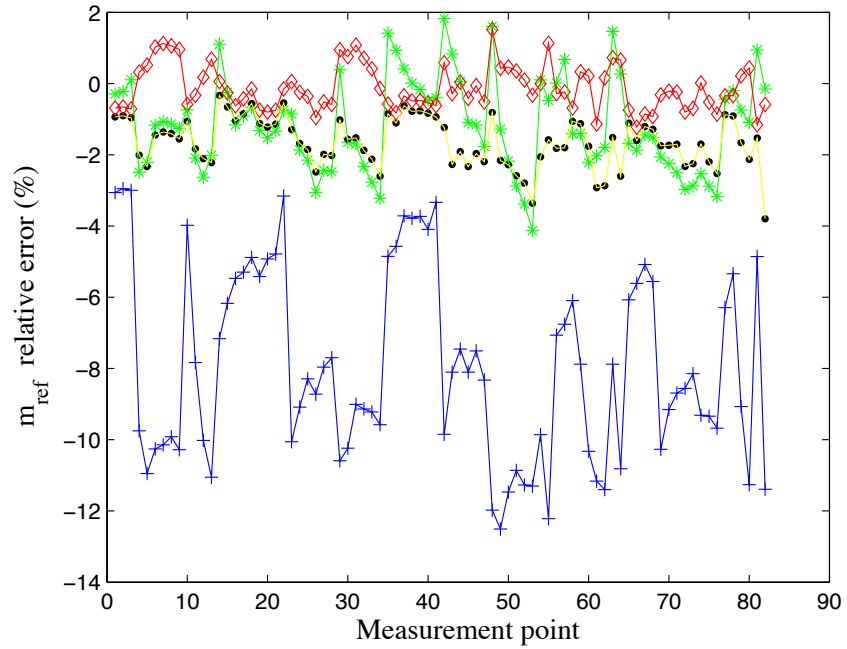


Figure 4-30: Refrigerant mass flow rate relative error

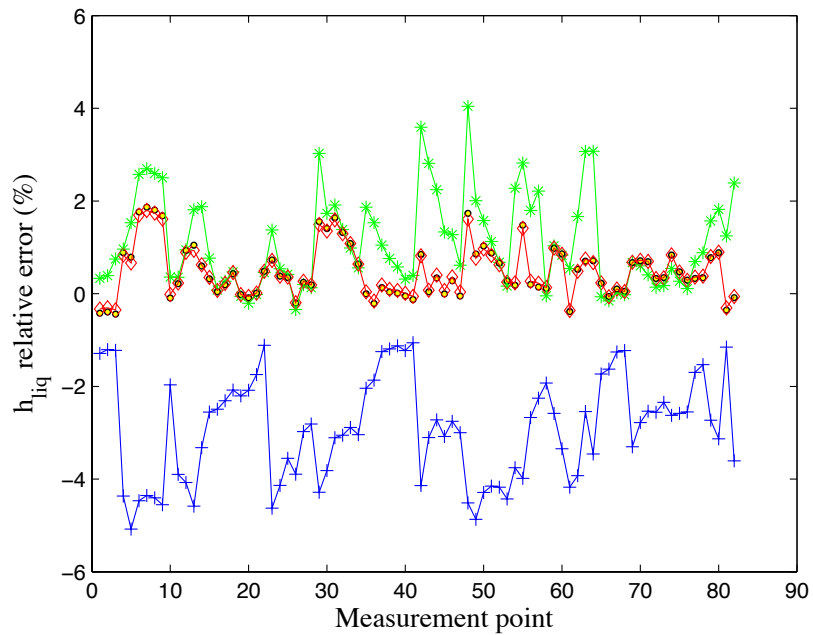


Figure 4-31: Condenser outlet enthalpy relative error

The compressor outlet pressure errors shown in Figure 4-32 also show similar behavior as for the condenser validation (Figure 4-24). Smaller differences from the condenser validation occur due to changes in the compressor outlet temperature and condenser heat (different from the measured values).

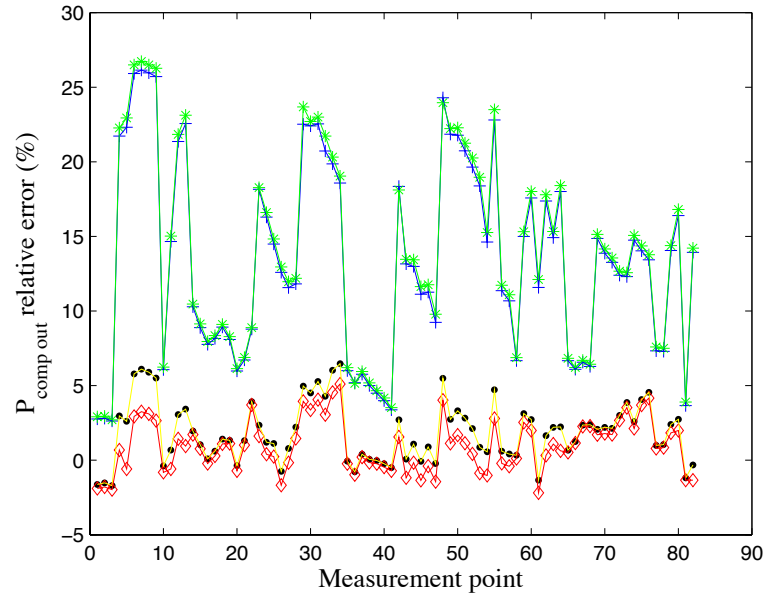


Figure 4-32: Compressor outlet pressure relative error

Although the compressor outlet pressure prediction is satisfying for M3 and M4 and not so much for M1 and M2, the compressor ratio errors show a somewhat different picture (Figure 4-33). The reason for these discrepancies lies with the large compressor inlet pressure errors for M4, which are again caused by the evaporating temperature errors, as mentioned before. The errors in pressure ratio can significantly influence the compressor speed and power calculations and hence, it is crucial to minimize them.

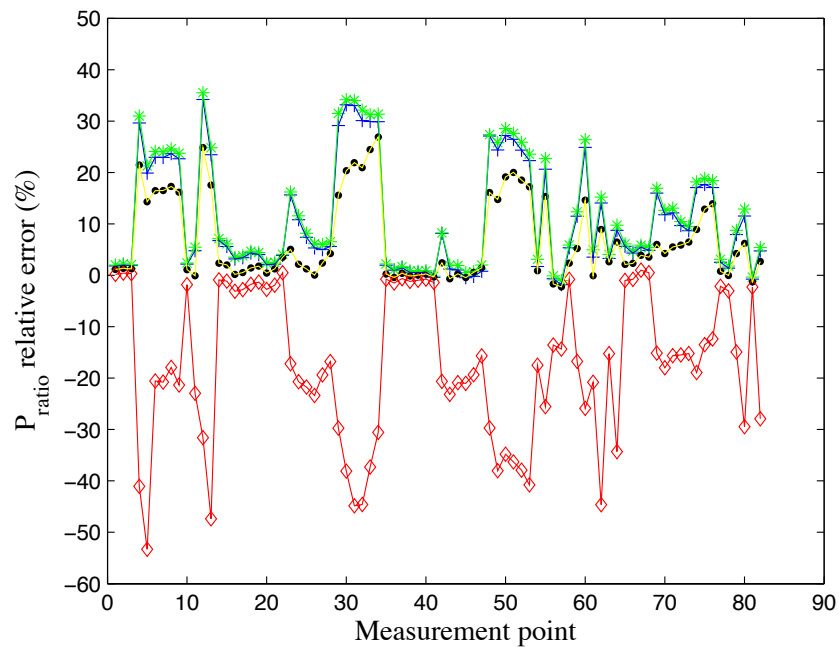


Figure 4-33: Pressure ratio relative error

In Figure 4-34 and Figure 4-35 it can be seen how the combination of the mass flow rate errors, compressor inlet temperature and pressure errors and compressor outlet pressure errors influence the compressor speed and power consumption. Although pressure ratio errors, mass flow rate errors and compressor outlet pressure errors influence other compressor parameters, the compressor inlet temperature and pressure have an even larger influence. The compressor inlet temperature and pressure influence the refrigerant volumetric flow rate, which then has a great effect on the compression process. One can see the sensitivity of the compressor process on the compressor inlet state from the results for M1 and M4. The model variation M4 that has the best prediction of the mass flow rate, evaporating temperatures and compressor outlet pressure among all four models. However, the large errors in the compressor inlet pressure have resulted in large compressor speed and power errors. On the other hand, the simplest model, M1, has shown the largest errors in mass flow rate, compressor inlet temperature and compressor outlet pressure prediction. But because the errors in the compressor inlet pressure are smaller than for M4, the predicted compressor speed and power are much closer to the measured values.

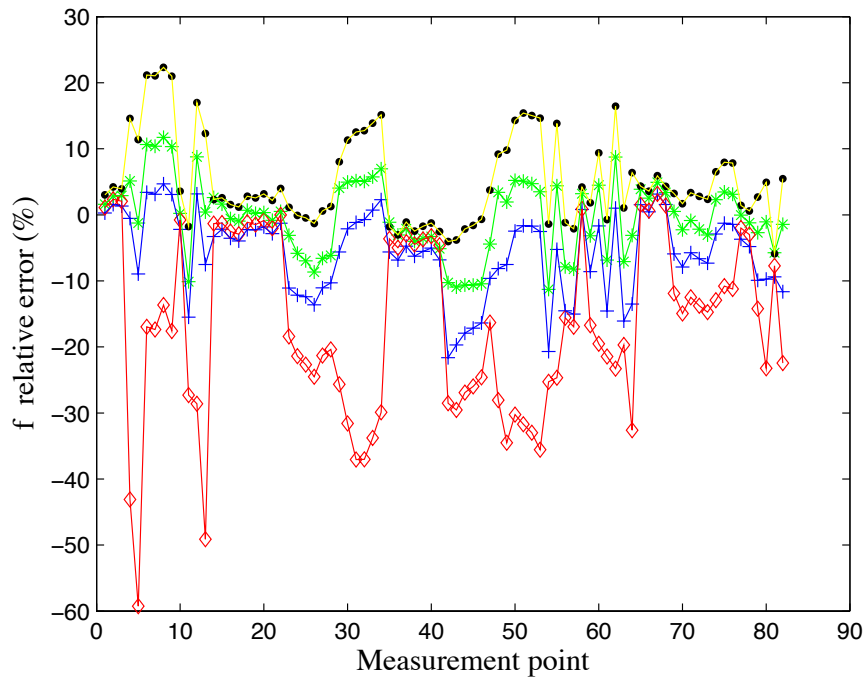


Figure 4-34: Compressor shaft speed relative error

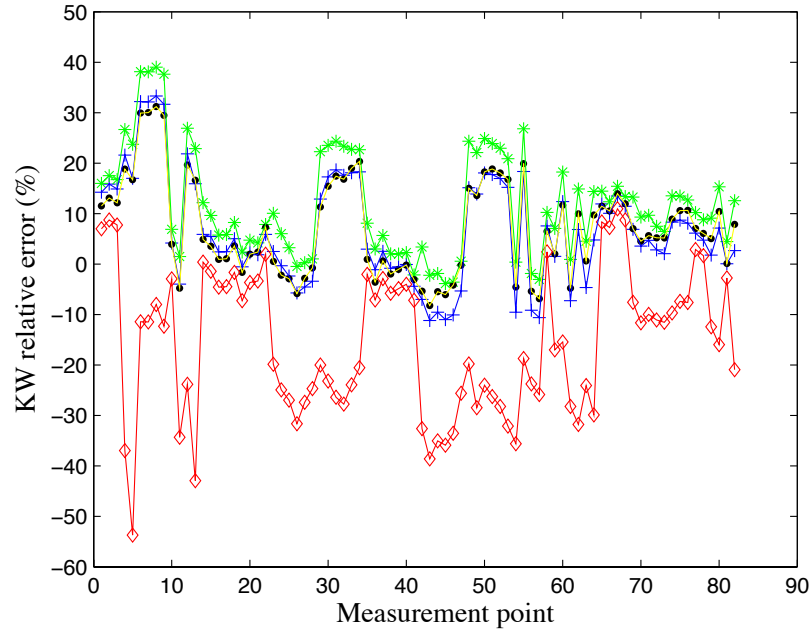


Figure 4-35: Compressor power relative error

The compressor outlet temperature is calculated from the compressor heat balance, so the errors in the temperature shown in Figure 4-36 follow the errors in the compressor power. The compressor sub-model validation has shown that in the case when the compressor power is equal to the measured power, the model tends to over-predict the compressor outlet temperature for up to 2%. The errors shown for the whole system comparison for M4 are significantly larger, as the result of the compressor power over prediction. Also, the power under-prediction for M1 – M3 is the reason for the large compressor temperatures under-prediction.

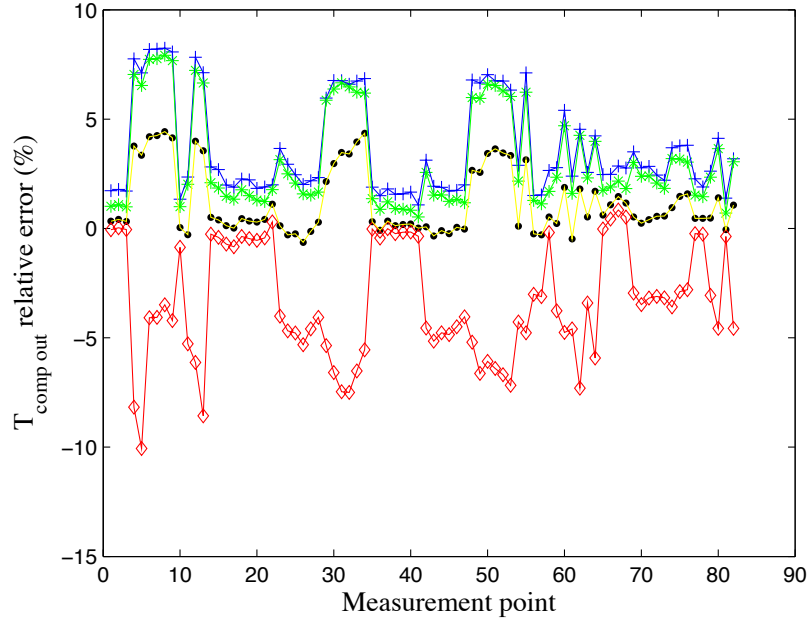


Figure 4-36: Compressor outlet temperature relative error

Since for the closed cooling cycle the sum of the cooling rate and compressor power needs to be equal to the condenser heat, the changes in the compressor power have also influenced the condenser heat, as can be seen in Figure 4-37. However, relative changes in the condenser heat were not so large as to significantly influence the condensing temperature, so the condenser temperature errors (Figure 4-38 and Figure 4-39) show very similar values as for the condenser sub-model validation.

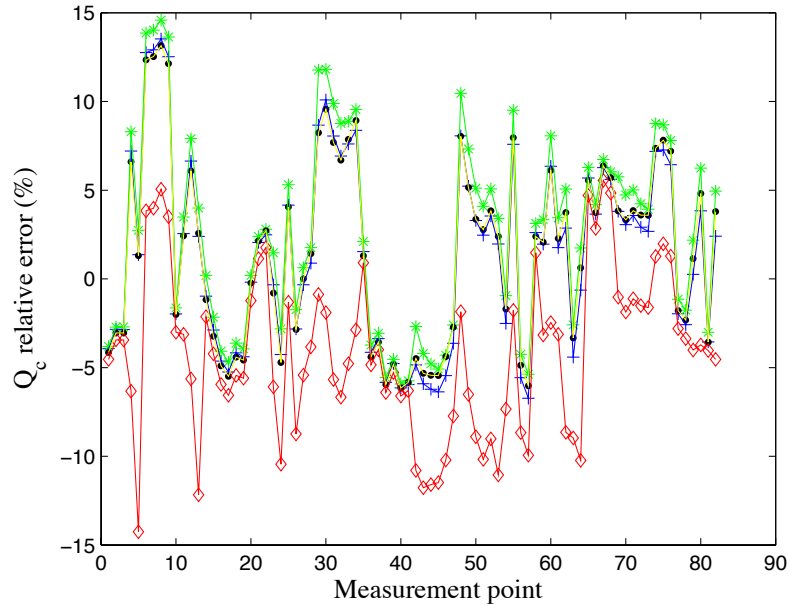


Figure 4-37: Condenser heat relative error

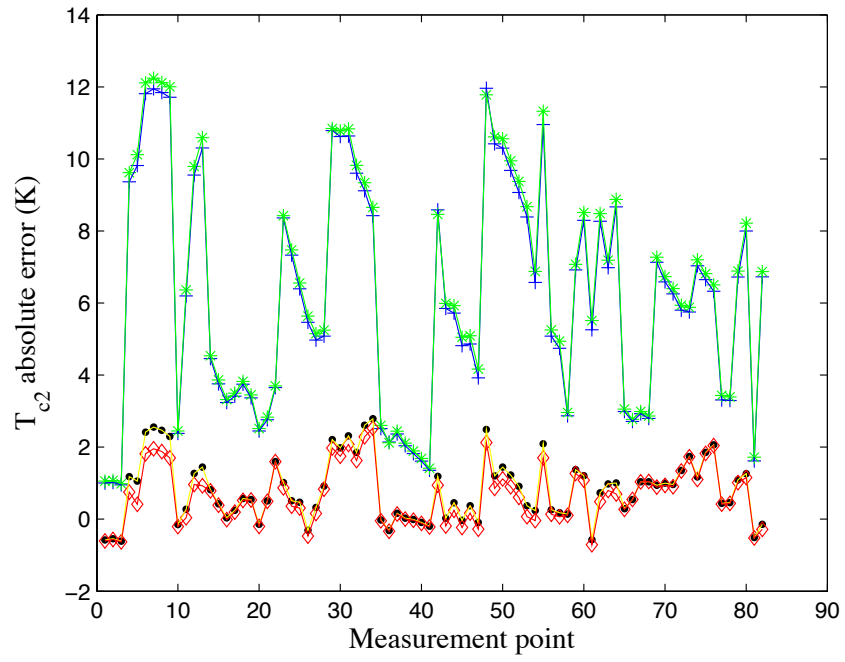


Figure 4-38: Condensing temperature absolute error

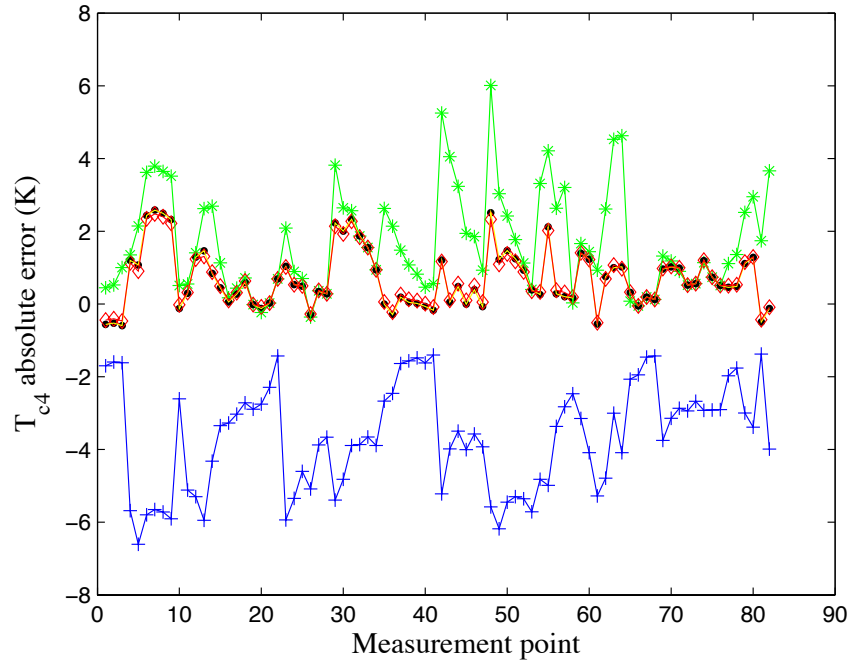


Figure 4-39: Condenser outlet temperature absolute error

The COP value is equal to the cooling rate to total power consumption ratio. Because the compressor power is different than the measurement, the compressor power errors shown in Figure 4-35 determine the COP errors (Figure 4-40).

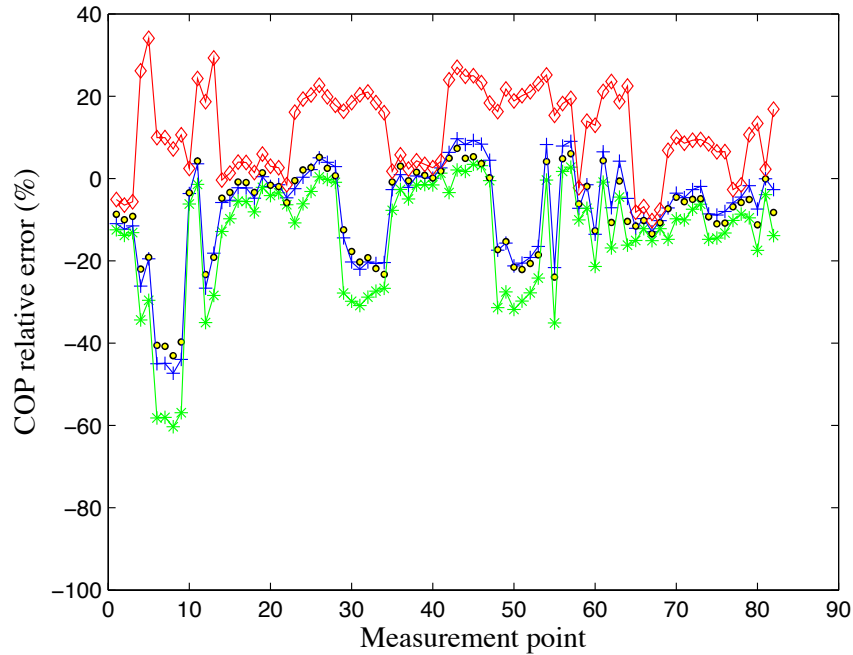


Figure 4-40: COP relative error

It can be seen from the comparison results that for most of the error metrics models M3 and M4 show better agreement with the measured data compared with the simple models M1 and M2. However, both models show significant errors for the COP value, the most important parameter in the energy consumption analysis. The large errors in COP for M4 are somewhat related to the errors in the compressor power correlation, but are much more related to the errors in the evaporating temperature. The error in temperature causes significant compressor inlet pressure error due to the reasons explained before. Since the compressor inlet state influences the pressure ratio and refrigerant volumetric flow rate, both of which have a strong impact on the compression process, it all results in large compressor power errors.

	RMS (%)				
	m_{ref}	T_{e1}	T_{e3}	P_{e1}	P_{comp_in}
M1	8.38	2.35	2.95	15.24	6.39
M2	1.75	2.30	2.29	14.91	6.08
M3	1.78	1.25	1.24	6.78	6.29
M4	0.64	1.29	1.28	7.12	14.95
	P_{comp_out}	P_{rat}	f	KW	T_{comp_out}
M1	14.94	0.90	8.52	12.34	4.25
M2	15.28	0.97	5.57	15.86	3.84
M3	2.77	0.41	8.43	11.82	1.91
M4	2.00	0.73	21.41	20.97	4.25
	Q_c	T_{c2}	T_{c4}	h_{liq}	COP
M1	5.44	2.15	1.29	3.12	14.71
M2	6.10	2.20	0.72	1.50	20.37
M3	5.39	0.38	0.35	0.75	13.98
M4	6.17	0.32	0.34	0.72	15.52

Table 4-6: System RMS errors for output variables for 4 different models

If the evaporating temperature showed better agreement with the measured data, the COP determined by M4 would show the best agreement with measured data among four model variations (Table 4-7). This will be shown using the same 20% increase in the evaporator airflow compared to the measured data. For this case, evaporator temperature errors decrease for all four models, but while for the M3 and M4 the predicted temperatures are close to the measured, for M1 and M2 the discrepancy between the predicted and measured values is still very large (Figure 4-41).

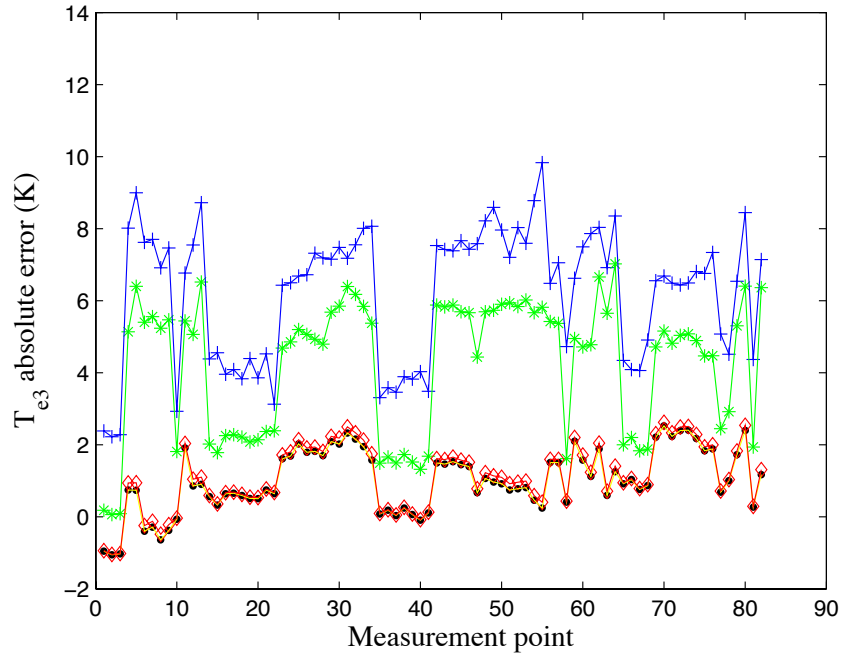


Figure 4-41: Evaporator outlet temperature absolute error for 20% larger evaporator airflow than the measured values

The changes in the evaporator temperatures will change the compressor inlet pressure and compression ratio, where now M4 shows the best prediction (Figure 4-42 and Figure 4-43).

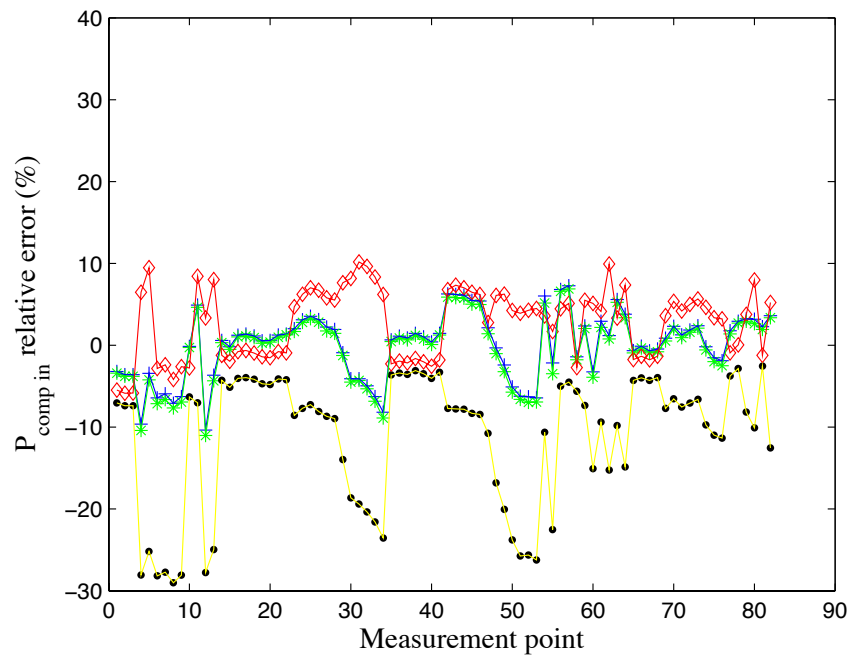


Figure 4-42: Compressor inlet pressure relative error for 20% larger evaporator airflow than the measured values

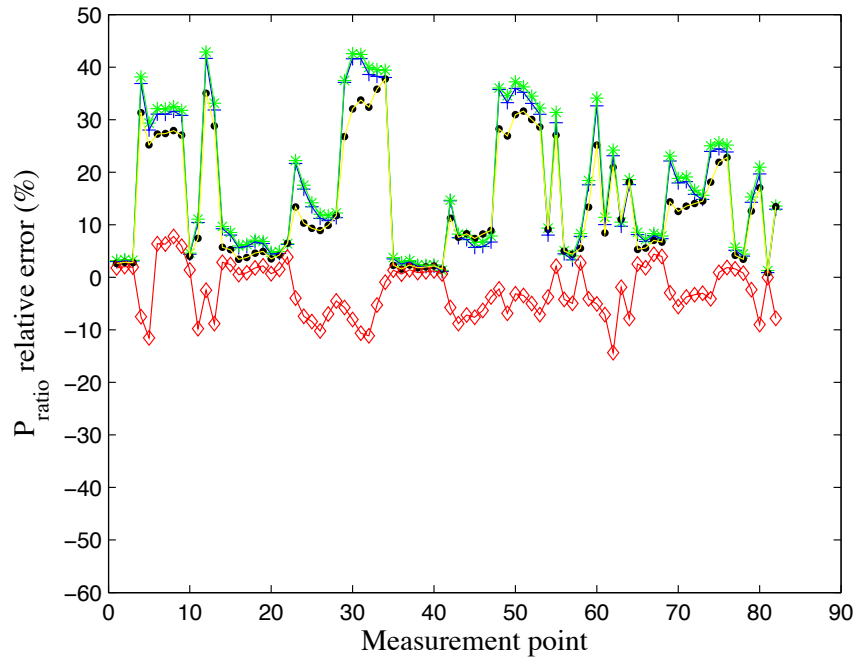


Figure 4-43: Pressure ratio relative error for 20% larger evaporator airflow than the measured values

Figure 4-44 and Figure 4-45 show that as expected, the compressor power and heat pump COP errors have significantly decreased for M4 and increased for M1 – M3. These changes are entirely due to better prediction of the evaporating temperature.

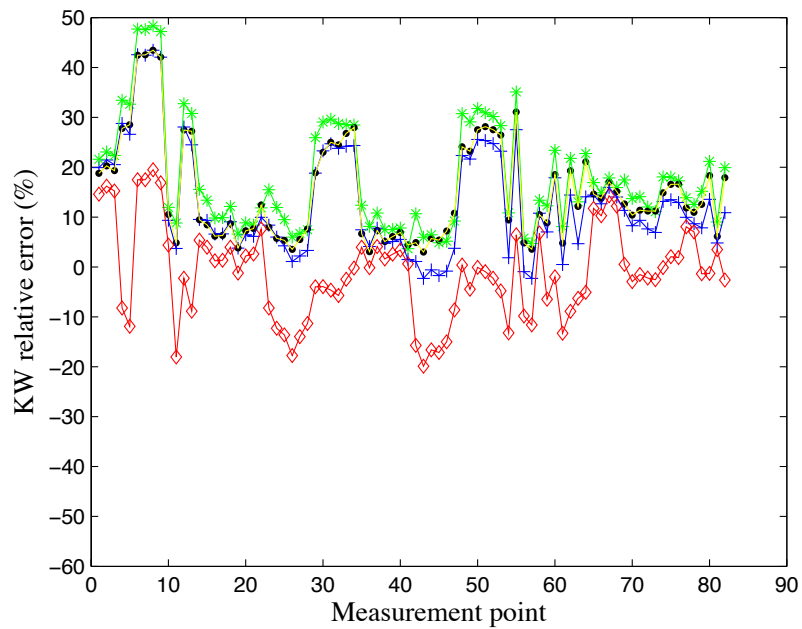


Figure 4-44: Compressor power relative error for 20% larger evaporator airflow than the measured values

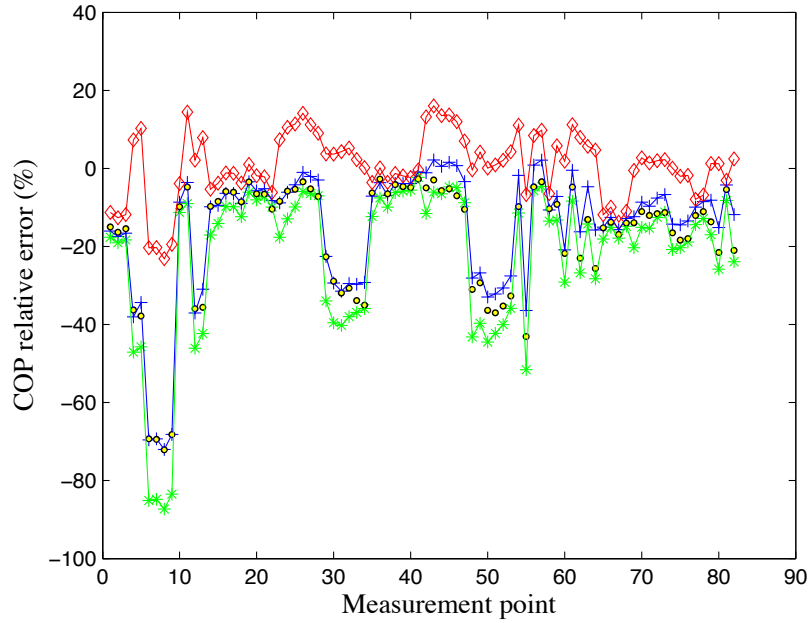


Figure 4-45: COP relative error for 20% larger evaporator airflow than the measured

It can be seen from Table 4-7 that when the evaporating temperatures are less than 2 K under-predicted, M4 shows the best agreement with measured data. For larger under-prediction, the compressor inlet pressure shows large errors for M4 and those errors result in large compressor power and heat pump COP errors.

	RMS (%)				
	m_{ref}	T_{e1}	T_{e3}	P_{e1}	P_{comp_in}
M1	8.10	1.70	2.31	10.42	3.98
M2	1.58	1.66	1.65	10.06	4.09
M3	1.47	0.48	0.48	2.61	13.79
M4	0.61	0.52	0.51	2.58	5.04
	P_{comp_out}	P_{rat}	f	KW	T_{comp_out}
M1	14.98	1.35	6.07	16.78	4.91
M2	15.30	1.42	8.20	20.92	4.48
M3	2.93	1.04	14.45	18.08	2.68
M4	2.18	0.06	6.83	9.32	1.86
	Q_c	T_{c2}	T_{c4}	h_{liq}	COP
M1	6.16	2.16	1.28	3.10	22.46
M2	6.91	2.21	0.71	1.48	29.38
M3	6.37	0.40	0.37	0.79	24.01
M4	4.43	0.35	0.36	0.78	8.51

Table 4-7: System RMS errors for output variables for 20% larger evaporator airflow than the measured values

The two simpler models M1 and M2 did not give satisfying estimation for COP for the case with 20% larger airflows. One can argue that the results would be better if the evaporator and condenser UA values were estimated more accurately. In that case, M1 and M2 errors would behave in similar fashion as for the model M3.

The model M3, which calculates the heat transfer coefficients for the heat exchanger geometry and given airflow rate, and which also includes evaporator desuperheating and condenser subcooling, did perform better than the simpler models for the most parameters. However, it does not take into account pressure drops in heat exchangers; these can cause significant errors for the evaporator, where pressure drops account for up to 20% of the evaporating pressure. The errors in the evaporator outlet pressure lead to serious under-predictions of the compressor speed and power consumption.

Finally, from the M4's comparison results it can be concluded that this was the only model that has shown good COP agreement with measured data for the case when the evaporator temperatures were well predicted (for less than 2K under-prediction). The condenser sub-model has shown the best accuracy between all three component sub-models, while the evaporator sub-model seems to be the most problematic. If the evaporator sub-model under-predicts the evaporating temperatures more than 2 K, it is not accurate enough for further energy consumption analysis since that error strongly influences the compressor inlet state, which then results in large compressor speed and power consumption predictions. In the future work the evaporator sub-model will be revisited to improve sub-model accuracy.

Chapter 5: Heat pump optimization

The heat pump model presented in Chapter 3 can be used to calculate heat pump performance for given input parameters: the cooling rate Q_e , zone temperature T_z , ambient temperature T_o , evaporator airflow V_z (or fan RPM), condenser airflow V_o (or fan RPM), evaporator desuperheating ΔT_{esh} , and condenser subcooling ΔT_{sc} . If the desuperheating and subcooling calculation option is turned off, only Q_e , T_z , T_o , V_z , and V_o need to be specified, and evaporator desuperheating and condenser subcooling are assumed to be zero. The same model can also be used to find the combination of input parameters that will give the optimal heat pump performance, meaning the lowest power consumption and maximum COP. By changing the evaporator and condenser airflow rate for a given cooling rate, zone and ambient temperature, desuperheating and subcooling temperature difference, the compressor speed and power will also change. For example, for an evaporator and condenser airflow increase, the compressor speed and power consumption will decrease, and the evaporator and condenser fan power will increase. The optimization algorithm can be used to find the airflows (and the corresponding compressor speed) for which the sum of the compressor power and fan power will be minimal. Although the final goal is to implement one of MATLAB's built-in optimization functions, the optimization is at this stage preformed using a grid search.

During the measurements, the “Mr. Slim” control algorithm has not been used, so the measured points do not have optimal fan and compressor speeds for given cooling load, zone and ambient conditions. However, the grid search was performed to analyze, first, how the predicted optimal operating point and maximum COP relate to the measured points for a given set of input parameters, and second, the sensitivity of COP values to different parameters. Because the model has some errors in predicted COP values compared with the measured data (Table 4-6) for the same input parameters, the maximum predicted COP was not directly compared with measured COP (COP_m). Instead, COP_m^* is calculated using measured Q_{e_m} , T_{z_m} , T_{o_m} , V_{z_m} , V_{o_m} , ΔT_{esh_m} , and ΔT_{sc_m} as inputs to the model, and then the maximum COP_{max} is found by changing:

- a) V_o (done for M1-M4)
- b) V_o and ΔT_{sc} (done only for M4)
- c) V_o and V_z (done only for M4)

The results of the comparison between the predicted optimal point and measured non-optimal point indicate the potential of optimizing the fan airflows and condenser subcooling. The predicted optimal points and their comparison with measured data are shown for each point and four model variations (M1 – M4) in Appendix B. A few example points will be more closely analyzed in this chapter.

5.1. Condenser airflow optimization

The first optimization is performed for all four model variations (M1-M4) using the grid search method for given: Q_{e_m} , T_{z_m} , T_{o_m} , V_{z_m} , ΔT_{esh_m} , and ΔT_{sc_m} . All input parameters, except the condenser airflow V_o , were taken from the measured data and the optimization variable V_o is changed in 0.05 m³/s increments to find the lowest power consumption and the corresponding COP_{max} . For the comparison, COP_m^* is calculated using the same measured data for inputs, and also measured V_{o_m} . The optimization and comparison results are given in Appendix B.

The condenser airflow rate influences the condensing temperature according to Equation (45). The condenser airflow change does not change UA values for M1 and M2 since they assume constant UA values (not a function of airflow), but it influences the air-side capacitance. In the model variations M3 and M4, both the UA value and the air-side capacitance change with airflow change. The fact that COP did not change significantly indicates that the COP value is not very sensitive to the condenser airflow. To understand this better, the results for the measurement point 8 will be more closely analyzed for M4. The measured airflow for that point is 0.44 m³/s and the predicted optimal airflow is 0.6 m³/s, while COP_m^* and COP_{max} are 3.2 and 3.3. The explanation for this trend can be seen if one plots how the power consumption for point 8 changes with the condenser airflow change (all other inputs stay constant):

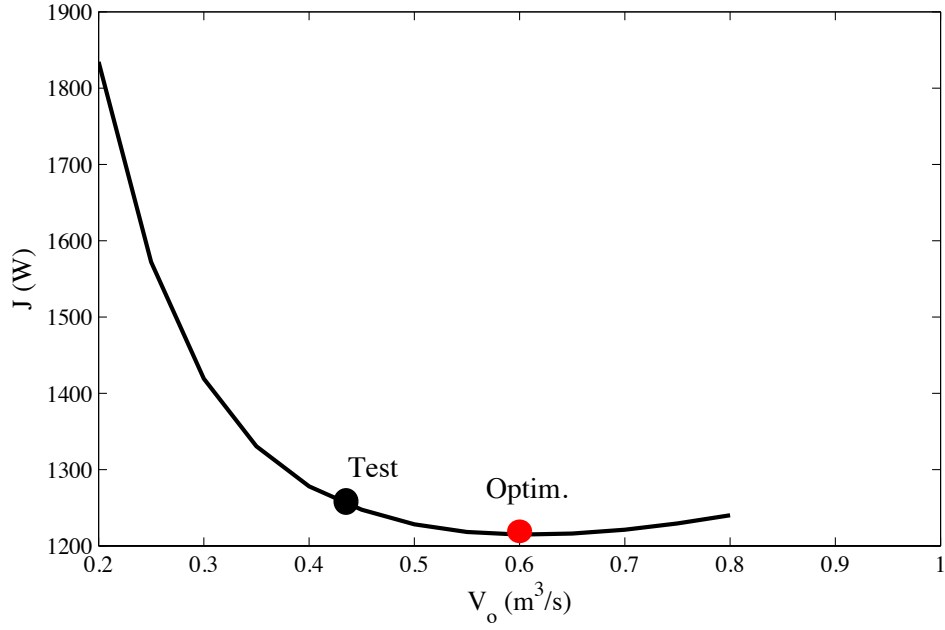


Figure 5-1: Total power consumption versus condenser airflow
for measurement point 8
($Q_e = 4048$ W, $T_z = 34$ °C, $T_o = 17$ °C, $\Delta T_{esh} = 1.5$ °C, $\Delta T_{sc} = 17.6$ °C)

The relevant parameters for the condensing region of the condenser are shown in Table 5-1 for the point 8. It can be seen that the combination of changes in the thermal capacitance and thermal effectiveness is not large enough to change the condensing temperature significantly (column 8 in the table shows the difference between the outside and condensing temperature).

	1	2	3	4	5	6	7	8
	V_o (m ³ /s)	h_{ex} (W/m ² K)	U_c (W/m ² K)	C_c (W/K)	ϵ_c (-)	$C_c * \epsilon_c$ (W/K)	Q_c (W)	$Q_c / (C_c * \epsilon_c)$ (K)
Meas.	0.44	57	1524	295	0.58	170	3381	19.9
Opt.	0.60	66	1683	360	0.51	181	3396	18.8

Table 5-1: Parameters for condensing region of the condenser for measured and optimal
condenser airflow for measurement point 8
($Q_e = 4048$ W, $T_z = 34$ °C, $T_o = 17$ °C, $\Delta T_{esh} = 1.5$ °C, $\Delta T_{sc} = 17.6$ °C)

As a different example we can take the measurement point 22, for which the power consumption changes more dramatically than for the point 8.

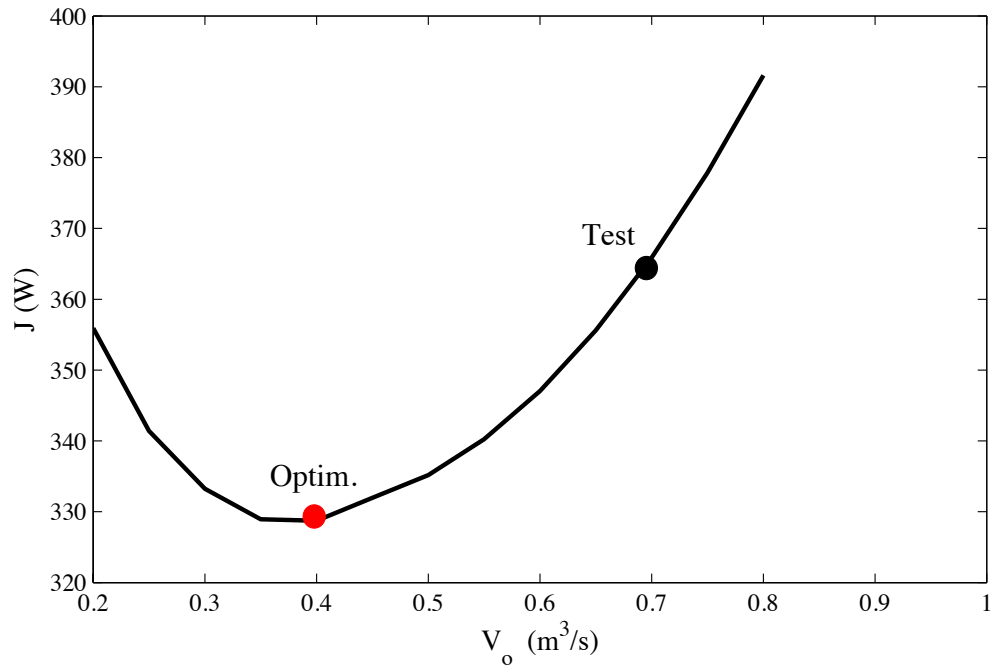


Figure 5-2: Total power consumption versus condenser airflow for measurement point 22
 $(Q_e = 1375 \text{ W}, T_z = 14 \text{ }^\circ\text{C}, T_o = 30 \text{ }^\circ\text{C}, \Delta T_{esh} = 0.7 \text{ }^\circ\text{C}, \Delta T_{sc} = 5 \text{ }^\circ\text{C})$

The measured and optimal airflows are 0.7 and 0.4 m³/s, and the total power consumption curve is relatively steep in that range (Figure 5-2). However, the absolute change in power increases COP for only 10 % (Table 5-2), which is still not as significant a change as when the evaporator airflow rate is optimized (Appendix B, Figure B- 12).

	Q_e (W)	m_{ref} (kg/s)	f (Hz)	J_e (W)	J_c (W)	KW (W)	J (W)	COP (-)
Measured	1375	0.0066	30	20	69	277	366	3.8
Optimal	1375	0.0066	30.5	20	15	293	328	4.2

Table 5-2: Parameters for measured and optimal condenser airflow for point 22

$$(Q_e = 1375 \text{ W}, T_z = 14 \text{ }^\circ\text{C}, T_o = 30 \text{ }^\circ\text{C}, \Delta T_{esh} = 0.7 \text{ }^\circ\text{C}, \Delta T_{sc} = 5 \text{ }^\circ\text{C})$$

5.2. Condenser airflow and subcooling optimization

The optimization is performed with model variation M4 using the condenser airflow V_o and subcooling temperature difference ΔT_{sc} as the optimization variables and the measured data Q_{e_m} , T_{z_m} , T_{o_m} , V_{z_m} , and ΔT_{esh_m} as other inputs to the model. In the grid search, the optimization variable V_o is changed in 0.05 m³/s increments and ΔT_{sc} in 2 K increments to find the lowest power consumption and corresponding COP_{max} . As explained in the previous section, COP_m^* is calculated using the same measured data for inputs and also measured V_{o_m} and ΔT_{sc_m} . The optimization results for M4 are given in Appendix B.

It is shown in the previous section that a change in the condenser airflow did not have a big influence on the COP value. One would expect that the subcooling temperature difference will have a noticeable impact, since larger subcooling requires a larger condenser heat transfer area or higher condensing temperature for the same area. However, the increase in subcooling can also result in a lower condenser outlet enthalpy and corresponding evaporator inlet enthalpy (they are equal in the model). Lower evaporator inlet enthalpy means higher enthalpy difference across the evaporator, lower refrigerant mass flow rate for the given cooling load, and lower compressor power due to the lower mass flow rate. The end result is a lower heat exchanged at the condenser (equal to the sum of the cooling rate and compressor power), which then lowers the condensing temperature (for the same airflow).

The sensitivity of COP to the subcooling temperature difference will be closely analyzed for the same measurement point 8. The measured condenser airflow and subcooling temperature difference for that point are 0.44 m³/s and 17.8 K and the predicted values are 0.8 m³/s and 8 K. The measured and optimal cooling process is shown in the same T-s diagram in Figure 5-3, where black represents the process with measured and red the process with optimal values.

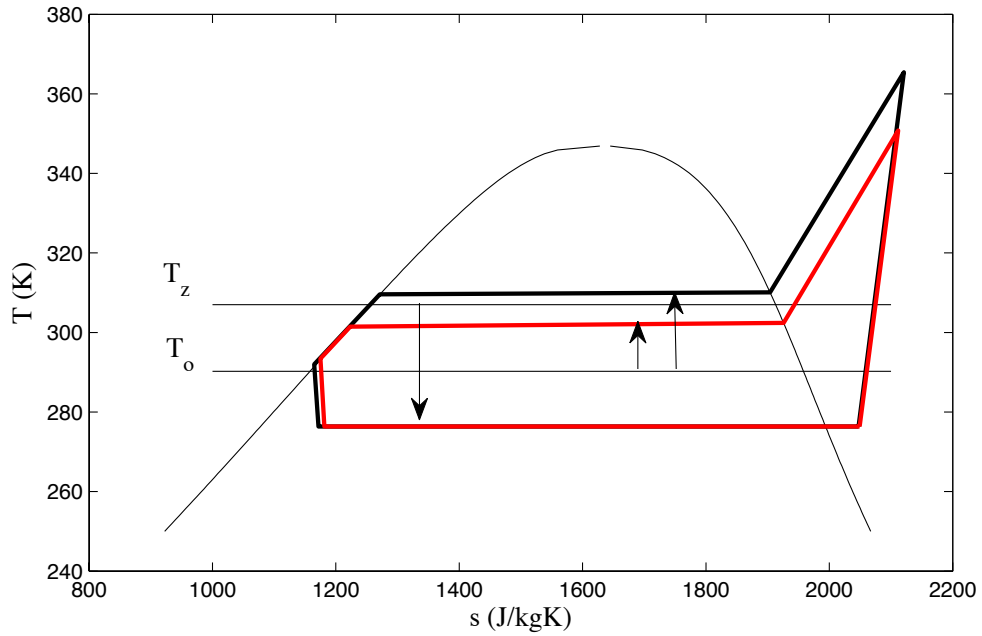


Figure 5-3: Cooling process T-s diagram for measured and optimal predicted condenser airflow and subcooling temperature difference for point 8

From the graph that shows how the total power changes with the change in condenser airflow and subcooling (Figure 5-4), it can be seen that for this particular point subcooling has an even smaller impact on the total power than the condenser airflow rate.

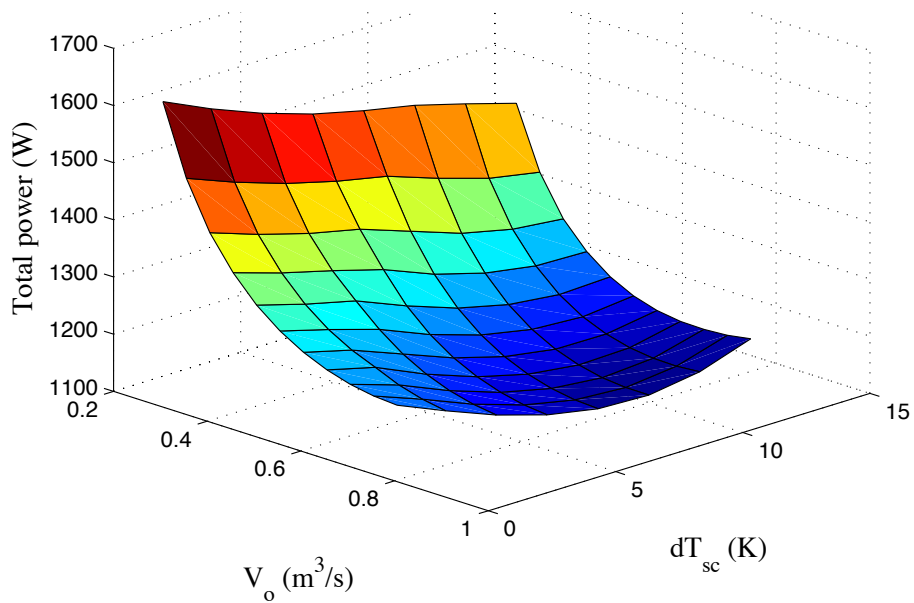


Figure 5-4: Total power consumption versus condenser airflow and subcooling temperature difference for point 8

The relevant parameters for the measured and optimal process (Table 5-3) show that although they have different condenser airflows and subcooling, the condenser outlet enthalpy stays almost the same and the change in pressure ratio due to the lower condensing pressure for the optimal case does not cause a large relative change in the compressor power consumption.

	Q_e (W)	T_{c_avg} (°C)	T_{c4} (°C)	h_{liq} (J/kgK)	m_{ref} (kg/s)	f (Hz)
Measured	4048	37	19	$2.32 \cdot 10^5$	0.0172	108
Optimal	4048	29	20	$2.35 \cdot 10^5$	0.0174	107
	J_e (W)	J_c (W)	KW (W)	J (W)	COP (-)	
Measured	24	22	1209	1255	3.2	
Optimal	24	91	1006	1121	3.6	

Table 5-3: Parameters for measured and optimal condenser airflow and subcooling temperature difference for point 8

$$(Q_e = 4048 \text{ W}, T_z = 34 \text{ °C}, T_o = 17 \text{ °C}, \Delta T_{esh} = 1.5 \text{ °C})$$

5.3. Evaporator airflow and condenser airflow optimization

In the final optimization, the sensitivity of COP value to both the evaporator and condenser airflow rates is analyzed. The evaporator fan speed stayed almost constant through the measurements and hence, the evaporator flow versus speed and power versus speed characteristics are not known. The evaporator airflow versus speed characteristic is assumed to be equal to that of the condenser fan and the power versus speed is scaled using condenser fan data, as explained in Chapter 3.

The optimization is performed for the model variation M4 using evaporator airflow V_z and condenser airflow V_o as the optimization variables, and measured data Q_{e_m} , T_{z_m} , T_{o_m} , ΔT_{esh_m} , and ΔT_{sc_m} as other inputs to the model. In the grid search both optimization variables are changed in $0.05 \text{ m}^3/\text{s}$ increments. COP_m^* is calculated using the same measured data as inputs, and also measured V_{z_m} and V_{o_m} .

The optimization results given in Appendix B show that the sensitivity of COP to the evaporator airflow is larger than for the condenser airflow. While the condenser airflow mostly influences the condensing pressure and compressor pressure ratio, the evaporator airflow influences the evaporating pressure and pressure ratio and, more importantly, it influences the compressor inlet state. For higher evaporator airflow, the evaporating temperature and pressure

increase and the compressor speed decreases due to higher density. Both of these result in a lower compressor power consumption per unit mass.

The first example of how the power consumption changes with the evaporator and condenser airflow change is shown for the measurement point 40, which has the typical summer day conditions. It can be seen from Figure 5-5 that for this particular measurement point the total power consumption changes significantly not just with the evaporator, but also with the condenser airflow. This is also shown in Appendix B (Figure B- 6) where only the condenser airflow rate is optimized. In that case, the change between COP_{max} and COP_m^* value was more obvious for this point than for the majority of other points.

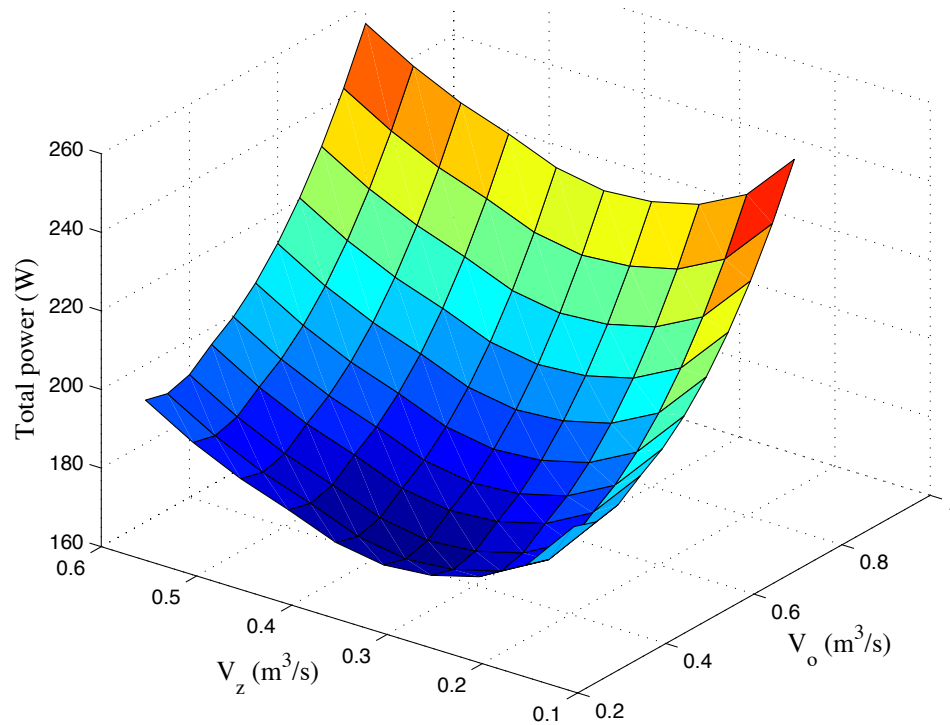


Figure 5-5: Total power consumption versus evaporator and condenser airflow for point 40
 $(Q_e = 1290 \text{ W}, T_z = 24 \text{ }^\circ\text{C}, T_o = 30 \text{ }^\circ\text{C}, \Delta T_{esh} = 2.6 \text{ }^\circ\text{C}, \Delta T_{sc} = 3.3 \text{ }^\circ\text{C})$

For the evaporator and condenser airflow optimization, both predicted optimal airflows were $0.35 \text{ m}^3/\text{s}$, while the measured are 0.14 and 0.63 . The optimized (red) and measured (black) cooling processes are shown in the T-s diagram in Figure 5-6:

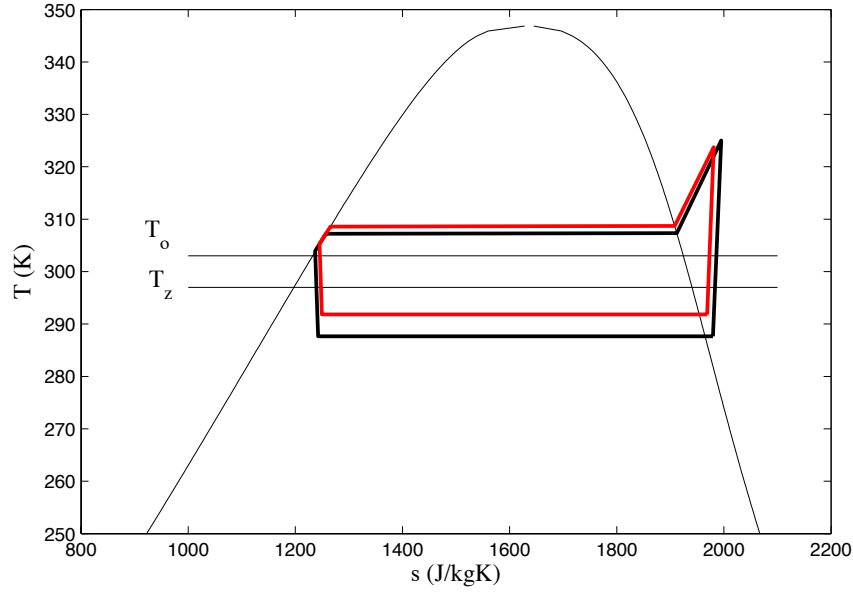


Figure 5-6: Cooling process T-s diagram for measured and optimal predicted evaporator and condenser airflow for point 40

$$(Q_e = 1290 \text{ W}, T_z = 24 \text{ }^{\circ}\text{C}, T_o = 30 \text{ }^{\circ}\text{C}, \Delta T_{esh} = 2.6 \text{ }^{\circ}\text{C}, \Delta T_{sc} = 3.3 \text{ }^{\circ}\text{C})$$

The parameters for three different cases for the same measurement point 40 are shown in Table 5-4. In the first case, all HPM inputs are from measured data, in the second case, the condenser airflow is optimized and the other inputs are from the measured data, and in the third case, the evaporator and condenser airflows are optimized and other inputs are from the measured data.

	$V_z(\text{m}^3/\text{s})$	$V_o(\text{m}^3/\text{s})$	$T_{e_avg} (^{\circ}\text{C})$	$T_{c_avg} (^{\circ}\text{C})$	$T_{c4} (^{\circ}\text{C})$	$m_{ref} (\text{kg/s})$
Case 1	0.14	0.63	14	34	31	0.0061
Case 2	0.14	0.35	14	36	33	0.0062
Case 3	0.35	0.35	19	35	32	0.0062
	$f (\text{Hz})$	$J_e (\text{W})$	$J_c (\text{W})$	$KW (\text{W})$	$J (\text{W})$	$COP (-)$
Case 1	19.6	25	49	147	221	5.8
Case 2	20.1	25	10	160	195	6.6
Case 3	17.4	33	10	123	166	7.8

Table 5-4: Parameters for point 40 for Case 1 (V_{z_m} and V_{o_m}), Case 2 (V_{z_m} and V_{o_opt}) and Case 3 (V_{z_opt} and V_{o_opt})

$$(Q_e = 1290 \text{ W}, T_z = 24 \text{ }^{\circ}\text{C}, T_o = 30 \text{ }^{\circ}\text{C}, \Delta T_{esh} = 2.6 \text{ }^{\circ}\text{C}, \Delta T_{sc} = 3.3 \text{ }^{\circ}\text{C})$$

A different example is the measurement point 8, for which the COP value did not change much when optimizing only the condenser airflow, but changed extremely when optimizing both airflows. It is important to note that the outside temperature for this point was lower than the inside temperature, and in reality, free-cooling could be used. However, even when the outside air temperature is lower than the inside and hence, free-cooling can be applied, the required supply air flow rate can be much larger than for the heat pump operation mode (smaller temperature difference between the supply air and the room temperature requires larger airflow rates). In that case, the fan energy could be larger than the energy to run the heat pump and free-cooling would not be beneficial.

From the grid search results for the measurement point 8 (Figure 5-7) it can be concluded that the power consumption for this point is much more sensitive to the evaporator than to the condenser airflow change.

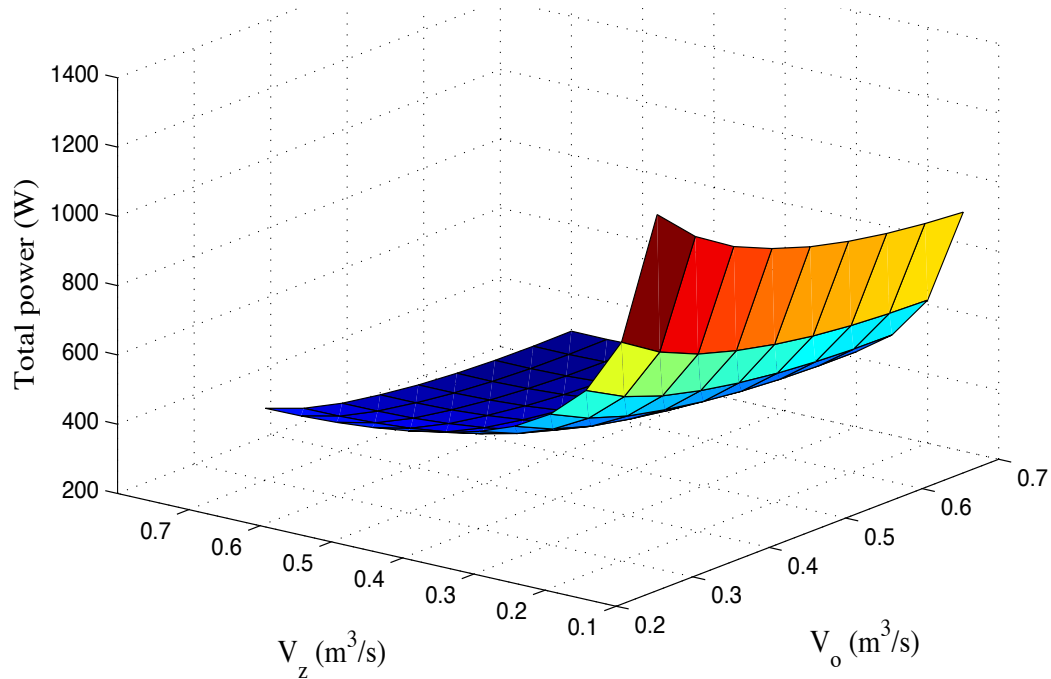


Figure 5-7: Total power consumption versus evaporator and condenser airflow for point 8
 $(Q_e = 4048 \text{ W}, T_z = 34 \text{ }^\circ\text{C}, T_o = 17 \text{ }^\circ\text{C}, \Delta T_{esh} = 1.5 \text{ }^\circ\text{C}, \Delta T_{sc} = 2 \text{ }^\circ\text{C})$

The below T-s diagram of the measured and optimized process visually explains why large differences in the COP value between two processes occur. Due to the large airflows, the optimized process cycle (red) is much more narrow compared to measured (black), and the

evaporating temperature is also higher, meaning the higher compressor inlet density and lower compressor speed and power.

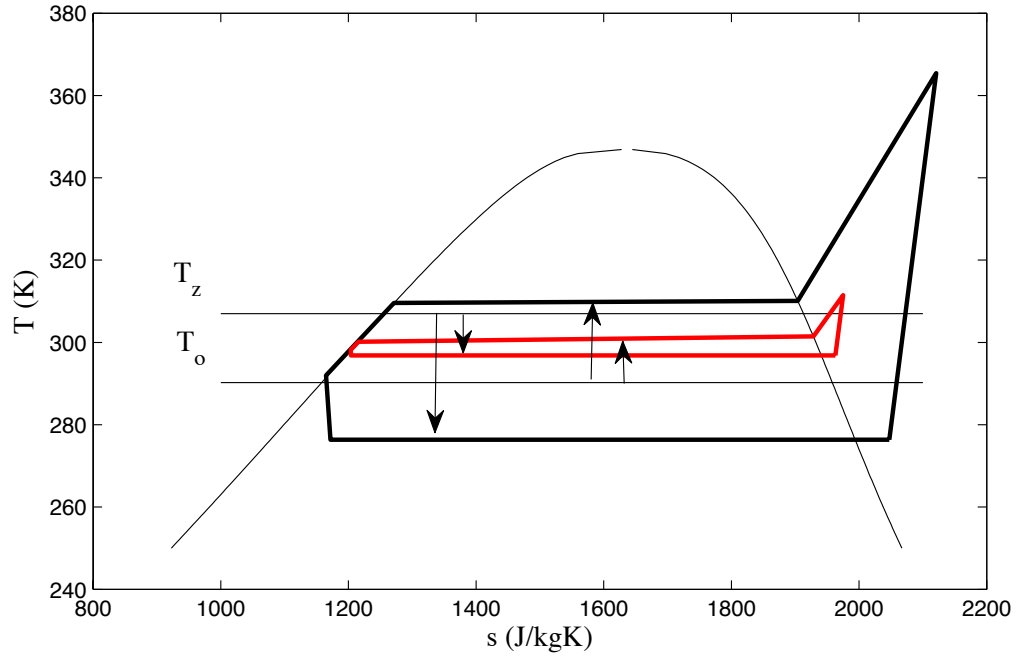


Figure 5-8: Cooling process T-s diagram for measured and optimal predicted evaporator and condenser airflow for point 8

$$(Q_e = 4048 \text{ W}, T_z = 34 \text{ }^{\circ}\text{C}, T_o = 17 \text{ }^{\circ}\text{C}, \Delta T_{esh} = 1.5 \text{ }^{\circ}\text{C}, \Delta T_{sc} = 17.6 \text{ }^{\circ}\text{C})$$

The power consumption sensitivity to the condenser and evaporator airflows change can be analyzed if we again compare the relevant parameters for three cases (measured, condenser airflow optimization and both airflows optimization):

	$V_z (\text{m}^3/\text{s})$	$V_o (\text{m}^3/\text{s})$	$T_{e_avg} (^{\circ}\text{C})$	$T_{c_avg} (^{\circ}\text{C})$	$T_{c4} (^{\circ}\text{C})$	$m_{ref} (\text{kg/s})$
Case 1	0.13	0.44	0	37	19	0.0172
Case 2	0.13	0.60	0	36	18	0.0171
Case 3	0.65	0.65	23	28	25	0.0181
	$f (\text{Hz})$	$J_e (\text{W})$	$J_c (\text{W})$	$KW (\text{W})$	$J (\text{W})$	$COP (-)$
Case 1	108	24	22	1209	1255	3.2
Case 2	106	24	44	1151	1219	3.3
Case 3	42	76	53	160	289	14

Table 5-5: Parameters for point 8 for Case 1 (V_{z_m} and V_{o_m}), Case 2 (V_{z_m} and V_{o_opt}) and Case 3 (V_{z_opt} and V_{o_opt})

$$(Q_e = 4048 \text{ W}, T_z = 34 \text{ }^{\circ}\text{C}, T_o = 17 \text{ }^{\circ}\text{C}, \Delta T_{esh} = 1.5 \text{ }^{\circ}\text{C}, \Delta T_{sc} = 17.6 \text{ }^{\circ}\text{C})$$

In addition to the point 8, points that also have higher zone than outside temperatures and hence show similar behavior and large COP differences in Figure B- 12 are the measurement points 5 – 9, 13, 54 and 55.

When plotted systematically for the given zone and ambient temperature and a range of cooling rates, the optimal evaporator airflow and condenser airflow show a recognizable pattern. In the example in Figure 5-9, the zone temperature was set to 25 °C, outside temperature to 30 °C and the cooling rate was changed from 2 kW to 3.2 kW in 0.4 kW increments. The optimal predicted airflows shift from lower values for lower cooling loads to higher airflows for higher loads. It is also important to recognize that for low partial-load ratios the sensitivity of the total power consumption to the evaporator and condenser airflow rates is high. Since the low-lift cooling system is run at lower part-load ratios most of the time, the optimization process is crucial for energy saving potential.

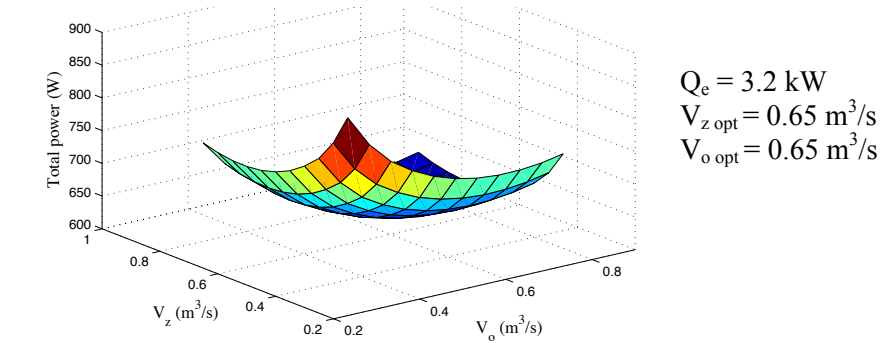
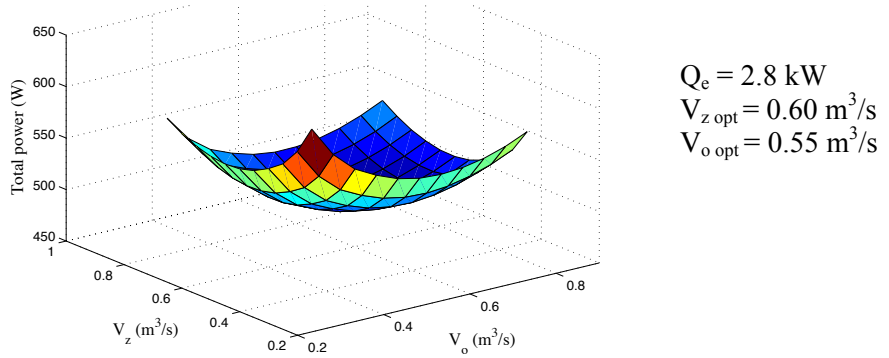
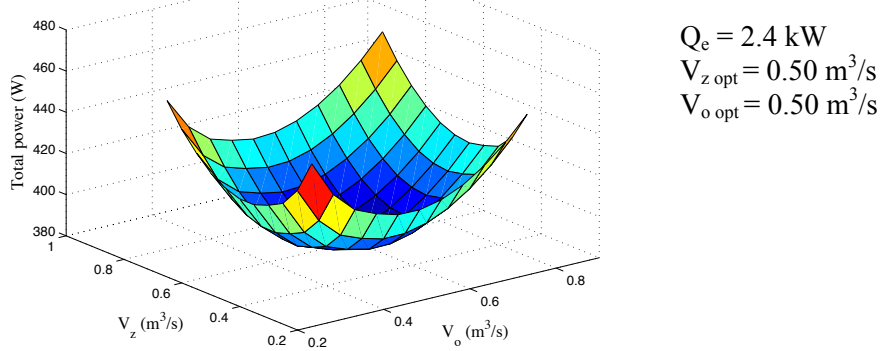
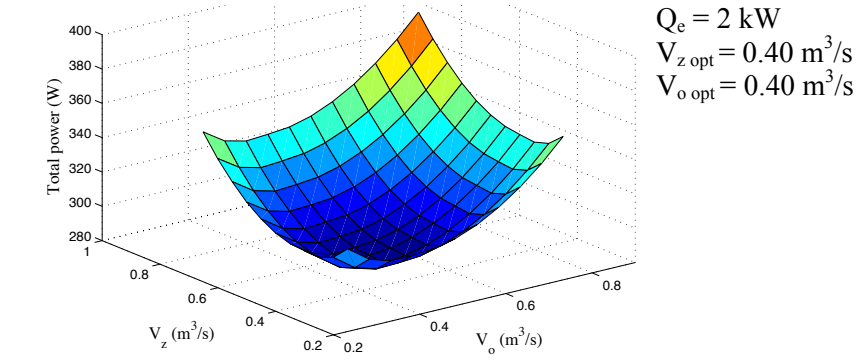


Figure 5-9: Total power consumption versus the evaporator and condenser airflows for different cooling rates
 $(T_z = 25 \text{ }^\circ\text{C}, T_o = 30 \text{ }^\circ\text{C}, \Delta T_{esh} = 2 \text{ }^\circ\text{C}, \Delta T_{sc} = 6 \text{ }^\circ\text{C})$

5.4. Heat pump optimal performance map

Although the optimization in this chapter was performed for only 82 measured points and a limited range of input parameters, the optimization algorithm can produce the optimal performance heat pump maps. One example is shown in Figure 5-10 for the zone temperature 25 °C, ambient temperatures 20 – 40 °C in 5 °C increments and cooling rates 0.8 – 4 kW in 0.4 kW increments.

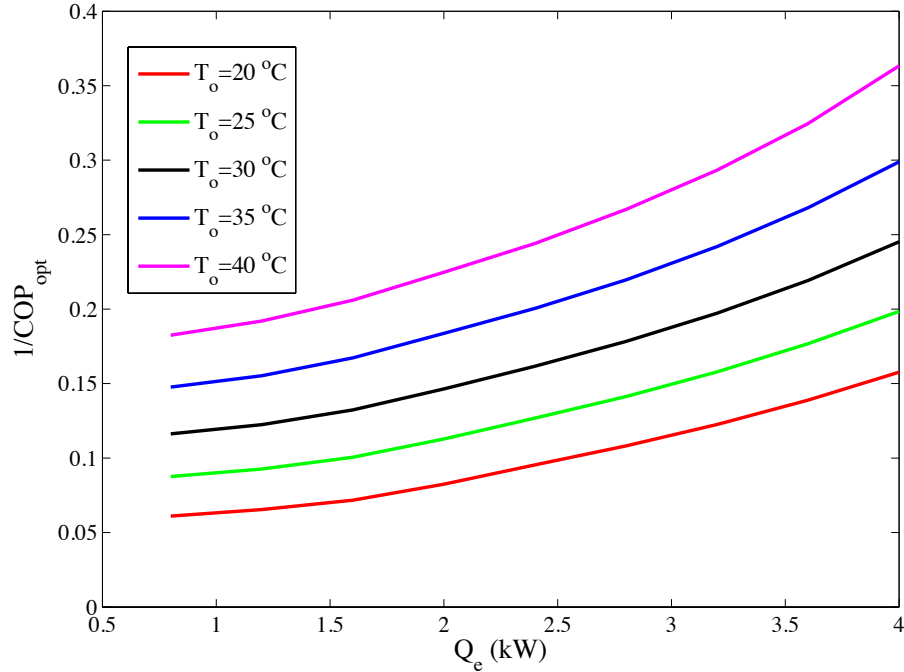


Figure 5-10: Heat pump performance map for the zone temperature 25 °C ($T_z = 25$ °C, $\Delta T_{esh} = 2$ °C, $\Delta T_{sc} = 6$ °C)

This map shows the potential for the heat pump energy savings when thermal storage, the important part of the low-lift cooling technology, is used. Thermal storage allows us to cool water during the night when T_o is lower and to store chilled water for the next day. The significant decrease in the power consumption can be seen in Figure 5-10 for given cooling load between, for example, a hot summer day with $T_o = 30$ °C and a summer night with $T_o = 20$ °C.

The heat pump map shown in Figure 5-10 predicts what is the lowest power consumption for the given cooling rate, ambient and zone temperature, meaning the power consumption for the optimal cooling cycle. However, it does not show how that cooling cycle can be achieved, which is the crucial information for the HVAC equipment control. The optimal process will be achieved for the specific combination of the evaporator airflow rate, condenser airflow rate and

the corresponding compressor speed. Since the airflow rate is proportional to the fan speed, using the optimizer algorithm, the optimal evaporator fan speed, condenser fan speed and compressor speed for given conditions can be predicted, which then completely defines the cooling cycle and HVAC operation point. The maps that show the evaporator airflow rate to compressor speed ratio and the condenser airflow to compressor speed ratio, both as functions of the cooling load and temperature difference are shown in Figure 5-11 and Figure 5-12.

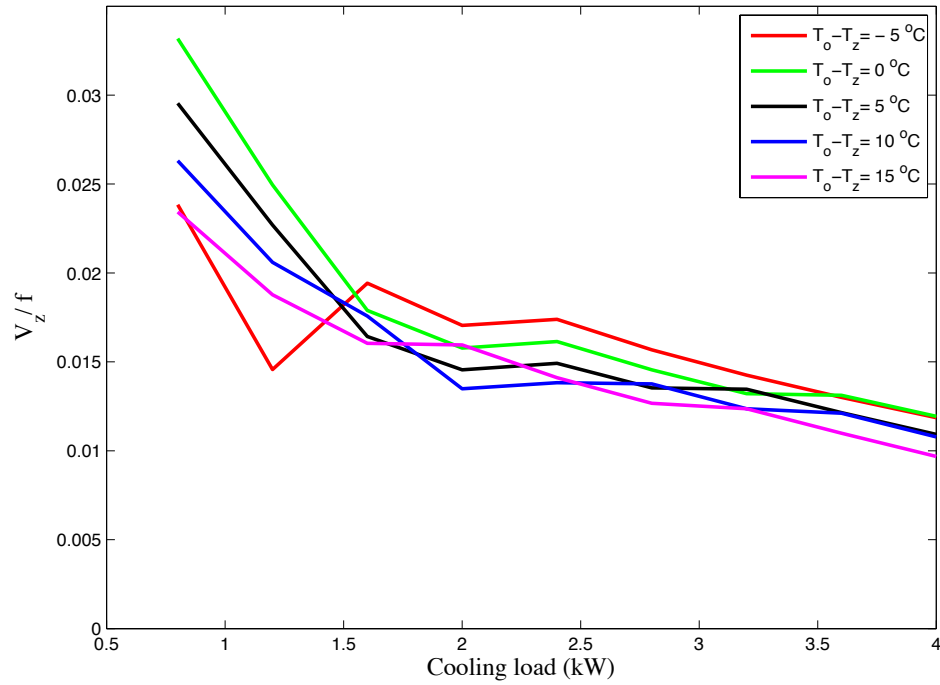


Figure 5-11: Evaporator airflow to compressor speed ratio map

$$(T_z = 25\text{ °C}, \Delta T_{esh} = 2\text{ °C}, \Delta T_{sc} = 6\text{ °C})$$

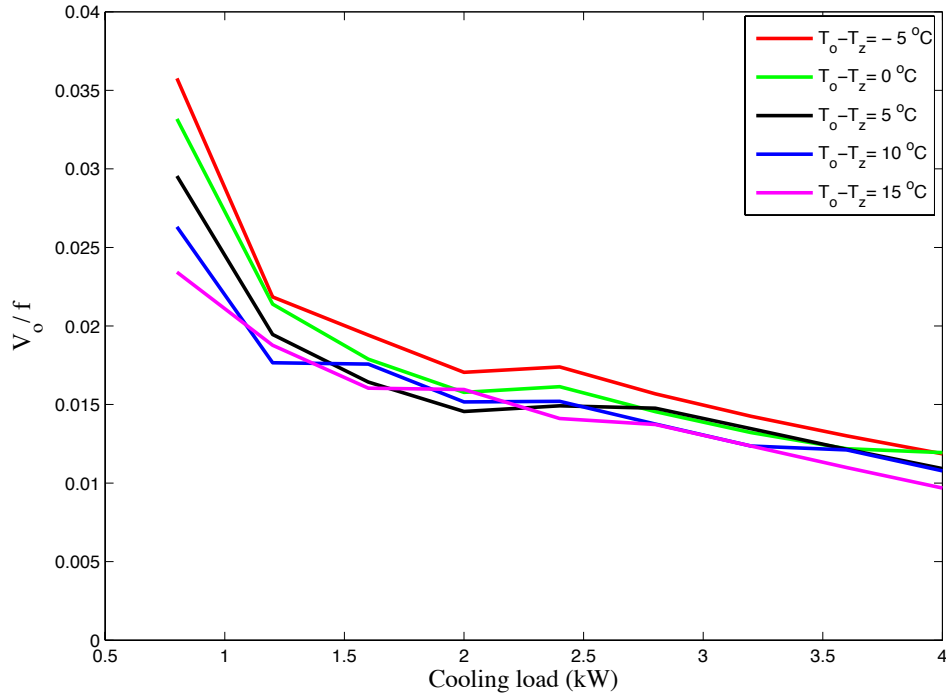


Figure 5-12: Condenser airflow to compressor speed ratio map

$$(T_z = 25\text{ °C}, \Delta T_{esh} = 2\text{ °C}, \Delta T_{sc} = 6\text{ °C})$$

Although curves in Figure 5-11 and Figure 5-12 show the expected general trend, some deviations for particular cooling loads can be noticed. One of the future work objectives will be to analyze and to improve these deviations, especially because these heat pump maps can be very useful in the simulation and control of larger mechanical systems. They predict not just the lowest power consumption for the given cooling rate, ambient temperature and zone temperature, but also the compressor speed and fan speeds needed to achieve that optimal operation point. One example of the potential usage is for the control of the low-lift cooling systems that are being implemented in the test rooms at MIT and Masdar Institute. If the cooling loads and weather forecast are predicted for the next day, the heat pump maps can be used to define how the optimal process should run, and what is the predicted minimal power consumption.

Chapter 6: Conclusion and future work

The steady-state heat pump model is developed from first principles using a component-modeling approach. The required model inputs are the cooling rate, zone and ambient temperature, evaporator and condenser airflow, and desired desuperheating and subcooling temperature differences. The steady-state operating point is then calculated for a given set of input parameters and the model output parameters are the power consumption, mass flow rate, compressor speed, condenser exchanged heat, temperatures and pressures in the evaporator, temperatures and pressures in the condenser, compressor inlet and outlet pressures and pressure drops in different heat pump regions.

The components being modeled are the evaporator, the compressor and the condenser, called in that order.

The compressor sub-model calculates the compressor speed, compressor power and discharge temperature for a given mass flow rate, compressor inlet state and outlet pressure. The shaft speed is calculated using the volumetric efficiency model and the compressor power is calculated as the power required for isentropic work, corrected by the combined efficiency that takes into account all losses in the compressor. The compressor outlet temperature is calculated from the compressor heat balance, where the lubricant oil is assumed to have a constant mass fraction.

The evaporator is divided into the evaporating and desuperheating region and then the heat balance is calculated for each region using the ϵ -NTU method. The condenser is modeled essentially the same as the evaporator, except it consists of the desuperheating, condensing and subcooling regions. The user has the option to either specify a constant UA value for each heat exchanger or to specify the heat exchanger geometry, in which case the program calculates the heat transfer coefficients for the geometry, airflow rate and refrigerant mass flow rate. The heat transfer coefficients are calculated separately for air stream, two-phase and single-phase refrigerant flows. The second user option is to include evaporator desuperheating and condenser subcooling into consideration, or to neglect them. If desuperheating and subcooling are neglected, zero evaporator desuperheating and zero condenser subcooling are assumed, and the whole evaporator is considered as the evaporating region and the condenser as the desuperheating and condensing regions. The user does not have the possibility to neglect the

desuperheating region in the condenser. The third user option is to choose whether the pressure drop inside the heat exchangers and the connecting pipes will be considered or not. If the pressure drop calculation option is turned on, the pressure drop is calculated separately for the two-phase and single-phase refrigerant flow. Including more of these phenomena will result in higher accuracy but also in longer computational time, so the user has the possibility to decide which amongst two objectives, accuracy or computational time, has the more important role.

The model is compared against 82 measured points collected from the Mitsubishi “Mr. Slim” heat pump by Nick Gayeski [20]. Some measured parameters have been used as the inputs to the heat pump model, and the other measured parameters are used for the comparison with the model outputs. The measured and predicted parameters were compared on the component and on the system level for four different model variations. The first variation is the model that does not consider evaporator desuperheating and condenser subcooling (both set to zero), has no pressure drops, and assumes constant UA values for both heat exchangers. The second variation is the same set-up as the first model, except evaporator desuperheating and condenser subcooling are included. The third model variation includes the heat transfer coefficient calculations, desuperheating and subcooling, while the fourth model has all options turned on. The results show significant differences between the models in the parameter predictions, especially between the first model (the simplest model), and the third and fourth model. For the majority of the parameters, the best accuracy was achieved using the third and fourth model. The exceptions were the compressor inlet pressure and power consumption, for which the fourth model did not perform accurately enough. However, it is shown that the model accuracy is strongly related to the evaporating temperature prediction, since that temperature influences the evaporator pressure drop and compressor inlet state, which in turn has an impact on the compressor power consumption. The evaporating temperature under-prediction leads to over-prediction of the calculated evaporator pressure drop, very low suction pressures and large over-prediction of the compressor power consumption. When predicted evaporating temperatures were closer to the measured (less than 2 K under-prediction), the fourth model has shown the best accuracy among all four model variations with the 6% RMS in COP.

Finally, the grid search model optimization is developed to find the optimal operation point, which is the point with the lowest power consumption for the given cooling rate, zone temperature and ambient temperature. The optimization variables can be the evaporator airflow rate, condenser airflow rate, condenser subcooling, or any combination of these. Using the heat pump optimization algorithm, the heat pump maps can be developed for a range of cooling

loads, zone temperatures and ambient conditions. These maps can be very useful in other simulation models where a heat pump is a part of the more complex system.

The main objective for the future work is the development of a faster optimization algorithm, which will probably go in the direction of using the MATLAB built-in optimization functions. From the grid search for all 82 measured points it seems that the power-airflow, power-subcooling and power-airflow-subcooling dependence curves and surfaces are smooth for the whole search area, which means that the gradient-based method could potentially be used. However, the code has some conditional statements (if-then constructs), which can hinder the performance of the gradient-based method. Another option would be to use genetic algorithms, which would overcome this problem, but also require much more computational time.

Regarding the component sub-models, the evaporator and condenser fan will be modeled using the fan laws rather than fitting polynomial curves to the measured data. Using power law functions is preferred because the iteration can safely go outside the training data range, which might not be the case with the polynomial curve fitting approach. Also, the six constants needed for the compressor model have been determined using the measurement data for all 82 points. It would be interesting to analyze what is the minimum number of experimental points (and at what operating conditions) that is sufficient for a relatively accurate compressor sub-model. It is shown that the evaporating temperature prediction strongly influences the model accuracy and hence it is important to show in the future work what input parameter errors and assumption have the strongest impact on the evaporating temperature errors. Also, an additional evaporator sub-model needs to be developed for the water-cooled instead of air-cooled evaporator since Armstrong's suggested low-lift cooling system is using hydronic radiant cooling.

Further, a free-cooling operation mode has not been modeled at this stage of the model development and it would be beneficial to have that option included, especially for low-lift cooling technology analysis.

Finally, as seen in part 5.4, all heat pump performance curves show the expected general trend, but for some of them, the bumps for particular input conditions occur. For the future work, it is important to address and resolve this problem, which might be related to heat pump model convergence or with particular parameter prediction accuracy.

References

- [1] Armstrong, P., Jiang, W., Winiarski, D.W., Katipamula, S., Norford, L.K. and Willingham, R. 2009. Efficient Low-Lift Cooling with Radiant Distribution, Thermal Storage and Variable-Speed Chiller Controls Part I: Component and Subsystem Models. *HVAC&R Research* 15(2), pp. 367-401.
- [2] Armstrong, P., Jiang, W., Winiarski, D.W., Katipamula, S., Norford, L.K. and Willingham, R. 2009. Efficient Low-Lift Cooling with Radiant Distribution, Thermal Storage and Variable-Speed Chiller Controls Part II: Annual Energy Use and Savings Estimates. *HVAC&R Research* 15(2), pp. 403-433.
- [3] ARI. 1999. ARI standard 540: *Positive Displacement Refrigerant Compressor and Compressor Units*. Air-conditioning and Refrigeration Institute, Arlington, Virginia.
- [4] Armstrong, P. 2009 – 2010. Personal Communication.
- [5] ASHRAE Handbook *Fundamentals*. 2009. American Society of Heating, Refrigerating and Air-Conditioning Engineers, Atlanta, USA.
- [6] Bertsch, S.S., and Groll, E.A. 2008. Two-Stage Air-Source Heat Pump for Residential Heating and Cooling Applications in Northern U.S. Climates. *International Journal of Refrigeration*, 31, pp. 1282 – 1292.
- [7] Braun, J.E., Mitchell, J.W., Klein, S.A., and Beckman, W.A. 1987. Models for Variable-Speed Centrifugal Chillers. *ASHRAE Transactions*, 93(1), pp. 1794-1813.
- [8] Browne, M.W., and Bansal, P.K. 1998. Challenges in Modeling Vapor-Compression Liquid Chillers. *ASHRAE Transaction*, 104(1a), pp. 474 – 484.
- [9] Browne, M.W., and Bansal, P.K. 2001. An Elemental NTU- ϵ Model for Vapor-Compression Liquid Chillers. *International Journal of Refrigeration*, 24, pp. 612 – 627,
- [10] Choi, J.Y., Kedzierski, M.A., and Domanski, P.A. 1999. *A Generalized Pressure Drop Correlation for Evaporation and Condensation of Alternative Refrigerants in Smooth and Micro-Fin Tubes*. National Institute of Standards and Technology, NISTIR 6333.
- [11] DOE/ORNL Heat pump design model MarkVI. Available at <http://www.ornl.gov/~wlj/hpdm/MarkVI.shtml>.
- [12] Domanski, P. A., and Didion, D. A. 1984. Mathematical Model of an Air-to-Air Heat Pump Equipped with a Capillary Tube. *International Journal of Refrigeration*, 7(4), pp. 249-255.
- [13] Damasceno, G. S., and Goldschmidt, V. W. 1987. *An Update of the August 1986 User's Guide of the Heat Pump Performance Model HN*. Report No. HL 87-37p. Ray W. Herrick Laboratories, Purdue University.

- [14] Damasceno, G. S., Rooke, S. P., and Goldschmidt, V. W. 1990. Comparison of Three Steady-State Heat Pump Computer Models, *ASHRAE Transactions*, 96(2), pp. 191-204.
- [15] Ellison, R. D., and Creswick, F. A. 1978. *A Computer Simulation of the Steady-State Performance of Air-to-Air Heat Pump*. Report No. ORNL/CON-16. Oak Ridge, Oak Ridge National Laboratory, Oak Ridge.
- [16] Ellison, R. D. , Creswick, F. A., Rice, C. K., Jackson, W.L. and Fischer, S. K. 1979. *Heat Pump Modeling: A Progress Report*. The 4th annual heat pump technology conference, Oklahoma State University, Stillwater, Oklahoma.
- [17] Feustel, H., and Stetiu C. 1995. Hydronic radiant cooling – preliminary assessment. *E&B* 22(3) pp. 193 – 205.
- [18] Fischer, S. K., Rice, C. K., and Jackson W. L. 1988. *The Oak Ridge Heat Pump Design Model: Mark III Version Program Documentation*. Report No. ORNL/TM-10192. Oak Ridge National Laboratory, Oak Ridge.
- [19] Fu, L., Ding, G., Su, Z., and Zhao, G. 1988. Steady State Simulation of Screw Liquid Chillers. *Applied Thermal Engineering*, 22, pp. 1731 – 1748.
- [20] Gayeski, N. 2009-2010. Personal Communication.
- [21] Gray, D.L., and Webb, R.L. 1986. Heat Transfer and Friction Correlation for Plate Finned-Tube Heat Exchangers Having Plain Fins. *Proceedings of Eight Int. Heat Transfer Conference*. San Francisco.
- [22] Hiller, C.C. 1976. *Improving Heat Pump Performance Via Compressor Capacity Control: Analysis and Test*. PhD Thesis. Massachusetts Institute of Technology.
- [23] Iu, I.S. 2007. *Development of Air-to-Air Heat Pump Simulation Program with Advanced Heat Exchanger Algorithm*. PhD thesis. Oklahoma State University.
- [24] Jähnig, D.I., Reindl, D.T., and Klein, S.A. 2000. A Semi-Empirical Method for Representing Domestic Refrigerator/Freezer Compressor Calorimeter Test Data. *ASHRAE Transactions* 101 (2).
- [25] Jeter, S.M., Wepfer, W.J., Fadel, G.M., Cowden, N.E., and Dymek, A.A. 1987. Variable Speed Drive Heat Pump Performance. *Energy*, Vol. 12, No. 12, pp.1289 – 1298.
- [26] Jin, H. 2002. *Parameter Estimation Based Model of Water Source Heat Pumps*. PhD thesis. Oklahoma State University.
- [27] Kim, M.H., and Bullard, C.W. 2002. Thermal Performance Analysis of Small Hermetic Refrigeration and Air-Conditioning Compressors. *JSME International Journal*, Vol.45, No.4.
- [28] McQuiston, F.C, Parker, J.D., and Spitler J.D. *Heating, Ventilating and Air Conditioning*. 6th Edition. Wiley.
- [29] Mitsubishi “Mr. Slim” technical data for model MSZ-A09NA. Available at http://www.mehvac.com/UploadedFiles/Resource/MSZ-Y-A09~24NA - GA24NA_Service_Manual_OB450D_3-2-09.pdf.

- [30] Nguyen, H. 1986. *Reversing Valve Heat Transfer and Pressure Drops and Their Effects on the Steady-State Performance of a Heat Pump*. PhD thesis. Purdue University.
- [31] Nguyen, H., and Goldschmidt, V.W. 1986. *A User's Guide to the Heat Pump Performance Model HN*. Report No. HL 86-27p. Ray W. Herrick Laboratories, Purdue University.
- [32] NIST Reference Fluid Thermodynamic and Transport Properties Database (REFPROP). Version 8.0. Available at <http://www.nist.gov/srd/nist23.htm>.
- [33] Schmidt, T.E. 1945-1946. Annexe G-5: *La Production Calorifique des Surfaces Munies d' Ailettes*. Annexe du Bulletin de L'Institut International du Froid.
- [34] Timm, M.L. 1991. An Improved Method for Calculating Refrigerant Line Pressure Drops. *ASHRAE Transactions*, 97 (1), pp. 194-203.
- [35] US Energy Information Administration. 2008. *Annual Energy Review*. Available at <http://www.eia.doe.gov/>.
- [36] Willingham, R.A. 2009. *Testing and Modeling of Compressors for Low-Lift Cooling Applications*. SM thesis. Massachusetts Institute of Technology.

Appendix A: Constant UA value estimate

The evaporator and condenser constant UA values for M1 and M2 are calculated using the standard operation data from “Mr. Slim” manual (Table A-1).

Indoor unit	Cooling capacity	Q_e	2.78	kW
	Evaporator airflow	V_e	0.142	m ³ /s
	Evaporator fan speed	w_e	1160	rpm
	Evaporator fan power	P_e	0.019	kW
	Inlet air temperature	$T_{air,in,e}$	16.7	°C
	Outlet air temperature	$T_{air,out,e}$	13.9	°C
Outdoor unit	Condenser airflow	V_c	0.511	m ³ /s
	Condenser fan speed	w_c	830	rpm
	Compressor + condenser fan power	J_{out}	0.85	kW
	Inlet air temperature	$T_{air,in,c}$	35	°C
Refrigerant	Suction temperature	T_{comp_in}	9	°C
	Condensing temperature	T_c	43.3	°C

Table A-1: Standard operation data for “Mr. Slim” [29]

Even for the standard operation point some values necessary for the UA value calculations are not given by the manufacturer, so several assumptions have been made:

- The evaporator outlet temperature T_{e3} is equal to the suction temperature (T_{comp_in})
- There is 2-3 °C desuperheating (ΔT_{esh}) in the evaporator, which was the typical overheating during the “Mr. Slim” experimental measurements
- From the total outdoor unit power specified by the manufacturer (J_{out}), 0.03 kW is the condenser fan power ($J_{c,as}$), based on the experimentally measured condenser fan power for 0.5 m³/s (condenser airflow given by the manufacturer for the standard operation data)

From these assumptions and the standard operation data, parameters for the UA value estimation are determined:

- Average evaporating temperature T_e is 6.5 °C ($T_{e3} - \Delta T_{esh} = 9 - 2.5$)
- Power dissipated in the compressor KW is 0.82 kW ($J_{out} - J_{c,as} = 0.85 - 0.03$)
- Condenser heat Q_c is 3.6 kW ($Q_e + KW = 2.78 + 0.82$)
- From the condenser heat (Q_c), condenser airflow (V_c) and condenser inlet air temperature ($T_{air,in,c}$), calculated condenser outlet air temperature $T_{air,out,c}$ is 41 °C.

The UA value is estimated using the logarithmic mean temperature difference:

$$p.UA_e = \frac{Q_e}{\Delta T_{\log m,e}} \quad (108)$$

$$p.UA_c = \frac{Q_c}{\Delta T_{\log m,c}} \quad (109)$$

where

$$\Delta T_{\log m,e} = \frac{(T_{air,out,e} - T_e) - (T_{air,in,e} - T_e)}{\ln \frac{T_{air,out,e} - T_e}{T_{air,in,e} - T_e}} \quad (110)$$

$$\Delta T_{\log m,c} = \frac{(T_c - T_{air,in,c}) - (T_c - T_{air,out,c})}{\ln \frac{T_c - T_{air,in,c}}{T_c - T_{air,out,c}}} \quad (111)$$

The estimated constant evaporator and condenser UA values are 220 W/K and 830 W/K respectively.

Appendix B: Optimization results

B.1. Condenser airflow optimization results

As mentioned in Chapter 5, the optimization was performed for all four model variations with the condenser airflow (V_o) as the optimization variable. All other input parameters (Q_{e_m} , T_{z_m} , T_{o_m} , V_{z_m} , ΔT_{esh_m} , and ΔT_{sc_m}) are taken from the measured data. Figure B- 1 shows how the optimal condenser airflow changes between M1 – M4. It can be seen that the optimal value curve shows very similar behavior for all four models and that the values for M1 – M4 are similar for a single measurement point.

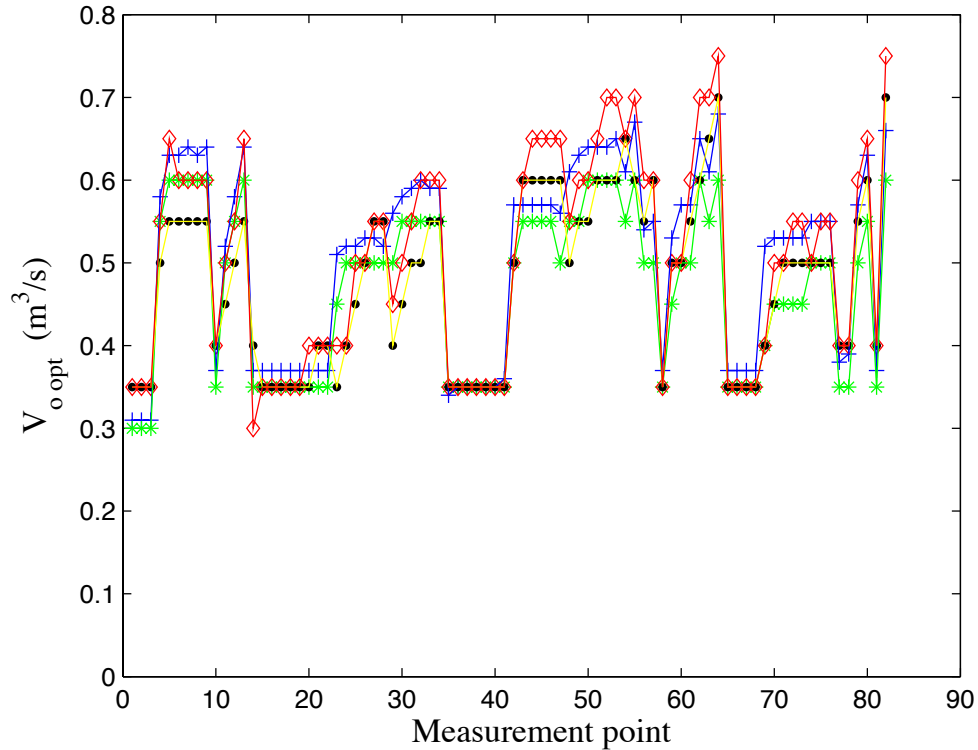


Figure B- 1: Optimal condenser airflow for M1 – M4

The comparison between the measured and optimal condenser airflow is shown in Figure B- 2. Because the optimal value curve shows similar trends for all four model variations, only the comparison for M4 is presented. The measured condenser airflow for a given point is, of course, equal for all four models, for which the optimal values are shown in Figure B- 1 (black are the measured and red are the predicted values).

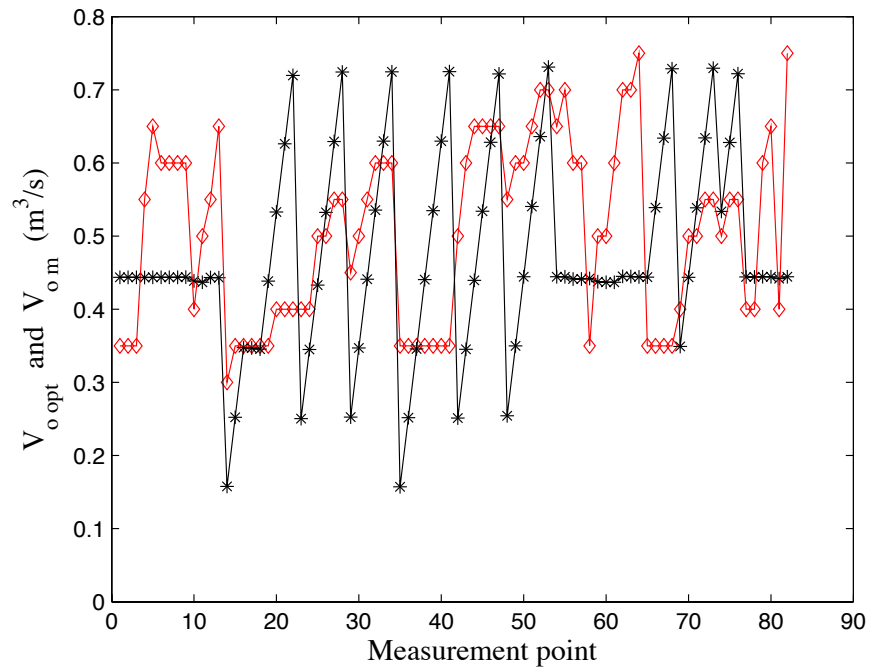


Figure B- 2: Measured and optimal condenser airflow for M4

Although results show differences between the optimal predicted and non-optimal measured condenser airflow, there is almost no change in the COP values according to the results shown for all four model variations in Figure B- 3 – Figure B- 6. Slight changes can be seen for points 1 – 3 and 35 – 41, which are the points with the lowest cooling rate, so small absolute changes in the total power consumption result in significant relative changes in the total power consumption and COP.

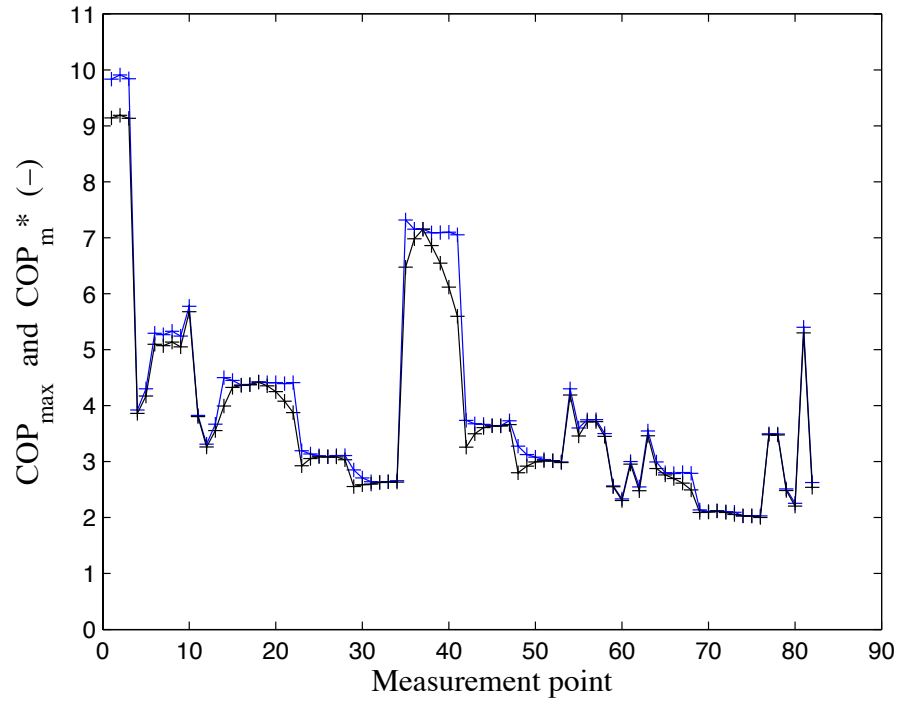


Figure B- 3: COP_m^* and COP_{max} for model M1

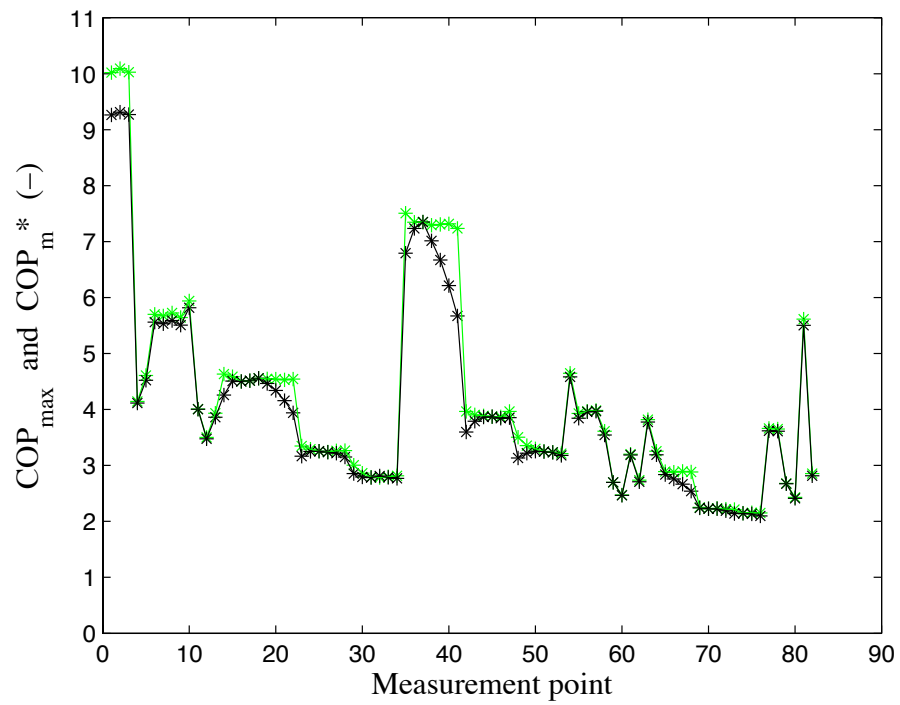


Figure B- 4: COP_m^* and COP_{max} for model M2

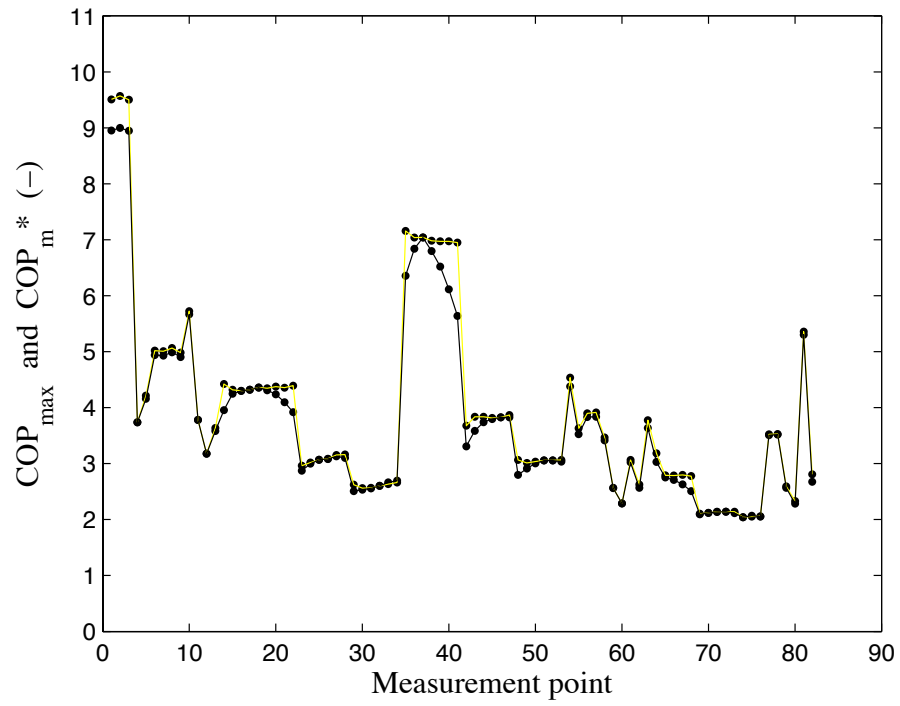


Figure B- 5: COP_m^* and COP_{max} for model M3

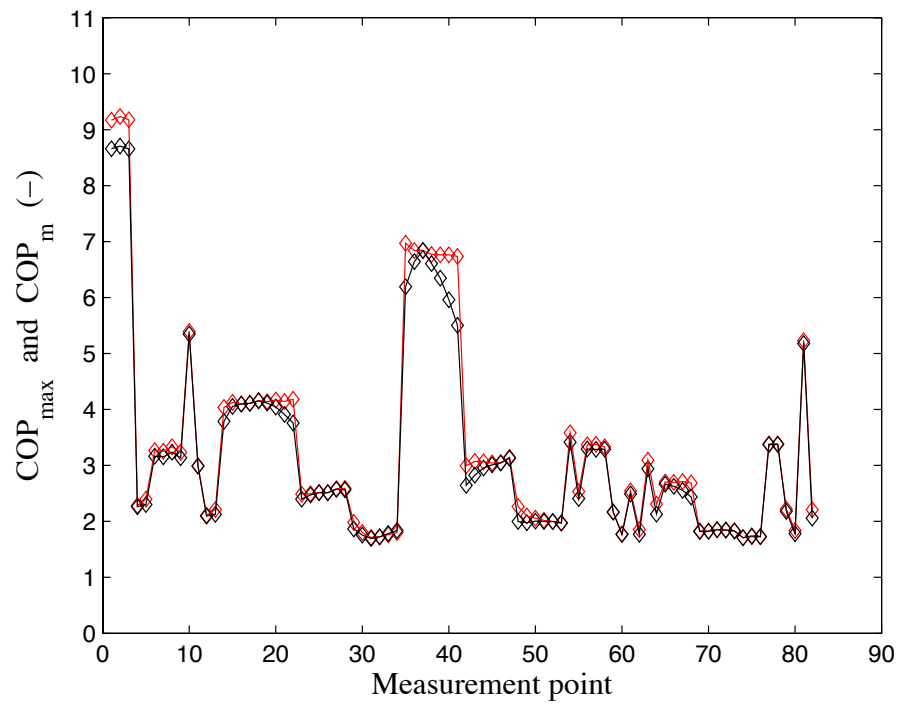


Figure B- 6: COP_m^* and COP_{max} for model M4

B.2. Condenser airflow and subcooling optimization results

The optimization is performed with model variation M4 using the condenser airflow V_o and subcooling temperature difference ΔT_{sc} as the optimization variables and the measured data Q_{e_m} , T_{z_m} , T_{o_m} , V_{z_m} , and ΔT_{esh_m} as other inputs to the model. From the predicted optimal condenser airflow rate and subcooling temperature difference shown in Figure B- 7 and Figure B- 8 (black are the measured and red are the predicted values) it can be seen that when the subcooling temperature is added as an optimizing variable, the optimal condenser airflows are somewhat different than the optima reported in section B.1, where only the condenser airflow is optimized. Also, the predicted optimal subcooling temperature differences are for most points lower than the measured ones.

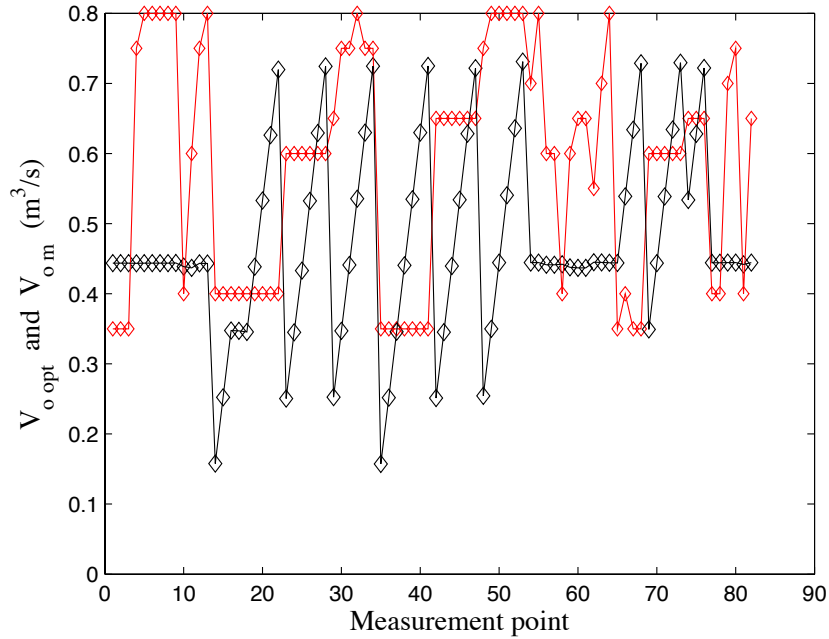


Figure B- 7: Measured and optimal condenser airflow for M4

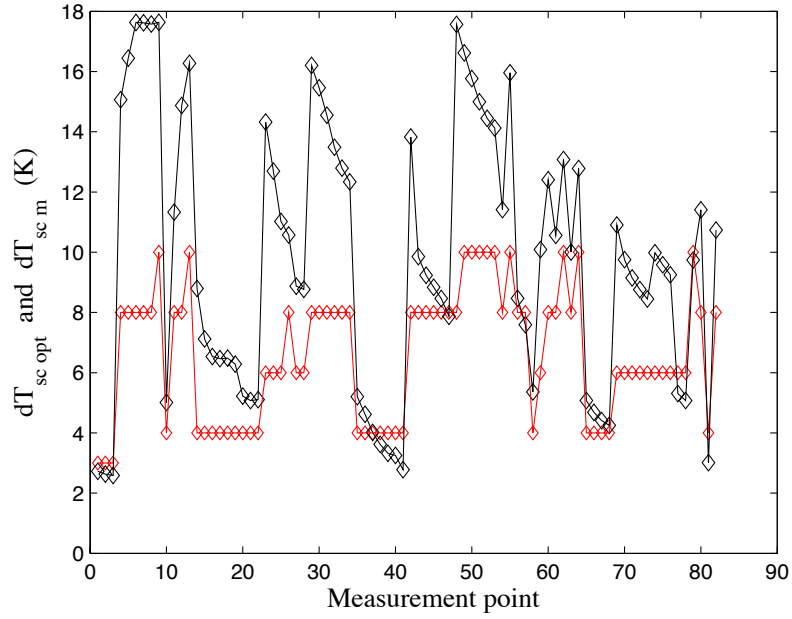


Figure B- 8: Measured and optimal condenser subcooling for M4

Despite the differences between the predicted optimal and measured values for both the condenser airflow and subcooling temperature difference, the COP comparison shows very small changes between COP_m^* and COP_{max} (Figure B- 9).

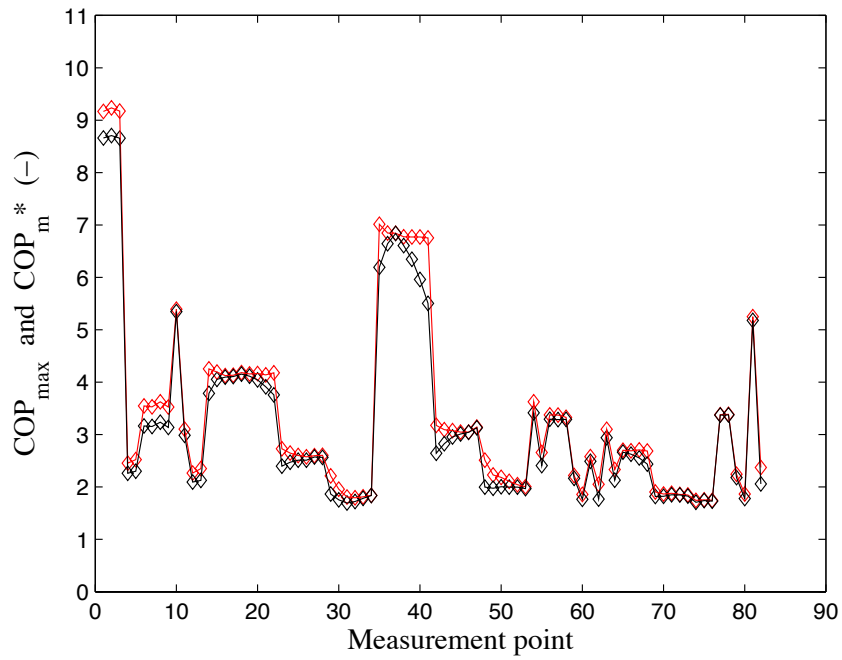


Figure B- 9: COP_m^* and COP_{max} for model M4

B.3. Evaporator airflow and condenser airflow optimization results

The optimization is performed for the model variation M4 using evaporator airflow V_z and condenser airflow V_o as the optimization variables, and measured data Q_{e_m} , T_{z_m} , T_{o_m} , ΔT_{esh_m} , and ΔT_{sc_m} as other inputs to the model.

The results show that the optimal evaporator airflows are much higher than the measured (Figure B- 10) and the optimal condenser airflows fluctuate from point to point in the similar fashion as for the previous optimizations (Figure B- 11), but the fluctuations have smaller amplitude than before (most of them are in the range from 0.3 to 0.55 m³/s).

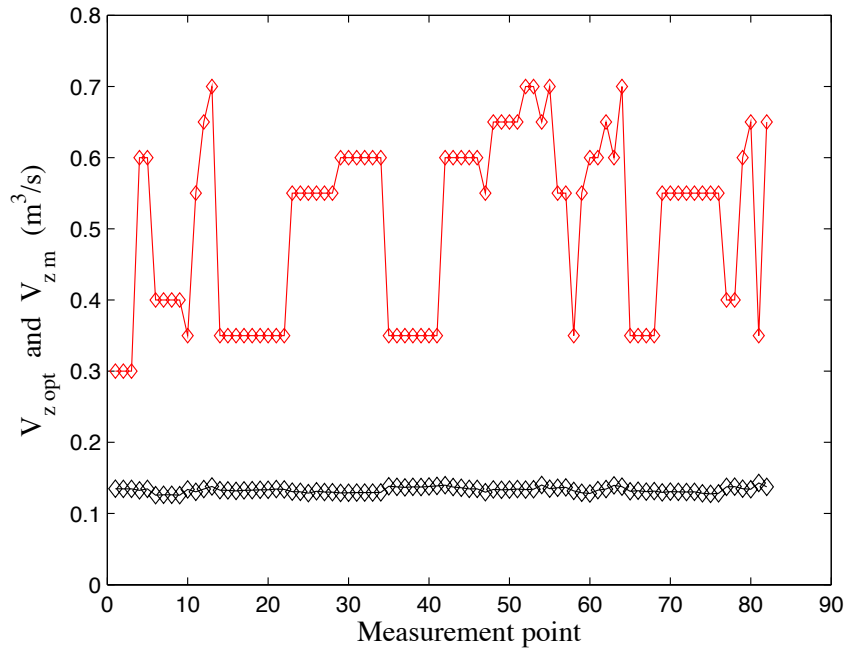


Figure B- 10: Measured and optimal evaporator airflow for M4

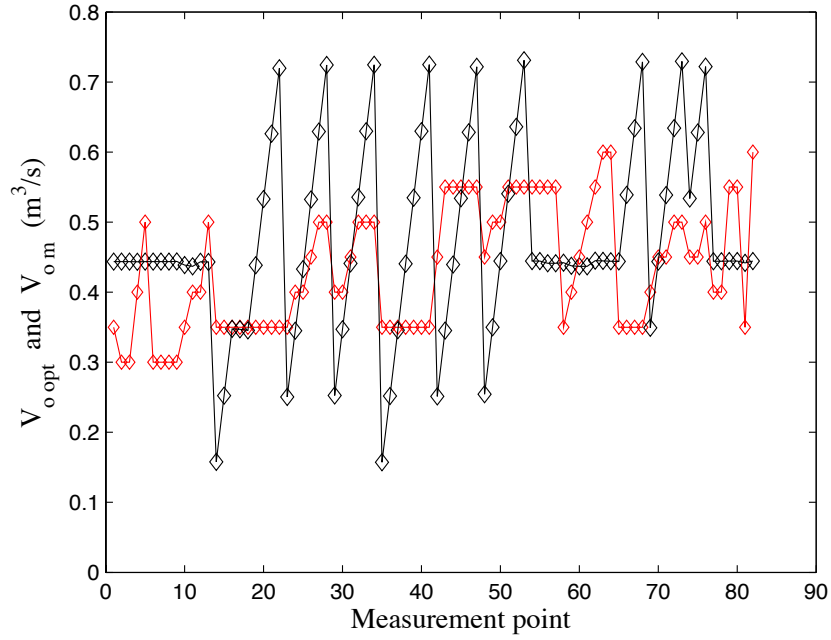


Figure B- 11: Measured and optimal condenser airflow for M4

In contrast to the previous optimization parameters, the COP values show significant sensitivity to the evaporator airflow:

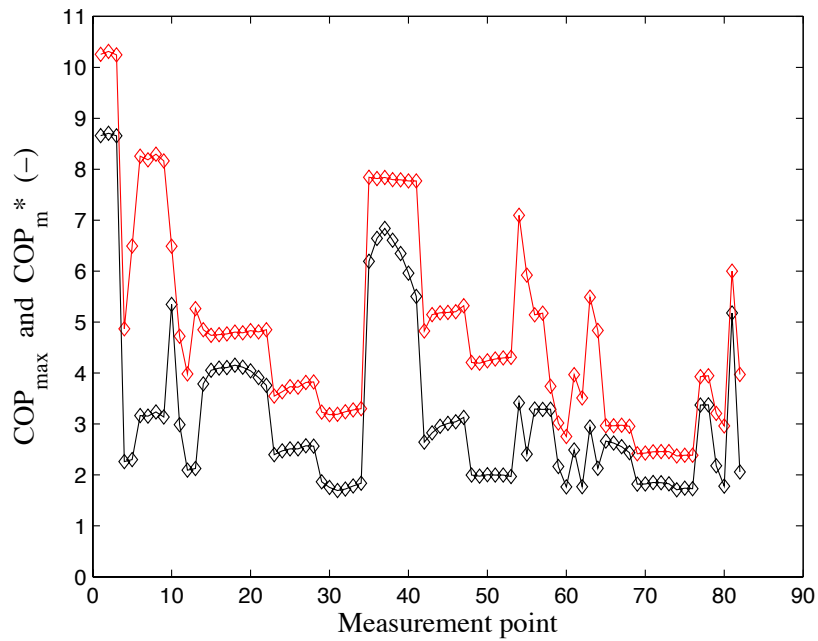


Figure B- 12: COP_m^* and COP_{max} for model M4

Appendix C: Measurement data

The parameters that are directly measured are the temperatures (except T_{c2}) and pressures, compressor shaft speed, compressor 3-phase power, condenser airflow rate, condenser fan speed, and condenser fan power. The cooling rate is calculated from a power measurement of load on the evaporator, as well as the temperature difference and heat transfer coefficient between the insulated zone served by the evaporator and its surroundings. The evaporator desuperheating is calculated as $T_{e3} - T_{e1}$. The condenser subcooling is calculated as $T_{c2} - T_{c1}$, where T_{c2} (average condensing temperature) is calculated using the assumption that the average condensing pressure is equal to the compressor outlet pressure $P_{comp.out}$. The evaporator airflow rate V_z is calculated from the cooling rate and the air-side temperature difference $T_{e,air,in} - T_{e,air,out}$. The refrigerant mass flow rate is calculated from the cooling rate and the evaporator enthalpy difference, where the assumption is made that the evaporator inlet enthalpy is equal to the condenser outlet enthalpy.

	T_z (°C)	T_o (°C)	T_{e1} (°C)	T_{e3} (°C)	T_{c1} (°C)	T_{c2} (°C)	T_{c4} (°C)	ΔT_{esh} (°C)	ΔT_{sc} (°C)	$T_{e,air,in}$ (°C)	$T_{e,air,out}$ (°C)	$T_{c,air,in}$ (°C)	$T_{c,air,out}$ (°C)
1	14.0	15.4	5.9	8.0	33.3	11.6	16.3	2.1	-4.7	14.9	8.2	15.4	17.7
2	14.0	15.3	5.8	7.9	33.3	11.5	16.3	2.1	-4.8	14.8	8.1	15.4	17.7
3	14.0	15.4	5.8	8.0	33.2	11.5	16.4	2.1	-4.9	14.8	8.2	15.4	17.7
4	14.0	16.0	-3.8	-1.2	84.6	27.4	17.9	2.7	9.6	17.4	-1.3	16.3	21.4
5	24.0	16.7	1.9	4.3	81.4	30.6	19.3	2.4	11.2	28.1	4.6	16.7	23.3
6	34.0	17.1	7.1	9.1	80.0	34.0	21.2	2.0	12.7	38.5	10.4	17.1	25.4
7	34.0	17.2	7.2	9.2	80.3	34.2	21.5	1.9	12.8	38.6	10.5	17.3	25.7
8	34.0	17.3	7.1	8.6	80.1	34.1	21.4	1.5	12.7	38.1	10.2	17.3	25.7
9	34.0	17.3	7.1	8.9	80.0	34.1	21.3	1.8	12.8	38.5	10.4	17.2	25.5
10	14.0	22.5	4.7	5.8	49.8	22.5	23.5	1.1	-1.0	15.6	6.7	22.7	26.3
11	14.0	22.5	0.7	1.9	68.4	29.6	23.5	1.2	6.0	17.0	1.8	22.4	28.3
12	14.0	22.5	-2.5	-0.2	96.1	34.4	24.4	2.3	10.0	17.0	-0.3	22.7	28.3
13	24.0	22.5	3.2	5.2	91.4	37.3	25.6	2.0	11.7	28.0	5.8	22.8	30.3
14	14.0	30.0	6.2	8.5	74.7	37.4	33.2	2.3	4.2	15.4	7.6	30.0	39.9
15	14.0	30.0	5.7	8.4	69.7	33.9	31.6	2.7	2.2	15.4	7.4	30.2	36.3
16	14.0	30.2	6.0	7.6	66.0	32.4	30.9	1.6	1.5	15.5	7.2	30.3	34.8
17	14.0	30.1	6.0	7.7	65.5	32.5	31.0	1.7	1.4	15.6	7.3	30.5	34.9
18	14.0	30.0	6.0	7.6	66.4	32.7	31.2	1.6	1.5	15.4	7.3	30.4	35.0
19	14.0	30.0	5.8	8.1	65.3	31.7	30.5	2.2	1.2	15.4	7.3	30.7	34.2
20	14.0	30.0	5.9	7.5	63.3	30.3	30.3	1.7	0.0	15.2	7.1	30.0	32.8
21	14.0	30.0	6.0	8.1	63.3	30.4	30.5	2.1	-0.1	15.6	7.4	30.3	32.9
22	14.0	30.0	6.1	6.8	63.1	31.2	31.2	0.7	0.0	15.3	7.2	30.9	33.4
23	14.0	30.0	1.8	3.5	90.4	42.7	32.6	1.6	10.1	16.6	2.9	30.6	40.5

24	14.0	30.0	1.6	3.2	84.7	39.7	31.4	1.5	8.3	16.7	2.8	30.5	37.5
25	14.0	30.0	1.7	3.1	81.4	37.6	31.2	1.4	6.4	16.7	2.5	30.2	35.5
26	14.0	30.0	1.5	3.0	78.8	36.0	30.1	1.6	5.9	16.7	2.5	30.1	34.3
27	14.0	30.0	1.5	3.8	78.1	34.9	30.9	2.2	4.1	16.7	2.5	29.8	32.9
28	14.0	30.0	1.4	3.7	78.0	34.7	30.8	2.2	3.9	16.6	2.5	30.1	32.8
29	14.0	30.0	0.4	1.8	106.6	46.6	34.3	1.4	12.3	16.9	1.2	30.1	41.9
30	14.0	30.0	-0.5	1.0	108.1	44.5	33.1	1.5	11.4	17.1	0.5	29.9	38.2
31	14.0	30.0	-0.6	0.1	106.9	43.5	33.1	0.7	10.4	17.2	0.2	30.0	36.6
32	14.0	30.0	-0.8	0.4	104.7	41.6	32.4	1.3	9.2	17.2	0.1	30.1	35.0
33	14.0	30.0	-1.0	1.0	104.0	40.5	32.1	2.0	8.4	17.2	0.2	30.2	34.1
34	14.0	30.0	-1.3	1.2	103.3	39.3	31.4	2.5	7.9	17.1	0.3	30.0	33.1
35	24.0	30.0	16.4	18.1	59.3	34.6	34.2	1.7	0.4	25.1	17.8	30.0	38.5
36	24.0	30.0	16.2	18.0	54.4	31.7	32.2	1.8	-0.5	25.3	17.6	30.1	35.6
37	24.0	30.0	16.0	17.9	53.6	30.8	32.0	1.9	-1.2	25.2	17.5	30.1	34.5
38	24.0	30.0	16.1	18.1	52.1	29.9	31.6	2.1	-1.6	25.5	17.7	29.9	33.4
39	24.0	30.0	15.9	18.1	51.6	29.3	31.3	2.2	-2.0	25.3	17.5	29.8	32.7
40	24.0	30.0	15.7	18.3	51.5	28.8	31.0	2.6	-2.1	25.3	17.5	30.0	32.3
41	24.0	30.0	15.9	17.6	49.5	28.4	31.1	1.7	-2.6	25.3	17.5	30.1	32.1
42	24.0	30.0	8.5	10.0	86.0	45.6	35.7	1.5	9.8	26.9	9.8	30.4	44.2
43	24.0	30.0	8.1	9.6	77.3	40.0	34.5	1.5	5.5	27.0	9.4	30.2	39.7
44	24.0	30.0	8.1	9.5	74.8	38.5	33.7	1.4	4.7	27.0	9.3	30.6	37.9
45	24.0	30.0	7.8	9.6	72.8	36.6	32.4	1.8	4.2	27.1	9.2	30.1	35.9
46	24.0	30.0	7.8	9.4	71.9	36.1	32.4	1.6	3.8	27.0	9.1	30.6	35.5
47	24.0	30.0	7.1	10.0	71.2	34.5	31.4	2.9	3.0	26.9	9.1	29.7	33.7
48	24.0	30.0	5.7	8.0	107.1	50.4	36.5	2.3	13.9	27.0	7.2	30.5	47.0
49	24.0	30.0	4.8	7.4	103.2	46.2	33.5	2.6	12.7	27.1	6.5	29.9	41.4
50	24.0	30.0	4.5	6.4	102.4	44.6	32.9	1.9	11.7	27.1	6.2	30.6	38.2
51	24.0	30.0	4.2	5.4	100.0	43.1	32.3	1.1	10.8	27.1	6.1	30.3	36.3
52	24.0	30.0	4.0	6.0	99.0	41.8	31.6	2.0	10.2	27.3	6.1	30.0	35.1
53	24.0	30.0	4.0	5.5	96.8	40.7	30.9	1.4	9.8	27.2	5.9	29.9	33.7
54	34.0	30.0	13.4	16.2	75.0	40.9	33.8	2.8	7.1	37.2	15.6	30.1	38.6
55	34.0	30.0	10.1	13.7	98.1	46.8	34.7	3.6	12.1	38.1	13.1	30.5	40.2
56	27.0	35.1	12.6	13.6	75.3	42.5	38.2	1.0	4.3	30.0	13.8	34.8	42.1
57	27.0	35.0	12.5	14.1	75.3	42.1	38.7	1.5	3.4	30.2	14.1	34.9	42.0
58	14.0	37.5	6.5	9.5	78.9	38.9	38.0	3.0	0.9	15.0	7.8	37.3	40.8
59	14.0	37.5	3.0	4.6	94.6	45.8	39.7	1.6	6.1	16.5	3.6	37.5	43.3
60	14.0	37.5	0.7	3.3	110.5	48.0	39.4	2.6	8.6	16.7	2.0	37.9	42.8
61	24.0	37.5	8.6	11.4	88.1	45.5	38.9	2.8	6.6	27.0	10.4	37.0	42.7
62	24.0	37.5	6.8	8.0	104.6	50.0	40.6	1.3	9.4	27.2	7.7	37.6	43.8
63	34.0	37.5	15.1	16.3	84.3	48.8	42.5	1.1	6.2	36.9	16.9	38.0	45.6
64	34.0	37.5	12.9	14.1	98.1	51.8	42.6	1.2	9.2	37.5	14.4	37.7	46.5
65	14.0	45.0	7.9	10.1	90.5	46.7	45.6	2.3	1.2	15.0	8.7	44.9	48.0
66	14.0	45.0	8.0	9.8	90.2	46.2	45.4	1.8	0.7	15.1	8.7	44.9	47.4
67	14.0	45.0	7.8	9.9	90.9	46.2	45.7	2.1	0.5	14.9	8.6	45.2	47.3
68	14.0	45.0	7.7	10.6	90.6	45.9	45.6	2.9	0.3	15.1	8.8	45.2	46.9
69	14.0	45.0	4.4	6.1	110.8	54.3	46.8	1.7	7.5	16.1	4.7	45.0	50.6

70	14.0	45.0	4.5	5.9	106.9	52.9	46.7	1.4	6.2	16.3	4.6	45.2	49.6
71	14.0	45.0	4.3	5.8	105.8	52.0	46.4	1.6	5.6	16.1	4.5	45.3	48.7
72	14.0	45.0	4.3	5.6	103.9	51.2	46.0	1.3	5.1	16.1	4.4	45.2	48.1
73	14.0	45.0	4.3	5.6	102.7	50.9	46.1	1.3	4.8	16.3	4.5	45.5	47.9
74	14.0	45.0	3.4	5.2	111.8	53.1	46.6	1.8	6.5	16.3	3.8	45.0	48.6
75	14.0	45.0	3.0	5.2	111.1	52.3	46.2	2.1	6.0	16.1	3.6	44.8	47.8
76	14.0	45.0	3.0	5.7	110.8	51.7	46.0	2.7	5.7	16.4	3.9	44.9	47.4
77	24.0	45.1	15.5	18.0	83.6	48.2	46.7	2.5	1.5	25.5	16.8	45.1	49.2
78	24.0	45.0	15.8	17.3	82.3	48.1	46.9	1.5	1.3	25.5	16.7	45.1	49.2
79	24.0	45.0	10.9	12.0	99.5	54.3	48.0	1.1	6.3	26.7	11.9	44.7	50.7
80	24.0	45.0	9.6	11.4	111.2	56.6	48.5	1.9	8.1	27.3	10.4	44.9	51.5
81	34.0	45.0	25.7	28.0	69.8	46.0	47.0	2.3	-0.9	35.6	27.4	45.1	48.2
82	34.0	45.0	15.2	15.9	102.3	56.6	49.2	0.7	7.4	36.9	16.3	44.7	52.3

	P _{e1} (kPa)	P _{e3} (kPa)	P _{comp.out} (kPa)	V _z (m ³ /s)	V _o (m ³ /s)	w _o (rpm)	f (Hz)	m _{ref} (kg/s)	Q _e (kW)	KW (kW)	Q _c (kW)	J _c (kW)
1	935.0	932.1	1149.6	0.13	0.44	752	19	0.00475	1.121	0.094	1.149	0.022
2	933.9	930.6	1147.1	0.13	0.44	751	19	0.00470	1.110	0.094	1.149	0.022
3	934.4	930.3	1148.5	0.13	0.44	752	19	0.00471	1.111	0.094	1.151	0.022
4	667.7	543.1	1784.6	0.13	0.44	751	95	0.01301	3.070	0.961	4.050	0.022
5	816.6	669.1	1938.9	0.13	0.44	752	95	0.01605	3.774	1.040	4.624	0.022
6	970.5	795.0	2112.4	0.13	0.44	752	95	0.01744	4.068	1.116	5.452	0.022
7	975.1	798.6	2127.6	0.13	0.44	751	95	0.01751	4.076	1.122	5.476	0.022
8	971.5	795.9	2120.0	0.13	0.44	752	95	0.01742	4.048	1.119	5.467	0.022
9	971.7	795.8	2118.8	0.13	0.44	752	95	0.01748	4.070	1.118	5.448	0.022
10	896.2	881.4	1564.3	0.13	0.44	742	30	0.00668	1.486	0.230	1.654	0.021
11	785.8	724.8	1889.3	0.13	0.44	739	60	0.01109	2.479	0.588	3.115	0.021
12	703.2	566.0	2138.0	0.13	0.44	751	95	0.01290	2.901	1.085	3.938	0.022
13	854.9	694.9	2295.9	0.14	0.44	751	95	0.01628	3.654	1.173	4.665	0.022
14	937.4	923.5	2301.7	0.13	0.16	287	30	0.00634	1.313	0.326	1.577	0.002
15	926.4	909.7	2106.9	0.13	0.25	439	30	0.00639	1.344	0.302	1.558	0.005
16	930.3	916.3	2029.5	0.13	0.35	571	30	0.00651	1.371	0.291	1.557	0.010
17	930.7	916.7	2034.9	0.13	0.35	571	30	0.00655	1.378	0.292	1.555	0.010
18	930.2	918.2	2046.3	0.13	0.35	569	30	0.00649	1.362	0.293	1.551	0.010
19	925.5	910.9	1993.3	0.13	0.44	742	30	0.00648	1.372	0.273	1.553	0.021
20	927.3	911.2	1922.4	0.13	0.53	869	30	0.00649	1.374	0.277	1.616	0.033
21	930.2	914.8	1928.5	0.13	0.63	991	30	0.00656	1.389	0.277	1.671	0.048
22	933.6	918.5	1967.0	0.13	0.72	1113	30	0.00658	1.375	0.283	1.658	0.069
23	811.5	748.7	2620.2	0.13	0.25	436	60	0.01071	2.231	0.756	2.895	0.005
24	810.7	747.6	2433.8	0.13	0.35	568	60	0.01085	2.281	0.715	2.815	0.010
25	810.0	745.5	2316.1	0.13	0.43	731	60	0.01090	2.295	0.688	3.065	0.020
26	803.1	739.5	2223.5	0.13	0.53	868	60	0.01098	2.333	0.665	2.893	0.033
27	800.1	735.9	2165.0	0.13	0.63	995	60	0.01087	2.306	0.649	2.916	0.049

28	798.4	734.2	2153.5	0.13	0.72	1119	60	0.01085	2.301	0.647	2.938	0.070
29	773.9	670.7	2873.0	0.13	0.25	439	80	0.01231	2.535	1.111	3.745	0.005
30	753.9	626.7	2737.0	0.13	0.35	571	89	0.01285	2.682	1.217	4.007	0.010
31	752.5	615.1	2668.4	0.13	0.44	747	93	0.01324	2.757	1.255	4.014	0.021
32	745.9	608.7	2549.6	0.13	0.54	872	93	0.01318	2.767	1.215	3.956	0.033
33	739.3	602.8	2483.2	0.13	0.63	996	93	0.01305	2.757	1.191	3.949	0.049
34	728.8	594.7	2414.0	0.13	0.72	1120	93	0.01288	2.742	1.165	3.942	0.070
35	1283.8	1272.1	2146.4	0.14	0.16	286	19	0.00593	1.220	0.171	1.392	0.002
36	1274.8	1263.1	1996.1	0.14	0.25	438	19	0.00606	1.271	0.155	1.356	0.005
37	1271.4	1260.3	1950.6	0.14	0.35	569	19	0.00604	1.268	0.151	1.355	0.010
38	1273.9	1261.5	1906.3	0.14	0.44	746	19	0.00612	1.292	0.146	1.346	0.021
39	1267.4	1256.3	1876.3	0.14	0.53	871	19	0.00610	1.290	0.143	1.355	0.033
40	1260.2	1249.4	1853.3	0.14	0.63	996	19	0.00606	1.290	0.142	1.336	0.049
41	1270.1	1258.3	1833.4	0.14	0.72	1120	19	0.00620	1.311	0.138	1.360	0.070
42	1013.9	931.1	2805.4	0.14	0.25	437	60	0.01409	2.877	0.802	3.489	0.005
43	1005.3	921.0	2454.2	0.14	0.35	568	60	0.01405	2.895	0.718	3.420	0.010
44	1002.2	917.8	2362.9	0.14	0.44	744	60	0.01396	2.896	0.695	3.379	0.021
45	990.9	908.7	2257.9	0.13	0.53	870	60	0.01377	2.895	0.669	3.357	0.033
46	989.8	907.8	2229.9	0.13	0.63	993	60	0.01378	2.896	0.661	3.374	0.049
47	969.5	890.5	2139.1	0.13	0.72	1116	60	0.01308	2.787	0.638	3.280	0.069
48	927.0	798.3	3138.1	0.13	0.25	442	84	0.01550	3.175	1.305	4.553	0.005
49	897.6	757.6	2846.2	0.13	0.35	575	88	0.01565	3.298	1.277	4.539	0.010
50	891.0	730.4	2742.5	0.13	0.44	752	93	0.01581	3.345	1.313	4.474	0.022
51	883.3	715.9	2644.6	0.13	0.54	878	95	0.01599	3.392	1.302	4.480	0.034
52	878.7	712.2	2564.2	0.13	0.64	1004	95	0.01589	3.402	1.274	4.528	0.050
53	876.6	707.9	2494.6	0.13	0.73	1128	95	0.01596	3.429	1.248	4.482	0.072
54	1179.0	1083.0	2508.0	0.14	0.44	753	60	0.01662	3.497	0.724	4.113	0.022
55	1069.2	893.6	2883.7	0.13	0.44	753	89	0.01842	3.897	1.329	5.285	0.022
56	1149.7	1079.7	2606.2	0.14	0.44	748	50	0.01316	2.618	0.609	3.051	0.021
57	1153.7	1083.3	2579.0	0.14	0.44	748	50	0.01325	2.629	0.603	3.030	0.021
58	947.0	924.7	2389.6	0.13	0.44	749	30	0.00612	1.218	0.337	1.542	0.021
59	847.9	773.3	2817.6	0.13	0.44	740	60	0.01076	2.104	0.796	2.876	0.021
60	784.5	681.9	2969.7	0.13	0.44	739	79	0.01201	2.373	1.129	3.500	0.021
61	1013.7	930.2	2799.3	0.13	0.44	739	60	0.01335	2.668	0.804	3.514	0.021
62	964.0	816.4	3108.5	0.13	0.44	753	95	0.01604	3.150	1.318	4.397	0.022
63	1252.2	1141.2	3020.9	0.14	0.44	753	60	0.01687	3.243	0.855	3.884	0.022
64	1163.8	1004.2	3241.5	0.14	0.44	752	81	0.01905	3.692	1.303	4.791	0.022
65	984.3	961.4	2882.5	0.13	0.44	752	30	0.00588	1.081	0.397	1.483	0.022
66	987.9	963.6	2844.7	0.13	0.54	877	30	0.00598	1.098	0.393	1.472	0.034
67	986.2	962.4	2842.9	0.13	0.63	1001	30	0.00586	1.074	0.393	1.475	0.050
68	983.4	961.1	2826.5	0.13	0.73	1125	30	0.00592	1.092	0.391	1.491	0.071
69	879.9	802.5	3428.4	0.13	0.35	574	60	0.01039	1.896	0.941	2.804	0.010
70	886.9	806.6	3324.0	0.13	0.44	752	60	0.01065	1.941	0.916	2.834	0.022
71	879.8	800.4	3252.7	0.13	0.54	876	60	0.01053	1.927	0.899	2.809	0.034

72	880.6	801.4	3192.6	0.13	0.63	1001	60	0.01061	1.945	0.885	2.812	0.050
73	882.8	803.3	3171.4	0.13	0.73	1126	60	0.01070	1.959	0.880	2.822	0.071
74	857.1	764.0	3338.2	0.13	0.53	870	68	0.01117	2.043	1.041	3.142	0.033
75	846.3	755.6	3274.8	0.13	0.63	993	68	0.01103	2.029	1.021	3.106	0.049
76	842.7	751.7	3230.4	0.13	0.72	1117	68	0.01102	2.039	1.012	3.088	0.069
77	1247.1	1217.6	2982.6	0.14	0.44	752	30	0.00802	1.471	0.406	1.781	0.022
78	1260.0	1228.5	2976.6	0.14	0.44	752	30	0.00817	1.485	0.405	1.788	0.022
79	1091.6	989.4	3431.1	0.13	0.44	753	60	0.01347	2.437	0.957	3.301	0.022
80	1045.1	916.3	3607.0	0.13	0.44	753	75	0.01515	2.755	1.300	4.009	0.022
81	1674.7	1653.0	2834.0	0.14	0.44	749	19	0.00753	1.375	0.218	1.516	0.021
82	1245.4	1096.4	3610.1	0.14	0.44	753	74	0.01833	3.303	1.294	4.557	0.022

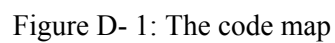
Table C- 1: Measured data [20]

Appendix D: Code

The code map is shown in Figure D- 1. The main function is Solver.m, for which the user needs to specify the cooling rate (in kW), zone temperature (in K), outside temperature (in K), evaporator airflow rate (in m³/s), condenser airflow rate (in m³/s), evaporator desuperheating (in K) and condenser subcooling (in K). The user also specifies different options for pressure drops, heat transfer coefficients, desuperheating and subcooling calculations:

esh_flag = 1 with evaporator desuperheating
esh_flag = 0 without evaporator desuperheating (set to zero desuperheating)
csc_flag = 1 with condenser subcooling
csc_flag = 0 without condenser subcooling (set to zero subcooling)
htc_flag = 1 heat transfer coefficient is calculated
htc_flag = 0 heat transfer coefficient taken as constants
(specified in Parameters.m function)
dP_flag = 1 pressure drop is calculated
dP_flag = 0 pressure drop is not calculated (set to zero)

The heat exchanger geometry and compressor constants are defined in Parameters.m function and they should be changed when a different heat pump than “Mr. Slim” is simulated.



Evaporator sub-model

```
function [mref, Tel, Te2, Te3, Pe1, Pe2, Pe3, yesh, dPe, dPesh,
exitflag] = Evaporator(Qe, hliq, Vz, dTesh, Tz, z0, esh_flag,
htc_flag, dP_flag, p)

options_e=optimset('LargeScale','off','Display','off','TolFun',0.001);

% air properties at zone temperature
rho_z = refpropm ('D','T',Tz,'P',p.Pamb,'air');% density [kg/m3]
cp_z = refpropm ('C','T',Tz,'P',p.Pamb,'air'); % thermal capac.[J/kgK]

% vapor quality at the end of evaporation
xoutep = 1;

mref      = 0;
Tel       = 0;
Te2       = 0;
Te3       = 0;
Pe1       = 0;
Pe2       = 0;
Pe3       = 0;
yesh      = 0;
dPe       = 0;
dPesh     = 0;
%+++++
% solving evaporator equations
[y,val,exitflag] = fsolve(@evaporator, z0, options_e);
%+++++
% evaluating output variables
mref      = y(1)*p.Cm;
Tel       = y(2)*p.CT;
if esh_flag
    yesh    = y(3)*p.CX1;
end
if dP_flag & esh_flag
    dPe     = y(4)*p.CP2;
    dPesh   = y(5)*p.CP1;
elseif dP_flag & ~esh_flag
    dPe     = y(3)*p.CP2;
end
%+++++
function result = evaporator(y)
    mref      = y(1)*p.Cm;
    Tel       = y(2)*p.CT;
    %.....
    % fix
    if Tel > Tz
        Tel=330;
        disp('Tel>Tz')
    end
    %.....

    Pe1 = refpropm('P','T',Tel,'Qe',1,p.Ref1,p.Ref2,p.Mix);
```

```

if esh_flag
    yesh = y(3)*p.CX1;
else
    yesh = 0;
    dTesh = 0;
end

if dP_flag & esh_flag
    dPe = y(4)*p.CP2;
    dPesh = y(5)*p.CP1;
elseif dP_flag & ~esh_flag
    dPe = y(3)*p.CP2;
    dPesh = 0;
elseif ~dP_flag
    dPe = 0;
    dPesh = 0;
end

yep = 1-yesh;

Pe2 = Pe1 - dPe;
Te2 = refpropm('T','P',Pe2,'Qe',1,p.Ref1,p.Ref2,p.Mix);
he2 = refpropm('H','P',Pe2,'Qe',1,p.Ref1,p.Ref2,p.Mix);
Pe3 = Pe2 - dPesh;

% EVAPORATING REGION

% refrigerant properties for evaporator region
[xinep, vinep, voutep, muep_l, muep_oil, hfgep, kep_l,...
...cpep_l, rhoep_l, rhoep_v] = prop_ep (Tel, Te2, hliq);
moil = p.xoil*mref; % mass flow of refrigerant oil [kg/s]

if htc_flag
    % heat transfer coefficient for evaporating region
    h_inep = htc_in2 (mref, xoutep, xinep, hfgep, muep_l,...
    ...kep_l, cpep_l, rhoep_l, rhoep_v, yep, 1, p);
    h_exep = htc_ex (Vz, Tz, 1, p);
    Uep = total_U (h_inep, h_exep, 1, p);
    UAep = yep*p.Aine*Uep; % [W/K]
else
    UAep = p.UAe;
end

% thermal capacitance and effectiveness for evaporating region
Cep = yep*rho_z*cp_z*Vz; % [W/K]
eff_ep = 1 - exp(-UAep/Cep);

if esh_flag

    % DESUPERHEATING REGION
    % properties at desuperheating region outlet
    Te3 = Tel + dTesh;

```

```

%.....
%fix
if Te3>Tz
    disp ('error Te3>Tz')
    Te3 = Te1 + 0.5;
end
%.....

he3 = refpropm('H','T',Te3,'P',Pe3,p.Ref1,p.Ref2,p.Mix);

% average properties for desuperheating region
Tesh_av = (Te2+Te3)/2;
Pesh_av = (Pe2+Pe3)/2;
[rhoesh_av, muesh_av, cpesh_av, kesh_av] = prop_esh...
...(Tesh_av, Pesh_av);

if htc_flag
    % heat transfer coeff. for desuperheating region
    h_inesh = htc_in1 (mref, muesh_av, muesh_av,...
...cpesh_av, kesh_av, yesh, 1, p);
    h_exesh = htc_ex (Vz, Tz, 1, p);
    Uesh = total_U (h_inesh, h_exesh, 1, p);
    UAesh = yesh*p.Aine*Uesh; % [W/K]
else
    UAesh = p.UAe;
end

% thermal capac. and effect. for desuperheating region
Cesh1 = mref*(he3 - he2)/(Te3-Te2);
Cesh2 = yesh*rho_z*cp_z*Vz;
Cesh_min = min([Cesh1,Cesh2]);
Cesh_max = max([Cesh1 Cesh2]);
eff_esh = Efficiency(Cesh_min,Cesh_max,UAesh);
else
    Te3 = Te2;
    he3 = he2;
end

% EQUATIONS THAT NEED TO BE SATISFIED
result(1) = mref*(he3 - hliq) - 1000*Qe;
result(2) = mref*(he2-hliq)/(Tz - Te1) - Cep*eff_ep;
if esh_flag
    result(3) = mref*(he3-he2)/(Tz - Te2) - Cesh_min*eff_esh;
end
if dP_flag & esh_flag
    result(4) = (dPe - Dp2ph (mref, moil, xinep, xoutep,...
...hfgep, vinep, voutep, muep_l, muep_oil, yep, p, 1));
    result(5) = dPesh - Dplph (mref, rhoesh_av, muesh_av,...
...yesh, p, 1);
elseif dP_flag & esh_flag ~0
    result(3) = dPe - Dp2ph (mref, moil, xinep, xoutep,...
...hfgep, vinep, voutep, muep_l, muep_oil, yep, p, 1);
end

```

```

% making sure that x's and dP's > 0
if yesh<0
    result = ones(size(y))*exp(-1e10*yesh);
end
if yesh>1
    result = ones(size(y))*exp(1e10*yesh);
end
if dPe<0
    result = ones(size(y))*exp(-1e10*dPe);
end
if dPesh<0
    result = ones(size(y))*exp(-1e10*dPesh);
end
if (Tz - Tel)<0
    result = ones(size(y))*10000;
end
end

end

%+++++
function [xin, vin, vout, mu_l, mu_oil, hfg, k_l, cp_l, rho_l,
rho_v] = prop_ep (Tel, Te2, hliq)
    Te_m = (Tel + Te2)/2;

    h_l = refpropm ('H','T',Tel,'Qe',0,p.Ref1,p.Ref2,p.Mix);
    if hliq < h_l
        xin = 0;
        rhoin = refpropm ('D','T',Tel,'Qe',0,p.Ref1,p.Ref2,p.Mix);
        disp ('hliq < h_l');
    else
        xin = refpropm ('Q','T',Tel,'H',hliq,p.Ref1,p.Ref2,p.Mix);
        rhoin = refpropm ('D','T',Tel,'H',hliq,p.Ref1,p.Ref2,p.Mix);
    end

    rhoout = refpropm ('D','T',Te2,'Qe',1,p.Ref1, p.Ref2, p.Mix);
    vin = 1/rhoin;
    vout = 1/rhoout;
    mu_l = refpropm ('V','T',Tel,'Qe',0,p.Ref1, p.Ref2, p.Mix);
    mu_oil = (250+(Te_m-273)/100*(3.7-250))*10^(-6)/1000;
    h_v = refpropm ('H','T',Te_m,'Qe',1,p.Ref1,p.Ref2,p.Mix);
    hfg = h_v - h_l; % heat of vaporisation
    k_l = refpropm ('L','T',Te_m,'Qe',0,p.Ref1,p.Ref2,p.Mix);
    cp_l = refpropm ('C','T',Te_m,'Qe',0,p.Ref1,p.Ref2,p.Mix);
    rho_l = refpropm ('D','T',Te_m,'Qe',0,p.Ref1,p.Ref2,p.Mix);
    rho_v = refpropm ('D','T',Te_m,'Qe',1,p.Ref1,p.Ref2,p.Mix);
end

%+++++
function [rho_av, mu_av, c_av, k_av] = prop_esh (T_av, P_av)
    rho_av = refpropm ('D','T',T_av,'P',P_av,p.Ref1, p.Ref2,p.Mix);
    mu_av = refpropm ('V','T',T_av,'P',P_av,p.Ref1, p.Ref2,p.Mix);
    c_av = refpropm ('C','T',T_av,'P',P_av,p.Ref1, p.Ref2,p.Mix);
    k_av = refpropm ('L','T',T_av,'P',P_av,p.Ref1, p.Ref2,p.Mix);
end

end

```

Suction pipe sub-model

```
function [Pcomp_in, dPs] = Suction_pipe (mref, Te3, Pe3, p)

% setting initial guess
dPs0 = 5; % [kPa]
options_s = optimset('LargeScale','off','Display','off');

% setting pressure drop equation
dPs = fsolve(@PressureDrop,dPs0,options_s);

% evaluating output variable
dPs;
Pcomp_in = Pe3-dPs;

%%%%%%%%%%%%%%%%%%%%%%%%%%%%%%%%%%%%%%%%%%%%%%%%%%%%%%%%%%%%%%%%%%%%%%%%%%%%%%

function result = PressureDrop (dPs)
    % properties for Te3 and average pressure in suction pipe
    Pcomp_in = Pe3-dPs;
    Ps_av = (Pe3+Pcomp_in)/2;
    rhos = refpropm ('D','T',Te3,'P',Ps_av,p.Ref1,p.Ref2,p.Mix);
    mus = refpropm ('V','T',Te3,'P',Ps_av,p.Ref1,p.Ref2,p.Mix);

    % equation that needs to be satisfied
    result = dPs - Dplph (mref, rhos, mus, 1, p, 2);
end

end
```

Compressor sub-model

```

function [Tcomp_out, f, KW, Q_oil, exitflag_m] = Compressor(mref,
Tcomp_in, Pcomp_in, Pcomp_out, To, z0, p)

options_m =optimset('LargeScale','off','Display','off','TolFun',1e-6);

Tcomp_out    = 0;
f             = 0;
KW            = 0;
Q_oil        = 0;

% properties at compressor inlet
rhocomp_in=refpropm('D','T',Tcomp_in,'P',Pcomp_in,p.Ref1,p.Ref2,p.Mix)
hcomp_in =refpropm('H','T',Tcomp_in,'P',Pcomp_in,p.Ref1,p.Ref2,p.Mix);
scomp_in =refpropm('S','T',Tcomp_in,'P',Pcomp_in,p.Ref1,p.Ref2,p.Mix);
rho_both=refpropm('D','P',Pcomp_out,'S',scomp_in,p.Ref1,p.Ref2,p.Mix);

% constants
ns = log(Pcomp_out/Pcomp_in)/log(rho_both/rhocomp_in);
cp = refpropm ('C','T',Tcomp_in,'P',Pcomp_in,p.Ref1,p.Ref2,p.Mix);
cv = refpropm ('O','T',Tcomp_in,'P',Pcomp_in,p.Ref1,p.Ref2,p.Mix);
k = cp/cv;
moil = p.xoil*mref; % mass flow of refrigerant oil [kg/s]
vdot = mref/rhocomp_in; % volumetric flow rate
Prat = Pcomp_out/Pcomp_in; % pressure ratio

%+++++
% calculating frequency
etaV = 1-p.C2*((Prat^(1/ns))-1);
f = (vdot + p.C3*(Pcomp_out-Pcomp_in)/1000)./(p.C1*etaV);
w = f*60/1800; % RPM/1800 RPM

% calculating power
eta_comb = p.C4 + p.C5*exp(p.C6*Prat);
KW = (1/eta_comb)*mref*(ns/(ns-1))*(Pcomp_in/rhocomp_in)*...
...((Prat^((ns-1)/ns))-1); % kW

% iterating discharge temperature
[y,val,exitflag_m] = fsolve(@compressor,z0,options_m);
Tcomp_out = y(1);

% checking
if Tcomp_out < To
    display ('Tcomp_out < To');
end

%+++++

function result = compressor (y)
    Tcomp_out      = y(1);

    if Tcomp_out> 430
        Tcomp_out=430;
    end

```

```

hcomp_out=refpropm('H','T',Tcomp_out,'P',...
...Pcomp_out,p.Ref1,p.Ref2,p.Mix);
Q_comp = mref*(hcomp_out-hcomp_in)/1000; % kW
Q_oil = moil*p.coil*(Tcomp_out-Tcomp_in)/1000; % kW

% equation that needs to be satisfied
result (1) = KW-Q_comp-Q_oil;
end

end

```

Discharge pipe sub-model

```
function [dPd] = Discharge_pipe (mref, Tcomp_out, Pcomp_out, p)

% setting initial guess
dPd0 = 5; % [kPa]
options_d = optimset('LargeScale','off','Display','off');

% setting pressure drop equation
dPd = fsolve(@PressureDrop,dPd0,options_d);

% evaluating output variable
dPd;

%%%%%%%%%%%%%%%%%%%%%%%%%%%%%%%%%%%%%%%%%%%%%%%%%%%%%%%%%%%%%%%%%%%%%%%%

function result = PressureDrop (dPd)
    % prop. for Tcomp_out and average pressure in discharge pipe
    Pc1 = Pcomp_out-dPd;
    Pd_av = (Pcomp_out+Pc1)/2;
    Rhod = refpropm ('D','T',Tcomp_out,'P',Pd_av,...
    ... p.Ref1,p.Ref2,p.Mix);
    mud = refpropm ('V','T',Tcomp_out,'P',Pd_av,...
    ...p.Ref1,p.Ref2,p.Mix);

    % equation that needs to be satisfied
    result = dPd - Dplph (mref, rhod, mud, 1, p, 3);

end

end
```

Condenser sub-model

```
function [Qc, hliq, Tc2, Tc3, Tc4, Pc1, Pc2, Pc3, Pc4, ysc, ycp,...
...ysc, dPcsh, dPcp, dPsc, dTsc_correction, exitflag] = ...
...Condenser(mref, Vo, Tc1, dTsc, To, z0,csc_flag,htc_flag,dP_flag, p)

options_c=optimset('LargeScale','off','Display','off','TolFun',
0.001);

% air properties at ambient temperature
rho_o = refpropm ('D','T',To,'P',p.Pamb,'air'); % density [kg/m3]
cp_o  = refpropm ('C','T',To,'P',p.Pamb,'air');% thermal capac.[J/kgK]

Qc      = 0;
hliq    = 0;
Tc2     = 0;
Tc3     = 0;
Tc4     = 0;
Pc1     = 0;
Pc2     = 0;
Pc3     = 0;
Pc4     = 0;
ycsh    = 0;
ycp     = 0;
ysc     = 0;
dPcsh   = 0;
dPcp    = 0;
dPsc    = 0;
Qsh     = 0;
Qcp     = 0;
Qsc     = 0;
dTsc_correction = 0;
dTsc_local = 0;
Divider_c=1;

%+++++

% solving condenser equations
[y,val,exitflag] = fsolve(@condenser, z0, options_c);

if exitflag < 0
    Divider_c=10;
    [y,val,exitflag] = fsolve(@condenser, z0, options_c);
end

%+++++

% evaluating output variables
Qc = Qsh + Qcp + Qsc; % [kW]
ycp = y(1)*p.CX2;
Pc1 = y(2)*p.C1000;
if csc_flag
    ysc = y(3)*p.CX1;
end
```

```

if dP_flag & csc_flag
    dPcsh = y(4)*p.CP1;
    dPcp  = y(5)*p.CP2;
    dPsc  = y(6)*p.CP1;
elseif dP_flag & ~csc_flag
    dPcsh = y(3)*p.CP1;
    dPcp  = y(4)*p.CP2;
end

ycp = 1 - ycsh - ysc;

%+++++

function result = condenser(y)

    ycp = y(1)*p.CX2;
    Pc1 = y(2)*p.C1000;

    if csc_flag
        ysc = y(3)*p.CX1;
    else
        ysc = 0;
        dTsc = 0;
    end

    if dP_flag & csc_flag
        dPcsh = y(4)*p.CP1;
        dPcp  = y(5)*p.CP2;
        dPsc  = y(6)*p.CP1;
    elseif dP_flag & ~csc_flag
        dPcsh = y(3)*p.CP1;
        dPcp  = y(4)*p.CP2;
        dPsc  = 0;
    elseif ~dP_flag
        dPcsh = 0;
        dPcp  = 0;
        dPsc  = 0;
    end

    ycsh = 1 - ycp - ysc;
    if ycsh < 0
        ycsh = 0.00000001;
    end

    Pc2 = Pc1 - dPcsh;
    Tc2 = refpropm('T','P',Pc2,'Q',1,p.Ref1,p.Ref2,p.Mix);
    Pc3 = Pc2 - dPcp;
    Tc3 = refpropm('T','P',Pc3,'Q',0,p.Ref1,p.Ref2,p.Mix);
    Pc4 = Pc3 - dPsc;
    Tc4_trial = Tc3 - dTsc;

    % solving case if Tc4 < To
    if csc_flag
        if Tc4_trial < To
            if (Tc3 - To) < 0.5

```

```

        dTsc_local = 0.01; % no desuperheating
    else
        dTsc_local = Tc3 - To - 0.5;
    end
    else
        dTsc_local = dTsc;
    end
    Tc4 = Tc3 - dTsc_local;
else
    Tc4 = Tc3;
end

% DESUPERHEATING REGION

if Tc2>Tc1
    disp ('error Tc2>Tc1')
    Tc1 = Tc2+0.1;
end

% properties in desuperheating region
hc2 = refpropm('H','P',Pc2,'Q',1,p.Ref1,p.Ref2,p.Mix);
hc1 = refpropm('H','T',Tc1,'P',Pc1,p.Ref1,p.Ref2,p.Mix);

% average properties for desuperheating region
Tsh_av = (Tc1+Tc2)/2;
Psh_av = (Pc1+Pc2)/2;
[rhosh_av, mush_av, cpsh_av, ksh_av] = prop_csh ...
...(Tsh_av, Psh_av);

if htc_flag
    % heat transfer coefficient for desuperheating region
    h_incsch = htc_in1 (mref, mush_av, mush_av, cpsh_av,...
    ...ksh_av, ycsch, 2, p);
    h_excsch = htc_ex (Vo, To, 0, p);
    Ucsh = total_U (h_incsch, h_excsch, 0, p);
    UAcsch = ycsch*p.Ainc*Ucsh;
else
    UAcsch = p.UAc;
end

% thermal capac. and effect. for desuperheating region
Ccsh1 = mref*(hc1 - hc2)/(Tc1 - Tc2);
Ccsh2 = ycsch*Vo*rho_o*cp_o;
Ccsh_min = min([Ccsh1 Ccsh2]);
Ccsh_max = max([Ccsh1 Ccsh2]);
eff_csh = Efficiency(Ccsh_min,Ccsh_max,UAcsch);

% heat exchanged in desuperheating region
Qsh = mref*(hc1 - hc2)/1000;

% CONDENSING REGION
% properties at condensing region outlet

hc3 = refpropm('H','P',Pc3,'Q',0,p.Ref1, p.Ref2, p.Mix);
Tc3 = refpropm('T','P',Pc3,'Q',0,p.Ref1, p.Ref2, p.Mix);

```

```

% refrigerant properties for condenser region
[vinc, voutc, muc_l, muc_oil, hfgc, kc_l, cpc_l,...
...rhoc_l, rhoc_v] = prop_cp (Tc2, Tc3);
moil = p.xoil*mref; % mass flow of refrigerant oil [kg/s]

if htc_flag
    % heat transfer coefficient for condensing region
    h_incp = htc_in2 (mref, 0, 1, hfgc, muc_l, kc_l, ...
...cpc_l, rhoc_l, rhoc_v, ycp, 0, p);
    h_excp = htc_ex (Vo, To, 0, p);
    Ucp = total_U (h_incp, h_excp, 0, p);
    UAcp = ycp*p.Ainc*Ucp; % [W/K]

else
    UAcp = p.UAc;
end

% thermal capacitance and effectiveness for condensing region
Ccp = ycp*rho_o*cp_o*Vo; % [W/K]
eff_cp = 1 - exp(-UAcp/Ccp);

% heat exchanged in condensing region
Qcp = mref*(hc2 - hc3)/1000;

% SUBCOOLING REGION

% properties at subcooling region outlet
hliq = refpropm('H','T',Tc4,'P',Pc4,p.Ref1, p.Ref2, p.Mix);
if hliq>hc3
    hliq = refpropm('H','T',Tc4,'Q',0,p.Ref1, p.Ref2, p.Mix);
end

% average properties for subcooling region
[rhosc_av, musc_av, cp_sc_av, ksc_av] = prop_sc (Tc3, Tc4);

if htc_flag
    % heat transfer coefficient for subcooling region
    h_insc = htc_in1 (mref, musc_av, musc_av, cp_sc_av,...
...ksc_av, ysc, 3, p);
    h_exsc = htc_ex (Vo, To, 0, p);
    Usc = total_U (h_insc, h_exsc, 0, p);
    UAsc = ysc*p.Ainc*Usc; % [W/K]
else
    UAsc = p.UAc;
end

if csc_flag
    % thermal capac. and effectiveness for subcooling region
    Csc1 = mref*(hc3 - hliq)/(Tc3-Tc4);
    Csc2 = ysc*Vo*rho_o*cp_o;
    Csc_min = min([Csc1 Csc2]);
    Csc_max = max([Csc1 Csc2]);
    eff_sc = Efficiency (Csc_min,Csc_max,UAsc);

```

```

        % heat exchanged in subcooling region
        Qsc = mref*(hc3 - hliq)/1000;
    end

    dTsc_correction = dTsc - dTsc_local;

    % EQUATIONS THAT NEED TO BE SATISFIED
    result(1) = Qcp*1000/(eff_cp*Ccp) - (Tc2 - To);
    result(2) = Qsh*1000/(eff_csh*Ccsh_min) - (Tc1 - To);
    if csc_flag
        result(3)=(Qsc*1000/(eff_sc*Csc_min)-(Tc3-To))/Divider_c;
    end
    if dP_flag & csc_flag
        result(4)=dPcsh-Dp1ph(mref, rhosh_av, mush_av, ycsh,p,4);
        result(5) = dPcp - Dp2ph (mref, p.xoil*mref, 1,0,hfgc,...
        ...vinc, voutc, muc_l, muc_oil, ycp, p, 0);
        result(6)=dPsc-Dp1ph (mref, rhosc_av, musc_av, ysc, p, 5);
    elseif dP_flag & csc_flag ~0
        result(3)=dPcsh-Dp1ph(mref, rhosh_av, mush_av, ycsh,p,4);
        result(4) = dPcp - Dp2ph (mref, p.xoil*mref, 1, 0,hfgc,...
        ...vinc, voutc, muc_l, muc_oil, ycp, p, 0);
    end

    % making sure that x's and dP's > 0

    if (1 - ycp - ysc) < 0
        result = ones(size(y))*exp(1e10);
    end
    if (1-ycp) < 0
        result = ones(size(y))*exp(1e10*ycp);
    end
    if ycsh < 0
        result = ones(size(y))*exp(-1e10*ycsh);
    end
    if ysc < 0
        result = ones(size(y))*exp(-1e10*ysc);
    end
    if dPcsh < 0
        result = ones(size(y))*exp(-1e10*dPcsh);
    end
    if dPcp < 0
        result = ones(size(y))*exp(-1e10*dPcp);
    end
    if dPsc < 0
        result = ones(size(y))*exp(-1e10*dPsc);
    end
end
end

```

```

%+++++

function [rho_av, mu_av, c_av, k_av] = prop_csh (T_av, P_av)

    rho_av=refpropm('D','T',T_av,'P',P_av, p.Ref1, p.Ref2, p.Mix);
    mu_av=refpropm('V','T',T_av,'P',P_av, p.Ref1, p.Ref2, p.Mix);
    c_av=refpropm('C','T',T_av,'P',P_av, p.Ref1, p.Ref2, p.Mix);
    k_av=refpropm('L','T',T_av,'P',P_av, p.Ref1, p.Ref2, p.Mix);

end

function [vin, vout, mu_l, mu_oil, hfg, k_l, cp_l, rho_l, rho_v] =
    prop_cp (Tc2, Tc3)

    rhoin = refpropm ('D','T',Tc2,'Q',1,p.Ref1, p.Ref2, p.Mix);
    rhoout = refpropm ('D','T',Tc3,'Q',0,p.Ref1, p.Ref2, p.Mix);
    vin = 1/rhoin;
    vout = 1/rhoout;
    mu_l = refpropm ('V','T',Tc3,'Q',0,p.Ref1, p.Ref2, p.Mix);
    Tc_av = (Tc2+Tc3)/2;
    mu_oil = (250+(Tc_av-273)/100*(3.7-250))*10^(-6)/1000;
    h_l = refpropm ('H','T',Tc3,'Q',0,p.Ref1, p.Ref2, p.Mix);
    h_v = refpropm ('H','T',Tc2,'Q',1,p.Ref1, p.Ref2, p.Mix);
    hfg = h_v - h_l;
    k_l = refpropm ('L','T',Tc3,'Q',0,p.Ref1, p.Ref2, p.Mix);
    cp_l = refpropm ('C','T',Tc3,'Q',0,p.Ref1, p.Ref2, p.Mix);
    rho_l = refpropm ('D','T',Tc3,'Q',0,p.Ref1, p.Ref2, p.Mix);
    rho_v = refpropm ('D','T',Tc2,'Q',1,p.Ref1, p.Ref2, p.Mix);
end

function [rho_av, mu_av, c_av, k_av] = prop_sc (Tc3, Tc4)
    T_av = (Tc3 + Tc4)/2;
    rho_av = refpropm ('D','T',T_av,'Q',0,p.Ref1, p.Ref2, p.Mix);
    mu_av = refpropm ('V','T',T_av,'Q',0,p.Ref1, p.Ref2, p.Mix);
    c_av = refpropm ('C','T',T_av,'Q',0,p.Ref1, p.Ref2, p.Mix);
    k_av = refpropm ('L','T',T_av,'Q',0,p.Ref1, p.Ref2, p.Mix);
end

end

```

System solver

```
function [mref, Te1, Te2, Te3, Pe1, Pe2, Pe3, hliq, yesh, dPep,...
...dPesh, Je, Pcomp_in, Pcomp_out, f, KW, Q_oil, Qc, Tc1, Tc2, Tc3,...
...Tc4, Pc1, Pc2, Pc3, Pc4, yesh, ysc, dPcsh, dPcp, dPsc, Jc,...
...dTsc_correction, exitflag] = Solver(Qe, Tz, To, Vz, Vo, dTesh,...
...dTsc, esh_flag, csc_flag, htc_flag, dP_flag)

close all
clc

options=optimset('LargeScale','off','Display','off','TolFun',0.000001);

global p
p = Parameters;

mref      = 0;
Te1       = 0;
Te2       = 0;
Te3       = 0;
Pe1       = 0;
Pe2       = 0;
Pe3       = 0;
hliq      = 0;
yesh      = 0;
dPep      = 0;
dPesh     = 0;
Pcomp_in  = 0;
Pcomp_out = 0;
f         = 0;
KW        = 0;
Qc        = 0;
Tc1       = 0;
Tc2       = 0;
Tc3       = 0;
Tc4       = 0;
Pc1       = 0;
Pc2       = 0;
Pc3       = 0;
Pc4       = 0;
yesh      = 0;
ysc       = 0;
dPcsh     = 0;
dPcp      = 0;
dPsc      = 0;
dTsc_correction = 0;
Divider   = 1;
Divider_s = 1;
%+++++
```

```

% INITIAL ASSUMPTIONS
mref0    = 0.016;
Te10     = 270;
yesh0    = 0.07;
dPep0    = 3;
dPesh0   = 1;
ycp0     = 0.8;
Pc10     = 2750;
ysc0     = 0.07;
dP10     = 10;
dP20     = 100;
hliq_as0 = refpropm ('H','T',285,'Qe',0, p.Ref1, p.Ref2, p.Mix);
Tcomp_out0 = 320;

% system
z0_s = [Pc10/p.C1000];

% evaporator
ze0_s = [mref0/p.Cm Te10/p.CT];

% % compressor
zm0_s = [Tcomp_out0];

% condenser
zc0_s = [ycp0/p.CX2, Pc10/p.C1000];

%%%%%%%%%%%%%%%%%%%%%%%%%%%%%%%%%%%%%%%%%%%%%%%%%%%%%%%%%%%%%%%%%%%%%%%%

% SYSTEM SOLVER
[z_s, val, exitflag_system] = fsolve(@Call_component_models_simple,
z0_s, options);

if (exitflag_system < 1)
    Divider_s = Divider_s*10;
    [z_s, val, exitflag_system] =
fsolve(@Call_component_models_simple, z0_s, options);
end

%%%%%%%%%%%%%%%%%%%%%%%%%%%%%%%%%%%%%%%%%%%%%%%%%%%%%%%%%%%%%%%%%%%%%%%%
% OUTPUT VARIABLES
Pcomp_out_s    = z_s(1)*p.C1000;
mref           = mref_s;
Te1            = Te1_s;
Te2            = Te2_s;
Te3            = Te3_s;
Pe1            = Pe1_s;
Pe2            = Pe2_s;
Pe3            = Pe3_s;
yesh           = yesh_s;
dPep           = dPep_s;
dPesh          = dPesh_s;
Pcomp_in       = Pcomp_in_s;
Pcomp_out      = Pcomp_out_s;
f              = f_s;

```

```

KW          = KW_s;
Qc          = Qc_s;
Tc1         = Tc1_s;
Tc2         = Tc2_s;
Tc3         = Tc3_s;
Tc4         = Tc4_s;
Pc1         = Pc1_s;
Pc2         = Pc2_s;
Pc3         = Pc3_s;
Pc4         = Pc4_s;
yesh        = yesh_s;
ycsh        = ycsh_s;
ycp         = ycp_s;
ysc         = xsc_s;
dPcsh       = dPcsh_s;
dPcp        = dPcp_s;
dPsc        = dPsc_s;
hliq        = hliq_s;

if (dP_flag) || (esh_flag) || (csc_flag) || (htc_flag)

    % evaporator
    ze0 = [mref_s/p.Cm Tel_s/p.CT];
    if esh_flag
        ze0 = [mref_s/p.Cm Tel_s/p.CT yesh0/p.CX1];
    end
    if dP_flag & esh_flag
        ze0=[mref_s/p.Cm Tel_s/p.CT yesh0/p.CX1 dP20/p.CP2
dP10/p.CP1];
    end
    if dP_flag & ~esh_flag
        ze0 = [mref_s/p.Cm Tel_s/p.CT dP20/p.CP2];
    end

    % compressor
    zm0 = [Tc1_s];

    % condenser
    zc0 = [ycp0/p.CX2, Pc1_s/p.C1000];
    if csc_flag
        zc0 = [ycp0/p.CX2, Pc1_s/p.C1000 ysc0/p.CX1];
    end
    if dP_flag & csc_flag
        zc0 = [ycp0/p.CX2 Pc1_s/p.C1000 ysc0/p.CX1 dP10/p.CP1
dP20/p.CP2 dP10/p.CP1];
    end
    if dP_flag & ~csc_flag
        zc0 = [ycp0/p.CX2, Pc1_s/p.C1000 dP10/p.CP1 dP20/p.CP2];
    end

    z0 = [Pc1_s/p.C1000, hliq_s/p.Ce5];

```

```

%+++++
% SYSTEM SOLVER

[z,fval,exitflag_system]=fsolve(@Call_component_models,z0,options);

%+++++
    if (exitflag_system < 1)
        Divider = Divider*10;
[z,fval,exitflag_system]=fsolve(@Call_component_models,z0,options);
    end

    % OUTPUT VARIABLES
    Pcomp_out    = z(1)*p.C1000;
    hliq         = z(2)*p.Ce5;

end

wz = interp1(p.flowdata_c(:,4),p.flowdata_c(:,1),...
... (Vz/0.00047194744322), 'linear', 'extrap'); %(rpm)
Je = (p.FanC1*(wz^3)+ p.FanC2*(wz^2)+ p.FanC3*wz+ p.FanE4)/1000;
%(kW)
wo =interp1(p.flowdata_c(:,4),p.flowdata_c(:,1),...
... (Vo/0.00047194744322), 'linear', 'extrap'); %(rpm)
Jc = (p.FanC1*(wo^3)+ p.FanC2*(wo^2)+ p.FanC3*wo+ p.FanC4)/1000;
%(kW)

%check if some fsolve didn't itterate
if (exitflag_system < 1) || (exitflag_e < 1) || (exitflag_m <
1) || (exitflag_c < 1)
    exitflag = 0
else
    exitflag = 2;
end
if (Te1>Tz) || (Te3>Tz)
    disp ('Te>Tz')
end
if Tc2>Tc1
    disp ('Tc2>Tc1')
end
if (To>Tc1) || (To>Tc2) || (To>Tc3) || (To>Tc4)
    disp ('To>Tc')
end

%+++++
function result = Call_component_models_simple (z_s)

    Pcomp_out_s = z_s(1)*p.C1000;
    %.....
    % fix
    if Pcomp_out_s < 300;
        Pcomp_out_s = 300;
    end
    %.....

    hliq_as=refpropm('H','P',Pcomp_out_s,'Qe',0,p.Ref1,p.Ref2,p.Mix);

```

```

% CALL EVAPORATOR MODEL
[mref_s, Te1_s, Te2_s, Te3_s, Pe1_s, Pe2_s, Pe3_s, yesh_s,...
...dPep_s, dPesh_s,exitflag_e] = Evaporator(Qe, hliq_as,Vz,...
...dTesh, Tz, ze0_s, 0, 0, 0, p);

Pcomp_in_s = Pe3_s;

% CALL COMPRESSOR MODEL
Tcomp_in_s = Te3_s;
[Tcomp_out_s, f_s, KW_s, Q_oil, exitflag_m] = Compressor...
...(mref_s, Tcomp_in_s, Pcomp_in_s, Pcomp_out_s, To, zm0_s,p);

% CALL CONDENSER MODEL
Tc1_s = Tcomp_out_s;
%.....
% fix
if Tcomp_out_s < To
    Tc1_s = To+20;
end
%.....
[Qc_s, hliq_s, Tc2_s, Tc3_s, Tc4_s, Pc1_s, Pc2_s, Pc3_s,...
...Pc4_s, ycsh_s, ycp_s, xsc_s, dPcsh_s, dPcp_s, dPsc_s,...
... dTsc_correction, exitflag_c] = Condenser(mref_s, Vo,...
... Tc1_s, dTsc, To, zc0_s, 0, 0, 0, p);

% SYSTEM EQUATION THAT NEEDS TO BE SATISFIED
result (1) = (Pcomp_out_s - Pc1_s)/Divider_s;

% SETTING NEW INITIAL GUESS
% evaporator
ze0_s = [mref_s/p.Cm Te1_s/p.CT];
% compressor
zm0_s = [Tcomp_out_s];
% condenser
zc0_s = [ycp_s/p.CX2, Pc1_s/p.C1000];

end
%+++++
function result = Call_component_models (z)

Pcomp_out_as = z(1)*p.C1000;
hliq_as      = z(2)*p.Ce5;

% CALL EVAPORATOR MODEL
[mref, Te1, Te2, Te3, Pe1, Pe2, Pe3, yesh, dPep, dPesh,...
... exitflag_e] = Evaporator(Qe, hliq_as, Vz, dTesh, Tz,...
... ze0, esh_flag, htc_flag, dP_flag, p);

% CALL SUCTION PIPE MODEL
if dP_flag
    [Pcomp_in, dPs] = Suction_pipe (mref, Te3, Pe3, p);
else
    Pcomp_in = Pe3;
end

```

```

% CALL COMPRESSOR MODEL
Tcomp_in = Te3;
[Tcomp_out, f, KW, Q_oil, exitflag_m] = Compressor...
...(mref, Tcomp_in, Pcomp_in, Pcomp_out_as, To, zm0, p);

% CALL DISCHARGE PIPE MODEL
if dP_flag
    [dPd] = Discharge_pipe (mref, Tcomp_out, Pcomp_out_as, p);
else
    dPd = 0;
end

% CALL CONDENSER MODEL
Tc1 = Tcomp_out;
[Qc, hliq, Tc2, Tc3, Tc4, Pc1, Pc2, Pc3, Pc4, yesh, ycp, ysc,...
...dPcsh, dPcp, dPsc, dTsc_correction, exitflag_c]=Condenser...
...(mref, Vo, Tc1, dTsc, To, zc0, csc_flag, htc_flag, dP_flag, p);

% SYSTEM EQUATION THAT NEEDS TO BE SATISFIED

result (1) = Pcomp_out_as/(Pc1+dPd) - 1;
result (2) = (hliq/hliq_as - 1)/Divider;

% SETTING NEW INITIAL GUESS
% evaporator
ze0 = [mref/p.Cm Tel/p.CT];
if esh_flag
    ze0 = [mref/p.Cm Tel/p.CT yesh/p.CX1];
end
if dP_flag & esh_flag
    ze0=[mref/p.Cm Tel/p.CT yesh/p.CX1 dPep/p.CP2,dPesh/p.CP1];
end
if dP_flag & ~esh_flag
    ze0 = [mref/p.Cm Tel/p.CT dPep/p.CP2];
end
% compressor
zm0 = [Tcomp_out];
% condenser
zc0 = [ycp/p.CX2, Pc1/p.C1000];
if csc_flag
    zc0 = [ycp/p.CX2, Pc1/p.C1000 ysc/p.CX1];
end
if dP_flag & csc_flag
    zc0 = [ycp/p.CX2 Pc1/p.C1000 ysc/p.CX1 dPcsh/p.CP1...
...dPcp/p.CP2 dPsc/p.CP1];
end
if dP_flag & ~csc_flag
    zc0 = [ycp/p.CX2, Pc1/p.C1000 dPcsh/p.CP1 dPcp/p.CP2];
end

end

%+++++
end

```

Constants

```
function p = Parameters;

% GENERAL PARAMETERS

p.Ref1 = 'R32';
p.Ref2 = 'R125';
p.Mix = [0.69761, 0.30239];
p.T_min = 137.44;
p.T_max = 346.86;

p.Mref = 72.585; % molar mass for R410A [kg/kmol]
p.Moil = 600; % molar mass for lubricant [kg/kmol]
p.Pamb = 101.325; % atmospheric pressure [kPa]
p.E = 1.5*10^(-6); % pipe roughnes [m]
p.kfin = 235; % fin thermal conductivity [W/mK]
p.loss180 = 1; % loss factor due to the turning of the flow [-]
p.loss_valve = 2; % service and reversing valves pressure loss factor
[
p.xoil = 0.04; % precentage of oil in the refrigerant [-]
p.coil = 1670; %specific heat of oil [J/kgK] NOT SURE, CHECK

%+++++

% COMPONENTS PARAMETERS

% evaporator parameters
LE = 0.62; %[m] evaporator length
HE = 0.34; %[m] evaporator height
WE = 0.0254; %[m] evaporator depth
fins_per_inch_e = 20; % number of fins per inch
N_pipes_e = 2*16; % total number of pipes, two branches
N_fins_e = LE*39.37007874*fins_per_inch_e;
p.dine = 0.00475; % tube inside diameter [m]
p.dexe = 0.0067564; % tube outside diameter [m]
p.Le = N_pipes_e*LE; % tube length [m]
p.Aine = p.dine*pi*p.Le; % inside area [m2]
p.Aexe = p.dexe*pi*p.Le; % outside area [m2]
p.Afine = 2*N_fins_e*(HE*WE-N_pipes_e*(pi*(p.dexe^2)/4));%fin area
[m2]
p.tfine = 0.0001016; % fin tickness [m]
p.S1e = 0.0127; % fin square side 1 [m]
p.S2e = 0.0387; % fin square side 2 [m]
p.sve = 0.018; % vertical distance between tubes [m]
p.she = 0.018; % horizontal distance between tubes [m]
p.sde = 0.00127; % distance between fins [m]
p.Amine = 0.03; % minimum flow area [m2]
p.Nturne_total_e = 2*16; % number of U-turns for the whole evaporator
p.localloss_evap = p.Nturne_total_e*p.loss180; % local pressure drop
factor in the whole evaporator
p.UAe = 220;
```

```

% condenser parameters
LC = 0.85725; %[m] evaporator length
HC = 0.504825; %[m] evaporator height
WC = 0.022225; %[m] evaporator depth
fins_per_inch_c = 18; % number of fins per inch
N_pipes_c = 2*12; % total number of pipes, two branches
N_fins_c = LC*39.37007874*fins_per_inch_c;
p.dinc = 0.00475; % tube inside diameter [m]
p.dexc = 0.0065278; % tube outside diameter [m]
p.Lc = N_pipes_c*LC; % tube length [m]
p.Ainc = p.dinc*pi*p.Lc; % inside area [m2]
p.Aexc = p.dexc*pi*p.Lc; % outside area [m2]
p.Afinc = 2*N_fins_c*(HC*WC-N_pipes_c*(pi*(p.dexc^2)/4));%fin area[m2]
p.tfinc = 7.62*10^(-5); % fin tickness [m]
p.S1c = 0.0215; % fin square side 1 [m]
p.S2c = 0.0222; % fin square side 2 [m]
p.svc = 0.018; % vertical distance between tubes [m]
p.shc = 0.018; % horizontal distance between tubes [m]
p.sdc = 0.00127; % distance between fins [m]
p.Aminc = 0.3; % minimum flow area [m2]
p.Nturnc_total_c = 2*12; % number of U-turns for the whole condenser
p.localloss_cond = p.Nturnc_total_c*p.loss180; % local pressure drop
factor in the whole condenser [-]
p.UAc = 830;

% suction pipe parameters
p.ds = 0.007925; % internal diameter [m]
p.Ls = 3; % pipe length [m]
p.locals = 10; % local pressure drop factor [-]

% discharge pipe parameters
p.dd = 0.007925; % pipe internal diameter [m]
p.Ld = 1.1; % pipe length [m]
p.locald = 10; % local pressure drop factor [-]

% compressor constants
p.C1 = 9.012585198e-006;
p.C2 = 4.0681827744500e-002;
p.C3 = 2.3901776617e-005;
p.C4 = 0.187485429274809;
p.C5 = 0.610814730911499 ;
p.C6 = -0.091200283613269;
%+++++
% constants used to calculate fan input power [-]
p.FanC1 = 5.949e-008;
p.FanC2 = -2.049e-005;
p.FanC3 = 0.01155;
p.FanC4 = -0.7439;
p.FanE4 = 22;

% condenser air flow to fan speed
p.flowdata_c = [300 1.345625 264.8868114 351.3086631;...
...450 2.103958333 414.1650269 549.2903218;...
...600 2.988125 588.2135836 780.1238822;...
...750 3.590625 706.815946 937.4213978;...
...900 4.519166667 889.5997389 1179.840149];

```

```
% FACTORS FOR RELATIVIZATION
p.Cm = 0.01;
p.CX2 = 1;
p.CX1 = 0.1;
p.CVe = 0.15;
p.CVc = 0.5;
p.CP1 = 10;
p.CP2 = 100;
p.C10 = 10;
p.C100 = 100;
p.C1000 = 1000;
p.Ce5 = 1e+005;
p.CT = 273;

end
```

Heat transfer coefficient calculations

External heat transfer coefficient calculations

```
function h_ex = htc_ex (Vex, Tex, evap_flag, p);

if evap_flag == 1 % for evaporator
    Amin = p.Amine;
    dex = p.dexe;
    sv = p.sve;
    sh = p.she;
    sd = p.sde;
    Rows = 2;
elseif evap_flag == 0 % for condenser
    Amin = p.Aminc;
    dex = p.dexc;
    sv = p.svc;
    sh = p.shc;
    sd = p.sdc;
    Rows = 1;
End

%+++++
% air properties at zone/ambient temperature
rho_ex = refpropm ('D','T',Tex,'P',p.Pamb,'air');
mu_ex = refpropm ('V','T',Tex,'P',p.Pamb,'air');
c_ex = refpropm ('C','T',Tex,'P',p.Pamb,'air');
k_ex = refpropm ('L','T',Tex,'P',p.Pamb,'air');
nu_ex = mu_ex/rho_ex;

%+++++

%air velocity in free area
wex = Vex/Amin;

Re_ex = dex*wex/nu_ex;
Pr_ex = mu_ex*c_ex/k_ex;
% j-factor for 4 rows
j4 = 0.14*(Re_ex^(-0.328))*((sv/sh)^(-0.502))*((sd/dex)^0.0312);
j = j4*0.991*((2.24*(Re_ex^-0.092))*((Rows/4)^-0.031))^...
... (0.607*(4-Rows))); % j-factor
St = j/((Pr_ex)^(2/3)); % j=St*Pr^(2/3)

h_ex = St*c_ex*wex*rho_ex; % St = h/(cp*w*rho)

end
```

Internal single-phase heat transfer coefficient calculations

```
function h_in1 = htc_in1 (mref, mu, mu_sur, cp, k, y, flag, p);

if flag == 1 % for evaporator
    m = mref/2;
    n = 0.4;
    din = p.dine;
    L = p.Le/2*y;
elseif flag == 2 % for condenser desuperheating
    m = mref/2;
    n = 0.3;
    din = p.dinc;
    L = p.Lc/2*y;
elseif flag == 3 % for condenser subcooling
    m = mref;
    n = 0.3;
    din = p.dinc;
    L = p.Lc*y;
end

Pr = mu*cp/k;
G = m/((din^2)*pi/4); % [kg/(s*m2)]
Re=(din*G)/mu;

if Re < 2300
    Nu = 1.86*((Re*Pr*din/L)^(1/3))*((mu/mu_sur)^0.14);
elseif Re > 10000
    Nu = 0.023*(Re^0.8)*(Pr^n);
else
    Nu = 0.023*(Re^0.8)*(Pr^n);
    disp ('2300 < Re < 10 000')
end

h_in1 = Nu*k/din; % [W/m2K]

end
```

Internal two-phase heat transfer coefficient calculations

```
function h_in2 = htc_in2 (mref, xout, xin, hfg, mu_l, k_l, cp_l,...
...rho_l, rho_v, y, evap_flag, p);

dT = 1;
if evap_flag == 1 % for evaporator
    din = p.dine;
    L = p.Le/2*y;
    G = (mref/2)/((din^2)*pi/4); % [kg/(s*m2)]
    Re_l = din*G/mu_l;
    C = 8.2*(10^(-3));
    n = 0.4;
    K = (xout - xin)*hfg/(L*9.81);

    Nu_l = C*((Re_l^2)*K)^n;
end
```

```

elseif evap_flag == 0 % for condenser
    din = p.dinc;
    L = p.Lc/2*y;
    G = (mref/2)/(din^2*pi/4); % [kg/(s*m2)]
    Re_l = din*G/mu_l;
    Pr_l = mu_l*cp_l/k_l;
    A = Re_l*((rho_l/rho_v)^0.5);

    if A < 20000
        Nu_l = 13.8*(Pr_l^(1/3))*((hfg/(cp_l*dT))^(1/6))*(A^0.2);
    else
        Nu_l = 0.1*(cp_l*mu_l/k_l)*(Pr_l^(1/3))*((hfg/(cp_l*dT))^...
        ... (1/6))*(A^(2/3));
    end

end

h_in2 = Nu_l*k_l/din;

end

```

Heat exchanger efficiency

```

function [eff] = Efficiency(C_min,C_max,yUA)

Crat = C_min/C_max;
NTU = yUA/C_min;

eff = 1-exp(1/(Crat*NTU^(-0.22)))*(exp(-NTU*Crat*NTU^(-0.22))-1));

end

```

U value calculation

```

function U = total_U (h_in, h_ex, evap_flag, p);

if evap_flag == 1 % for evaporator
    rin = p.dine/2;
    tfin = p.tfine;
    S1 = p.S1e;
    S2 = p.S2e;
    Afin = p.Afine;
    Aex = p.Aexe;
    Ain = p.Aine;
elseif evap_flag == 0 % for condenser
    rin = p.dinc/2;
    tfin = p.tfinc;
    S1 = p.S1c;
    S2 = p.S2c;
    Afin = p.Afinc;

```

```

    Aex = p.Aexc;
    Ain = p.Ainc;
end

m_fin = (2*h_ex/(p.kfin*tfin))^0.5; % fin parameter
alfa = (S1/2)/rin;
beta = S2/S1;
R_ratio = 1.28*alfa*((beta-0.2)^0.5);
fi = (R_ratio-1)*(1+0.35*log(R_ratio));
factor = m_fin*rin*fi;
eta_fin = (tanh(factor))/factor; % fin efficiency
eta_s = 1-Afin/(Aex+Afin)*(1-eta_fin); % total surface efficiency

U = (Ain/(eta_s*h_ex*(Aex+Afin))+1/h_in)^(-1); % based on internal
surface area p.Ain [W/m2K]

end

```

Pressure drop calculations

Internal single-phase pressure drop calculations

```
function dp = Dplph (mref, rho, mu, y, p, part_flag);

if part_flag == 1 % evaporator, desuperheating region
    mdot_loc = mref/2;
    d = p.dine;
    local = p.localloss_evap/2*y;
    L = p.Le/2*y;

elseif part_flag == 2 % suction pipe
    mdot_loc = mref;
    d = p.ds;
    local = p.locals + p.loss_valve + p.loss_valve; % 180 turns +
    service and reversing valve
    L = p.Ls;

elseif part_flag == 3 % discharge pipe
    mdot_loc = mref;
    d = p.dd;
    local = p.locald + p.loss_valve + p.loss_valve; % 180 turns +
    service and reversing valve;
    L = p.Ld;

elseif part_flag == 4 % condenser, desuperheating region
    mdot_loc = mref/2;
    d = p.dinc;
    local = p.localloss_cond/2*y;
    L = p.Lc/2*y;

elseif part_flag == 5 % condenser, subcooling region
    mdot_loc = mref/2;
    d = p.dinc;
    local = p.localloss_cond/2*y;
    L = p.Lc/2*y;

end

G = mdot_loc/(d^2*pi/4); % [kg/s*m2]
Re = G*d/mu;
f0 = 0.005;
options = optimset('Display','off');
f = fsolve(@(f) 1/f^0.5 - (1.74-
2*log10(2*p.E/d+18.7/(Re*f^0.5))),f0,options); % Colebrook equation

dp = (f*L/d+local)*G^2/(2*rho)/1000; % [kPa]

end
```

Internal two-phase pressure drop calculations

```

function dp = Dp2ph (mref, moil, xin, xout, hfg, vin, vout, muref,...
...muoil, y, p, evap_flag);

if evap_flag == 1
    din = p.dine;
    L = p.Le/2*y;
    Nturn = p.Nturne_total_e/2*y;
elseif evap_flag == 0
    din = p.dinc;
    L = p.Lc/2*y;
    Nturn = p.Nturnc_total_c/2*y;
end

x1 = xin*(mref/2)/(mref/2+moil/2);
x2 = xout*(mref/2)/(mref/2+moil/2);
deltax = abs (x2-x1);

K = deltax*hfg/(L*9.81);
Ain = din^2*pi/4;
G = (mref/2)/Ain; % total mass velocity [kg/s*m2]

% calculating viscosity of mixture for all liquid state
foil_in = (moil/2)/(moil/2+(1-xin)*mref/2); % mass fraction of oil at
inlet
foil_out = (moil/2)/(moil/2+(1-xout)*mref/2); % mass fraction of oil
at outlet
foil_av = (foil_in + foil_out)/2; % averaged mass fraction of
lubricant
noil = foil_av*(p.Mref/p.Moil)/(1-foil_av+foil_av*(p.Mref/p.Moil)); %
molar fraction of oil
nref = 1-noil; % molar fraction of refrigerant
k = 0.58; % emphirical exponent
ksiref = (p.Mref^k)*nref/((p.Mref^k)*nref+(p.Moil^k)*noil);
ksioil = p.Moil^k*noil/(p.Mref^k*nref+p.Moil^k*noil);
muM = exp((ksiref*log(muref)+ksioil*log(muoil))); % viscosity of
mixture [Ns/m2]

Re = G*din/muM;

if (Re/K)>2
    fNavg = 0.00506*(Re^-0.0951)*(K^0.1554); %two-phase friction
factor
else
    fNavg = 0.00506*(Re^-0.0951)*(K^0.1554);
    disp ('Pierres condition for fN is not satisfied');
end

xm = (x1+x2)/2; % average vapor quality

if evap_flag == 1
    vm = xm*vout; % specific volume at xm for evaporator
elseif evap_flag == 0

```

```

        vm = xm*vin; % specific volume at xm for condenser
    end

    dplocal = Nturn*p.loss180*(G^2)*vm/2; % local losses

    dp = ((fNavg*L*(vout+vin)/din+abs(vout-vin))*(G^2) + dplocal)/1000;

    %.....
    % fix
    if dp > 200
        dp=200;
    end
    %.....

end

```